Spring 2018

Biomonitoring in Seattle: Spatial Variation and Source-Determining of Airborne Pollutants in High-Traffic Areas

Saba Asefa
Western Washington University, sabaroas1@gmail.com

Biomonitoring in Seattle: Spatial Variation and Source-Determining of Airborne Pollutants in High-Traffic Areas

By

Saba Asefa

Accepted in Partial Completion
of the Requirements for the Degree
Master of Science

ADVISORY COMMITTEE

Dr. Bernard Housen, Chair

Dr. Brady Foreman

Dr. Troy Abel

GRADUATE SCHOOL

Dr. Gautam Pillay, Dean

Master's Thesis

In presenting this thesis in partial fulfillment of the requirements for a master's degree at Western Washington University, I grant to Western Washington University the non-exclusive royalty-free right to archive, reproduce, distribute, and display the thesis in any and all forms, including electronic format, via any digital library mechanisms maintained by WWU.

I represent and warrant this is my original work, and does not infringe or violate any rights of others. I warrant that I have obtained written permissions from the owner of any third party copyrighted material included in these files.

I acknowledge that I retain ownership rights to the copyright of this work, including but not limited to the right to use all or part of this work in future works, such as articles or books.

Library users are granted permission for individual, research and non-commercial reproduction of this work for educational purposes only. Any further digital posting of this document requires specific permission from the author.

Any copying or publication of this thesis for commercial purposes, or for financial gain, is not allowed without my written permission.

Saba Asefa

05/01/2018

Biomonitoring in Seattle: Spatial Variation and Source-Determining of Airborne Pollutants in High-Traffic Areas

A Thesis
Presented to
The Faculty of
Western Washington University

In Partial Fulfillment
Of the Requirements for the Degree
Master of Science

by
Saba Asefa
May 2018

Abstract

Although transportation is a large source of air particulate pollution in the U.S., air quality is currently not routinely monitored on the street level or using methods that could routinely determine particulate composition. In this study, we will use biomonitoring- using biological organisms (in this case tree leaves) as sample collectors- and magnetic characterization of particulate matter (PM) to provide a simple and inexpensive alternative air quality monitoring apparatus that is at the human spatial level, can collect micron-sized particles, and can be found in closely-spaced locations, so that there is a dense area collection network. Magnetic methods such as SIRM and magnetic susceptibility have been used to gauge PM concentrations on the street level (Hoffman et al 2014, Kardel et al 2011, Lehndorff & Schwark 2004, Maher et al 2008) using biomonitors such as tree leaves. Total PM concentrations correlate well with measured magnetic values on leaf surfaces because PM contains magnetic particles sourced from iron impurities in fossil fuel vehicle exhaust, brake dust, and other vehicle sources (Sagnotti et al 2009). The geographic focus of this study is the Seattle area because it has the most traffic in the Pacific Northwest (Seattle Department of Transportation) and because a mix of residential and community activities are located near sites of industry that include manufacturing, warehousing, commercial, container shipping and support activities, concentrated in the south Seattle Duwamish Valley (Abel et al 2015). This study uses rock-magnetic methods (SIRM, magnetic hysteresis) and imaging (SEM) to characterize types of particulates, and map the spatial variation of Seattle's air pollution. Magnetic saturation and susceptibility values for Duwamish Valley samples were higher than those of Capitol Hill samples. Coniferous leaves and deciduous leaves had similar magnetic values. The magnetic intensity of samples in a 300 mT field did not change when the field was 1 T, meaning the magnetic particles are composed of one magnetic mineral. Morphology and chemical makeup of magnetic particles varied within leaf samples, ranging from ~5-40 microns in diameter and from 0-93% Fe content. Cluster analyses determined that there are three sets of sources, but are not conclusive on whether some leaf samples have a mixture of source material on their surfaces.

Table of Contents

List of Figures and Tables

Figure **Page**

Table

Introduction

Air Quality and Human Health

Air quality is an issue that is important to human health and therefore has been studied and regulated to ensure that the air humans breathe is not harmful. Air pollutants, such as ozone, CO, SO_2, lead, ammonia, volatile organic compounds, and particulate matter are extensively monitored and regulated. In the United States the most abundant air pollutants are particulate matter and CO, while in the Pacific Northwest region they are particulate matter and ozone (Northwest Clean Air Agency 2017) . The main sources of pollution in Seattle are industrial emissions from the southwest industrial area and mobile emissions from the traffic across the city (Environmental Science Associates 2016). In addition, there can be seasonal variation in air quality related to factors such as forest wildfires and higher wood-burning emissions during winter months as people heat their homes (Environmental Science Associates 2016).
PM concentrations in air have a direct correlation with human respiratory issues, such as asthma and other chronic respiratory diseases and cardiovascular diseases, especially in children and infants (Schwartz et al 1993, Brook et al 2010, Lin et al 2002, Koenig 2000, Curtis et al 2006, Zeger et al 2008).

PM that is smaller than 10 microns in diameter (PM_{10}) poses a great threat to human health because it can bypass mucous filters and travel deep in the lungs (Shwartz et al 1993), while PM that is smaller than 2.5 microns in diameter tends to have a negative impact on the respiratory and cardiovascular systems, including the alveoli, which are the sites of diffusive gas exchange (Brook et al 2010). A recent study suggests that human exposure to PM particles that are less than 200 nm diameter can lead to Alzheimer's disease (Maher et al 2016). Because of these health issues, the Environmental Protection Agency (EPA) and state-level agencies monitor

and regulate levels of PM_{10} and $PM_{2.5}$ concentrations. The EPA has developed an Air Quality Index (AQI) to assess air quality, which includes the following five criteria pollutants under the Clean Air Act: ground-level ozone, CO, SO_2, NO_2, and particulate matter (EPA Clean Air Act, Section 112). National air quality monitors are installed regionally in order to report the AQI ranging from "Good" to "Hazardous" depending on the AQI value, which is based on the concentrations of the various pollutants in mass per air volume ($\mu g/m^3$) (See Appendix VI.1). In the Pacific Northwest, Puget Sound Clean Air Agency has air monitors that track air quality over time (See Appendix VI. 2).

Although the EPA observes air quality using air quality monitors, it does not have a mechanism to ascertain the specific source of the pollutants in a small-scale area or the ability to routinely distinguish the composition of particulates, though the EPA is able to report data for concentrations of different of sources on the county-level (See Appendix VI.3). According to the EPA, the main sources of PM_{10} and $PM_{2.5}$ in the Seattle area (King County) are dust, fuel combustion, miscellaneous sources (bulk gasoline terminals, commercial cooking, gas stations, and waste disposal), automobile, and industrial processes. However, there is no reference to where exactly these sources are located within the county, the composition of the pollutants, or how these sources may vary on a smaller spatial scale.

Even though the air quality standards regulate PM_{10} and $PM_{2.5}$, they do not specify or monitor the composition of these particles. An example of an un-regulated and less monitored component of total particulate matter are metallic particles. Metallic PM is associated with statistically significant increases in heart rate, blood pressure, and lung function decrease (Ristovksi et al 2012, Cakmak et al 2014). Transportation and industrial emissions are a large source of metallic air particulate pollution in the United States (Maher et al 2007), yet the spatial

distribution of this type of pollution is poorly constrained. Understanding the concentrations and spatial variations of particulate matter (PM), especially metallic PM, at the human-scale is important in order to mitigate and reduce human exposure.

Air Quality Monitor Challenges

Air quality monitors are often installed far apart (~ 5-10 km or more) and do not allow for fine-scale spatial coverage of an area; therefore, detailed spatial variation in pollution, and its source is hard to determine. Recent studies have found significant spatial variation in air pollution in many cities (Kaur, Nieuwenhuijsen, Colvile 2005; Knibbs, Cole-Hunter, Morawska 2011; Pattinson, Longley, Kingham 2014, Strum 2016). Sparse networks of stationary air pollution monitors are expensive and not readily adaptable to capture interurban heterogeneity and identify pollution spikes (Kumar et al 2015). A national air quality evaluation noted that "… these scale issues, at opposite ends of the spatial spectrum, challenge the current assessment framework that emphasizes regional air quality management" (NSTC 2013). Seattle has 4 air quality monitors spaced approximately 8-10 km apart from each other located in the International District, Duwamish Valley, Beacon Hill, and South Park (Puget Sound Clean Air Agency) (See Appendix VI.4).

The air quality monitors currently used are automated and can detect small PM_{10} and $PM_{2.5}$ particles (Mitchell et al., 2010), but the particles are not collected (Snyder et al 2013), so their composition cannot be determined. This makes assessing sources of transportation-produced and industrial ambient particulate concentrations difficult with the current air quality monitor system. The difficulties of the current air quality monitors have inspired many scientists and companies to find solutions. For example, a recent study done in Portland on Cadmium (Cd)

levels in the air, which found that the existing air monitors were unable to detect high levels of Cd near two stained glass factories because of the spacing of the monitors (Donovan et al 2016). The study analyzed the concentrations of Cd in 346 moss samples growing on urban trees along a randomized grid. The issue of spatial resolution of air pollutants at the street level is also a concern for Google and is the focus of a project in conjunction with the Environmental Defense Fund to map the street variability of air pollutants, including PM_{10} and $PM_{2.5}$ (Larson 2017). In this study, we will address the questions of the spatial variation of airborne PM within a city and how landscapes/foliage affect the variability of PM. We will assess the sources of PM based on comparisons of chemical compositions and magnetic properties of the sources and PM.

Biomonitoring

Biomonitoring- using biological organisms as sample collectors- provides a simple and inexpensive alternative air quality monitoring apparatus that is at the human spatial level, can collect micron-sized particles, and can be found in closely-spaced locations. Trees are excellent biomonitors because they are long-living organisms that can take up heavy metal PM from the soil, water, and air (Medejon et al 2006). Because different parts of the tree can absorb iron, the iron from the soil can also work its way through the tree's vascular network and eventually to the leaves' veins. The amount of iron in the roots compared to in the leaves varies greatly across different plant types and there is no conclusive evidence that a certain part of the plant absorbs iron more than the rest of the parts (Ancuceanu et al 2015).

The leaves of the tree collect the airborne particles on their surfaces (Kardel et al 2011, Mitchell et al 2010, Hoffman et al 2014). Magnetic measurements are used to gauge metallic

PM collected on the leaves' surfaces, and a detailed study has found the levels of metallic PM are in general proportional to the overall concentrations of PM (Ristovski et al 2012).

To evaluate the level of PM concentrations, particle sizes, and compositional information in leaves, we will use a set of magnetic properties that depend on leaf surface structure, leaf maturity, and particulate pollutant level. Saturation isothermal remnant magnetization (SIRM) provides variations in concentration and composition, saturation magnetization (Ms) determines overall concentration, remanent magnetization (Mr) suggests the amount of $PM_{2.5}$, coercive force (Hc) provides variations in composition, and magnetic susceptibility provides a measure of total particles (including non-metallic and metallic) (Kardel 2011). This study will also compare deciduous and coniferous leaves to understand how the different leaf characteristics record air quality as measured by these magnetic methods.

Background

Current Air Pollution Monitoring Systems

Air pollution sensors measure PM in three different ways - light scattering, light absorption, and direct particle mass measurements, each method with its own limitations (Snyder et al 2013). For example, light scattering is not a direct mass measurements and does not measure ultra-fine (< 0.1 microns) particles. Light absorption uses a relatively large device and is costly. Lastly, direct particle mass is sensitive to changes in temperature and humidity (Snyder et al 2013). The Puget Sound Clean Air Agency air quality monitors in Seattle use all of these methods. Another limitation of existing air monitoring techniques is that the Air Quality Index are averages from a metropolitan's entire system, which can obscure significant neighborhood PM variations. Air quality monitors can only detect particles at the microscale,

which is not fine enough for the smallest particulates that are the most detrimental to human health. In contrast, biomagnetism can measure fine nanoscale PM, is low cost to maintain, is not sensitive to temperature and humidity, and is sensitive to spatial variation (Kardel et al 2011).

Biomonitoring

The SIRM and magnetic susceptibility methods have been used to gauge PM concentrations on the street level (Hoffman et al 2014, Kardel et al 2011, Lehndorff & Schwark 2004, Maher et al 2008) in many different places. Airborne PM concentrations directly correlate to the measured magnetic values on leaf surfaces because PM contains magnetic particles from iron impurities released from fossil fuel vehicle exhaust, and other vehicle sources such as brakes (Sagnotti et al 2009). Magneto-mineralogical analysis of road dust and soils using SEM images suggest magnetite-like minerals and spherules are common in PM and contribute to the magnetic signal in PM concentrations (Rai et al 2014). The magnetic susceptibility of each leaf sample reflects the total composition of the dust deposited on the leaf, and is most often dominantly influenced by ferrimagnetic minerals, which have higher susceptibility values, but susceptibility variations can also be produced by large changes in concentration of paramagnetic (silicate mineral dusts) and diamagnetic (quartz, carbon (soot), and the H2O and C-compound leaf substrate) (Rai et al 2014).

SIRM, which involves measuring the magnetic remanence of samples once removed from an induced magnetic field, indicates the total concentration of magnetic grains and can be used as a proxy for PM concentrations (Muxworthy et al 2003). Additionally, SEM image analysis of magnetic particles in PM concludes that the magnetic particles are commonly spherules of magnetite with a maghemite coating (Sagnotti et al 2009). This type of road dust settles on the surface of leaves and is collected by the stomata on the surface.

Studies have compared the air quality-monitoring capabilities of soils, fruits, and leaves (Madejon 2006); "hairy" vs smooth leaves (Kardel 2011); and the relationship between time of year and pollution (Mitchell 2010). What all the studies have in common is that magnetic biomonitoring data are well correlated with the amount of PM in the air. Most studies have focused on deciduous leaves (Hoffman et al 2014, Kardel et al 2011, Maher et al 2008), but few studies have compared deciduous and coniferous leaves (Lehndorff & Schwark 2004, Zhang et al 2006). It is important to better understand how coniferous leaves may collect and retain PM because they live all year round unlike deciduous leaves, which are only present in the spring and summer. Expanding this technique to coniferous leaves will potentially allow a year-round sampling of PM, and to also evaluate the effectiveness of these types of plants to serve as screens to filter out PM.

Biomonitoring Leaves as Airborne PM Remediation

Besides studying variations of concentration and sources of PM, and the relative efficiency of different types of leaves to capture airborne PM, this study can also move toward evaluating possible mitigation strategies to reduce/shield human exposure to PM- by evaluating the screening effects of foliage on PM levels. Because roadside leaves absorb PM, they also can reduce the amount of PM in the air. Modelling studies of PM_{10} indicate that concentration of these particulates can be reduced by 1-60% via interaction with trees, and other work that used empirical data found that trees lining streets reduced the PM_{10} concentration by greater than 50% (Maher et al 2013). Another study (Kessler 2013) used models to predict the reduction of PM_{10} concentrations by 60% over a short period of time, while the average reduction over a year is in a range of 7-30%. Therefore, plant leaves are not only useful for monitoring air pollution, they are also valuable for air pollution mitigation. The dual benefit of monitoring and remediation is a

valuable argument in favor of using biomonitoring in addition to the current pricier and less spatially accurate air pollution monitors. For instance, a South Seattle coalition of community organizations installed the city's first "green wall" to mitigate localized industrial pollution levels. With the support of the EPA's Environmental Justice and Collaborative Problem Solving Program, this community hopes to reduce PM by 60% by building a 13 by 126 feet wall of plants to capture the polluted air (Bernard 2016). In this study, we will explore the mitigation factor of trees in an urban setting as distance increases from the probable source of PM in specific areas.

The Study Area

The geographic focus of this study is the Seattle area because it has the most traffic in the Pacific Northwest (Seattle Department of Transportation) and because it is a large center for industry (See Appendix VI.5) include manufacturing, warehousing, commercial, container shipping and support activities, concentrated in the south Seattle Duwamish Valley (Abel et al 2015), all of which create PM air pollution. The two sites for the study are Capitol Hill (the control site) and the Duwamish Valley based on the distribution of coniferous and deciduous trees, the relation of heavily air polluted areas to human populations, and the fact that the Duwamish area is an EPA superfund site. According to the Puget Sound Clean Air Agency's air monitor stationed in the Duwamish Valley, the air has low amounts of $PM_{2.5}$, but the location of the air monitor does not necessarily reflect the whole Duwamish Valley area. The Duwamish Valley has long been referenced as a community with environmental injustices because of the high pollution from the industrial sources, including an industrial diesel rail yard.

Based on a Cumulative Health Impacts Analysis, the 132,000 population of this community is more likely to live in poverty, not graduate from high school, and have chronic health issues than any other part of Seattle (Gould & Cummings 2013). Duwamish Valley

residents are more likely to be hospitalized for asthma than residents of King County, and one area of concern is the extent to which asthma incidence may be directly linked to PM air concentrations. Because the residents are more likely to live in poverty, they are less likely to move to another area to escape the industrial air pollution (Abel and White 2011, Abel and White 2015). Therefore, a better understanding of these possible sources of PM, how these variations may correlate with available health measures, and viable options for mitigation of PM levels is needed.

Methods

Field work

We chose two study areas in Seattle based on the amount of traffic, the amount of industrial land use, and the proximity to schools and housing units. One area of the study focuses on Capitol Hill in Seattle because it contains a mixture of land uses - significant traffic, with a residential/light industrial mix of buildings, with at least one school. In addition to Capitol Hill, the other site is the Duwamish Valley area, where one of the current air monitors is located.

Using Seattle land use data and tree data from the SDOT website, we collected 100 tree leaves/needles from a 1 km^2 area in Capitol Hill and Duwamish Valley each in the afternoon on June 11-12, 2017. We collected Douglas fir (*Pseudotsuga menziesii*) for coniferous and Big Leaf maple (*Acer macrophyllum*) for deciduous and put the samples in paper envelopes. The sampling and lab preparation methods are based on Kardel et al 2010.

In addition to collecting leaf samples, we collected dust samples of a gas-powered car engine exhaust manifold valve and a diesel exhaust pipe to later compare the magnetic characteristics of the dust samples to that of the leaves. The car valve was sampled from a 1989 Volvo 740 GLE, the diesel exhaust pipe was sampled from a construction truck. The dust was brushed off of the engine valve and was swabbed from the exhaust pipe of the construction truck.

Community Scientists

Before collection my own samples, we worked with students at the Cleveland Magnet High School in Seattle to collect samples from the Duwamish Valley and South Beacon Hill area for comparison with the Capitol Hill area and my own samples from the Duwamish area. The students collected samples of coniferous and deciduous leaves from around the southern Seattle site area in a variety of land use areas – park, industrial, school, and a heavily trafficked road. We collected the samples from the students and conducted the magnetic assessment that contributed to their own report of air quality in the Duwamish and South Beacon Hill areas (Figure 1, See Appendix III). We followed the same sample preparation and measurement procedures as conducted in Capitol Hill and Duwamish Valley/ South Beacon Hill so that there are no variables in sample collection that would mislead the analysis.

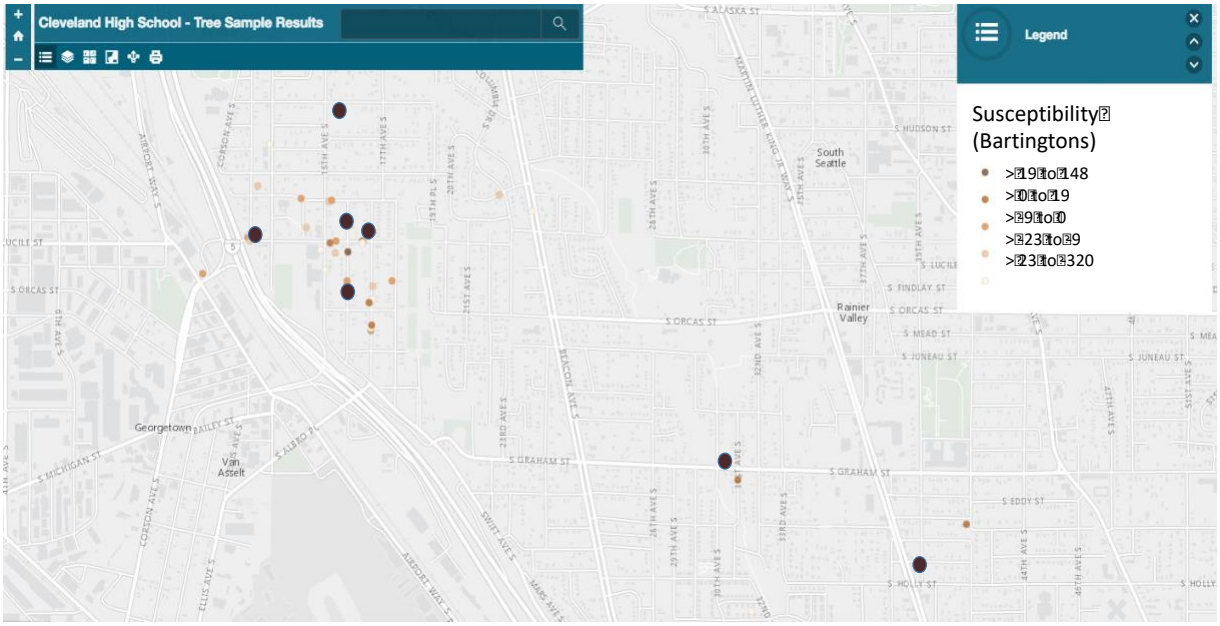

Figure 1:Map of susceptibility values from leaves collected by Cleveland High School students with largest susceptibility values' location points enlarged. Susceptibility values in Bartington units.

Magnetic Parameters

The SIRM was measured using an ASC Scientific IM-10-30 Impulse Magnetizer and a 2-G Enterprises 755 Cryogenic Magnetometer. The ratio of SIRM/magnetic susceptibility can reflect the size of the magnetic minerals in the sample. Low values of SIRM/magnetic susceptibility indicate larger grain sizes because there is less concentration of magnetism (based on the SIRM value) compared to the amount of magnetic grains (based on the magnetic susceptibility value) (Rai et al 2014). The measured samples are mass-normalized per kilogram to better capture variations in concentration. Although the collection of particles on the surface is not the exact equivalent of measuring particle concentration per volume of air, as modern air

quality monitors do, the mass-normalization of the leaf samples provides a measure of concentration proportional to the air quality instruments' measurements.

The saturation magnetization (Ms) (See Appendix VI.6) value gauges the overall concentration of the magnetic portion of the PM (Tauxe et al 1996). The saturation remnant magnetization (Mr) and the coercive force (Hc) (See Appendix VI.7) are useful values to estimate size and composition of magnetic grains (Tauxe et al 1996). Ms/Mr ratios determine the squareness of the hysteresis loops; values closer to 1 are more square and are more likely to have single-domain types of permanent magnetization. This ratio also adds to the characterization of grain size and shape (Day et al 1977). Fourier transforms of the magnetic hysteresis data are used to determine if there are more than one source or type of particle based on the forms of the hysteresis loop (Tauxe et al 1996).

Magnetic Corrections and Detection Limits

Magnetic hysteresis results generally had strong enough signal to produce well-defined hysteresis loops, (Figure 2).

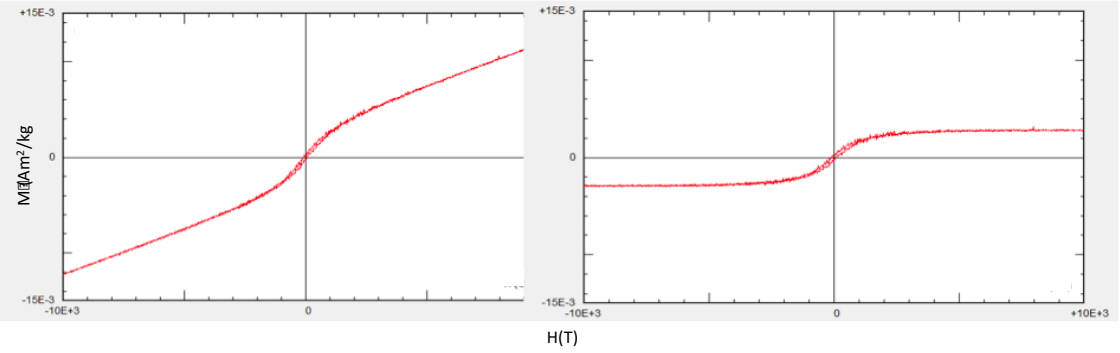

Figure 2: Slope Field correction of sample 55 from the Duwamish Valley area. Left: Original hysteresis plot with no slope correction, Right: Slope-corrected hysteresis.

After each leaf was run through the VSM, the raw data (Figure 10a) was then corrected for the high-field slope (Figure 10b) that is the combined result of paramagnetic contributions by mineral (Fe/Mn silicate) dusts, and the diamagnetic response of the C and H2O of the leaf material. Some of the slope-corrected hysteresis data had very weak magnetic signals, which resulted in horizontal lines, indicating a paramagnetic signature and low/no magnetic material.

Detection limits for magnetic samples were calculated based on the Ms values of pure magnetite (90,000 mAm^2/kg) (Dunlop and Ozdemir 1997). By dividing the measured Ms values by the pure Ms value of magnetite, we was able to estimate the amount of magnetite needed on a leaf surface to produce that value of Ms.

Most values were about 10,000 times smaller than the Ms value of pure magnetite (See Appendix V). The smallest Ms value that is still well-defined is 0.3554 mAm^2/kg; and anything below that value is less likely to be accurate data. Samples below the detection baseline are excluded from further analyses, but the locations will be noted as that indicates low(er) values of PM.

This approach can also be used to evaluate the Fe concentrations for plant material reported by Ancumeanu et al (2015), to see how the Fe content inferred from the magnetic measurements in this study compare. They reported an average amount of Fe of 489.4 mg per kg of leaf tissue (Ancuceanu et al 2015), which converts to 0.00018282 mAm^2/kg Ms by dividing the value by 90,000 mAm^2/kg and then taking the inverse. Because the Fe (and derived Ms values) content of the interiors of average plant material is so low compared to the Ms values measured from the leaves collected for this study, we conclude that internal Fe content has only a negligible influence on these measurements.

Magnetic Characterizations

Based on a comparable study (Kardel et al 2011), we oven-dried the samples at 45º C for 2 days, dry-weighed them, and tightly packed them in gel capsules. We recorded the Ms, Mr, and the Hc of the samples using the Princeton Measurements Corporation MicroMag 3900 Vibrating Sample Magnetometer (VSM) for hysteresis. The parameters for the VSM were maximum magnetization of 750 mT, increments of 10 mT, averaging time between 0.5 milliseconds and 1.0 seconds, pause time of 2.0 seconds. we measured the magnetic susceptibility using the AGICO KLY3-S Magnetic Susceptibility Kappabridge in the Western Washington University Pacific Northwest Paleomagnetic Laboratory. Samples obtained from the high school students were measured for susceptibility using the Bartington MS-2 dual frequency susceptibility meter We magnetized the samples at 300 mT and 1 T using the ASC Scientific IM-10-30 Impulse Magnetizer and obtained the magnetic moment with the 2-G Enterprises 755 Cryogenic Magnetometer. All of the measured units were mass-normalized in order to have a baseline of comparison between the samples (Table 1). Although the parameters are measured on flat surfaces – the leaves – the volume-normalized units are more comparable to the volume-normalized units that standard air monitors use. We obtained the exhaust particles of samples of the car and diesel parts and took residual particles off of the industrial sample, put the particles into gel capsules, and ran these samples using the same measurements as the leaf samples to evaluate the assemblage of the PM. All of the magnetic data are in the Appendices in order to have a cohesive display of the data.

Table 1: Unit conversions of volume-normalized magnetic measurements, where A is amperes, m is meters, kg is kilograms, and SI is the International Standard of Units.

Measurement	Raw Units	Normalized Units
Ms	Am^2	Am^2/kg
Mr	Am^2	Am^2/kg
Hc	T	T
Susceptibility (Kappabridge)	SI	m^3/kg
Susceptibility (Bartington)	1×10^{-5} SI	1×10^{-5} SI
Magnetic Moment	A/m	Am^2/kg
Ms of Magnetite		90 Am^2/kg

Imaging and Chemical Characterization

We mounted the 200 samples on stubs and coated them with gold-palladium coating before imaging them in a Vega TS 5136MM Scanning Electron Microscope at 15 kV and 10 nm resolution housed at Western Washington University. While in the SEM, we used the Energy Dispersive X-ray analysis and backscatter detector at 15 kV, 128 eV resolution, and 102.4 amplitude to acquire chemical spectra of the particulates on each sample. We measured magnetic particle sizes using the measuring tool in the SEM software.

Comparisons of different land uses and of leaf type

The Ms and the susceptibilities were mapped and analyzed using ArcGIS to determine if there are significant spatial variations in the magnetic properties of the leaves/needles in the study areas. Correlations between the magnetic particle concentration and environmental parameters (traffic counts, proximity to roads and railways, industrial lands) were tested. The results were compared separately between the conifer sample groups and the deciduous sample groups to compare and contrast their particle capture and retention characteristics using paired t-tests.

Hierarchical Clustering

To identify source of PM on the leaves' surfaces, we use Squared Euclidean Distance cluster analysis, which is used to find similar groups based on the different variables within the data. Using IBM SPSS Statistics software, we input combinations of the data set, including magnetic, chemical, and leaf types, and the software output taxonomical clusters. Hierarchical cluster analysis takes one data point and compares it to the next, and so on until it forms groups of data points that are most similar to each other. The resulting dendrogram displays the clusters and the representative cases along with the amount of points that overlap with each case point. The distance displayed on the axis opposite of the observations axis is the distance between the data points (Steinbach and Kumar 2005).

Results

Magnetic Properties

Magnetic Hysteresis (See Appendix I)

Southern Seattle leaves have Hc values have a narrow spread that is centered around a mean of 6.5 mT; the Ms values have a wider standard deviation with a mean of 1.5 mAm^2/kg; and the Mr values have a wide range with a mean of 36.6 $\mu Am^2/kg$ (Figure 3). Histograms of hysteresis values show the spread of the frequencies of a range of values – all with a sample size

of 100.

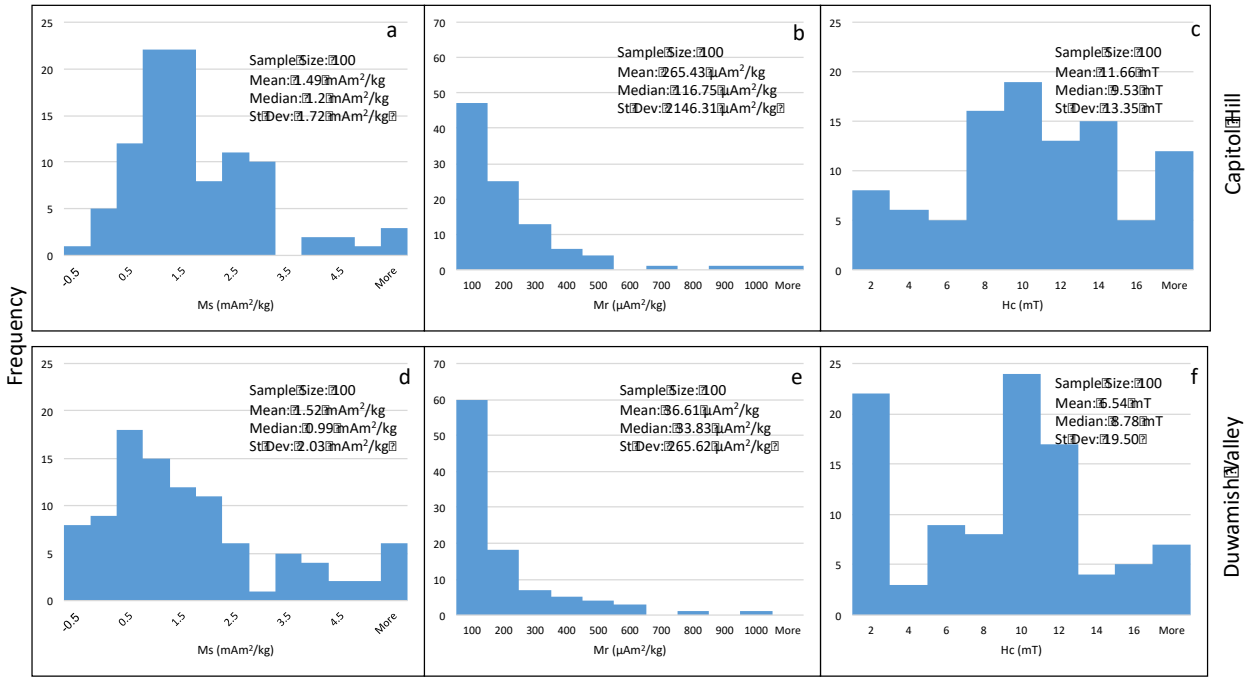

Figure 3: Histograms of the Ms, Mr, and Hc values for leaves in the Capitol Hill and Duwamish Valley areas with sample size, mean, median, and standard deviation values . a) Capitol Hill Ms values, b) Capitol Hill Mr values, c) Capitol Hill Hc values, d) Duwamish Valley Ms values, e) Duwamish Valley Mr values, f) Duwamish Valley Hc values.

Capitol Hill samples have Hc values between 4 and 30 mT, Ms values between 0.5 and 5.5 mAm^2/kg, and Mr values more consistently between 100 and 1000 $\mu Am^2/kg$. The Hc range is narrow with a mean value of 10.30 mT; Ms range is slightly wider with a mean of 1.49 mAm^2/kg; and the Mr values are very narrowly spread with a mean of 265.43 $\mu Am^2/kg$ (Figure 4). The overall shapes of the hysteresis loops are similar to the southern Seattle hysteresis loops, except that many of the Capitol Hill Hysteresis loops have larger gaps in the middle (Figure 5), which indicates that they have larger Hc values.

Comparing deciduous and coniferous samples, the Ms values of leaves collected near each other (less than 1 meter apart) were similar (Figure 6). However, based on Pearson 2-tailed analysis, the Ms and type of leaf are not significantly correlated at the 0.01 level (Figure 7). A

paired t-test (null hypothesis $\mu=0$) of all of the coniferous needles and deciduous leaves that grew near each other revealed that the Ms values are not significantly different, with a p-value of 0.386. Both deciduous and coniferous values of Ms (Figures 8,9) vary by location.

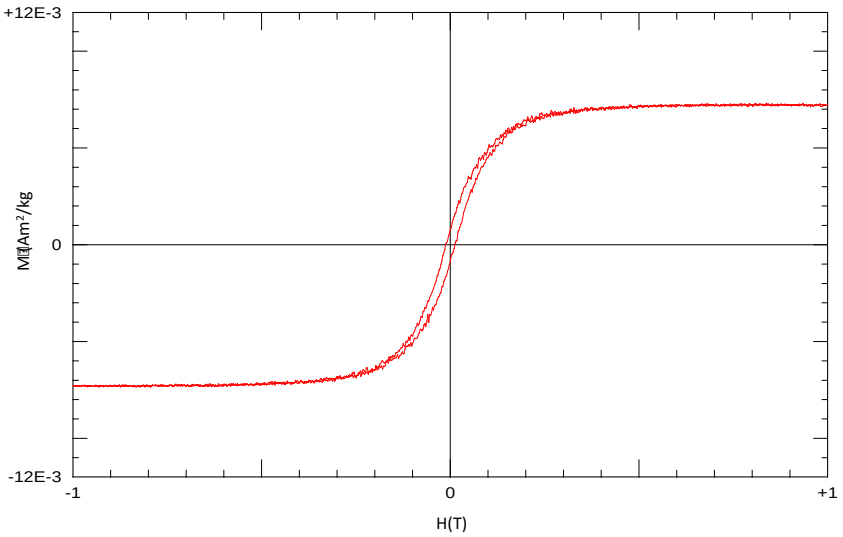

Figure 4: Hysteresis loop of deciduous leaf sample CH76 ~20 meters inside the edge of Cal Anderson Park in Capitol Hill.

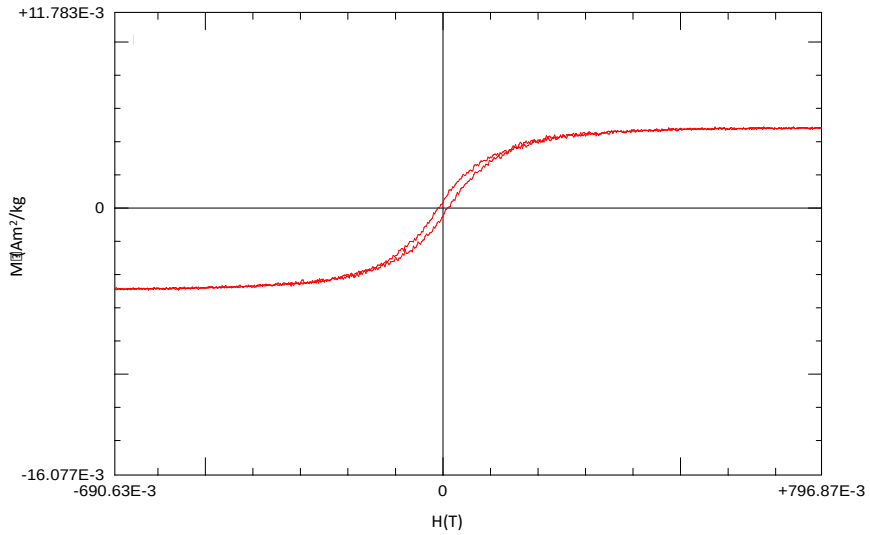

Figure 5: Hysteresis loop of coniferous leaf sample DW8 50 meters east of I-5 highway in Duwamish Valley.

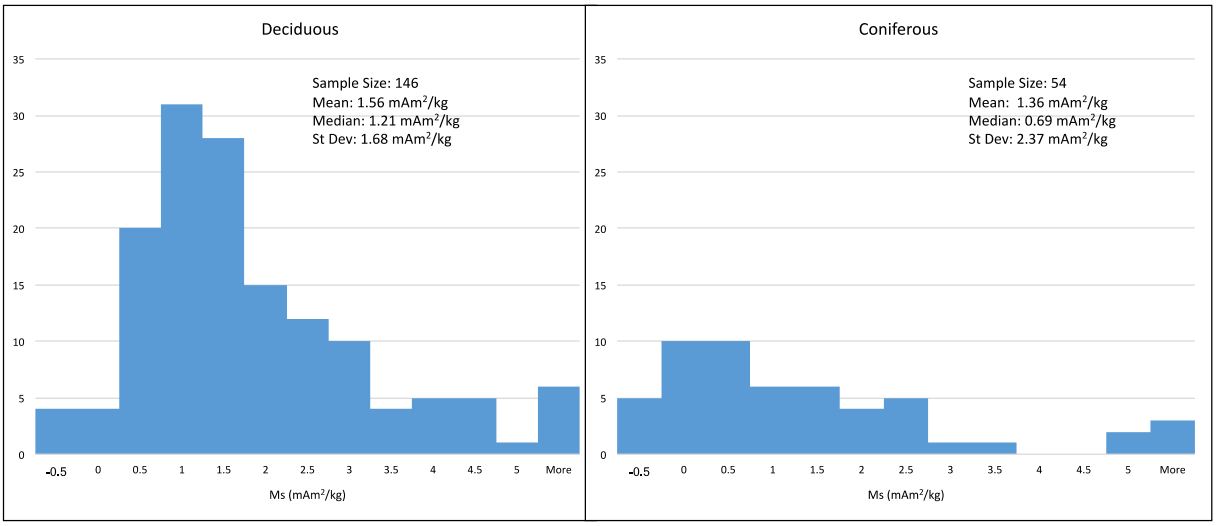

Figure 6: Histograms of the Ms values of deciduous leaves versus coniferous leaves with sample size, mean, median, and standard deviation values.

Correlations

		Type	Ms (mAm^2/kg)
Type	Pearson Correlation	1	-.071
	Sig. (2-tailed)		.317
	N	201	201
Ms (mAm^2/kg)	Pearson Correlation	-.071	1
	Sig. (2-tailed)	.317	
	N	201	204

Figure 7: Two-tailed Pearson correlation test between type of leaf (coniferous or deciduous) and Ms value, where N is the sample size.

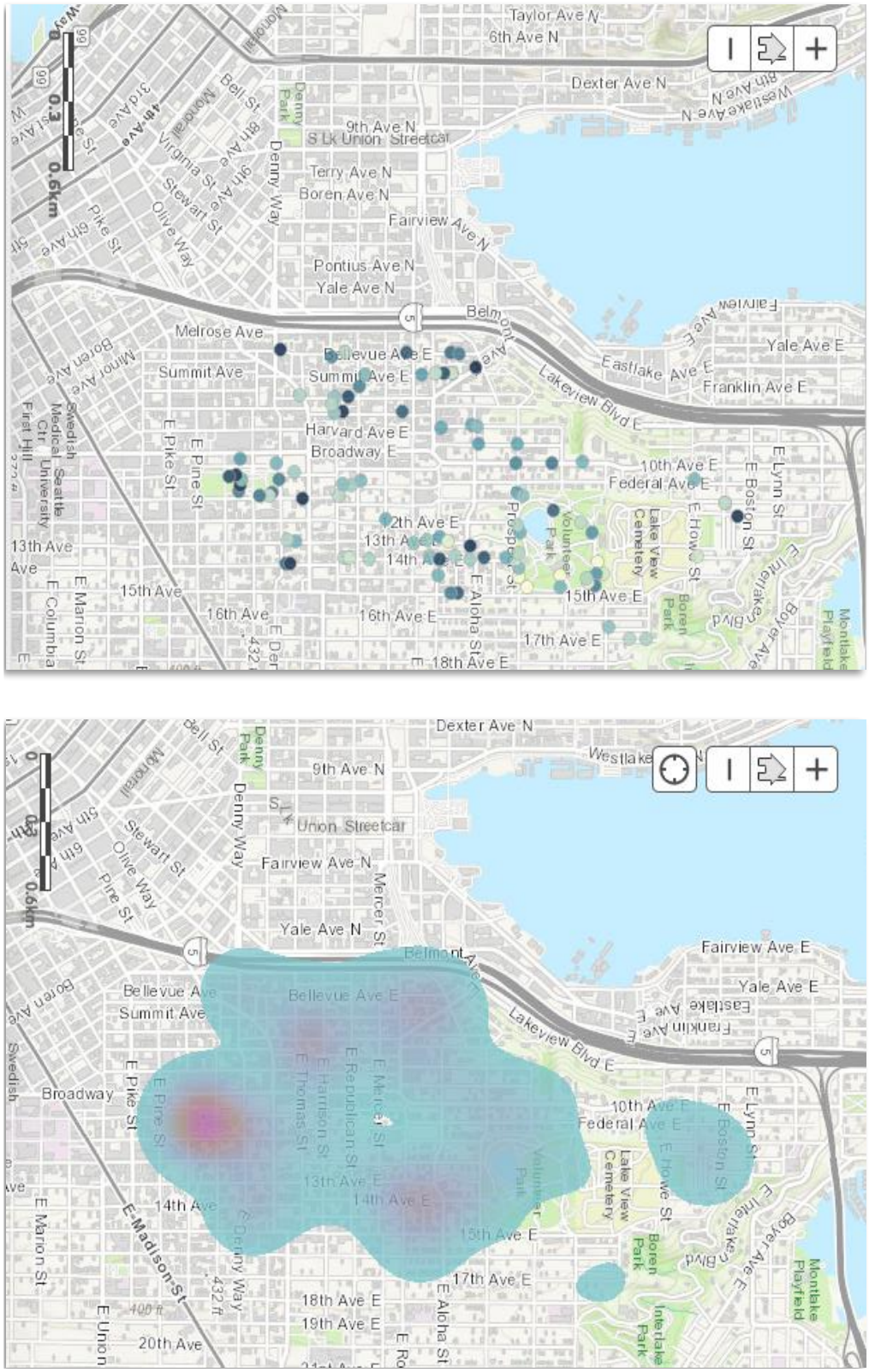

Figure 8: Left: Map of Ms values in Capitol Hill.. Darker blues indicate higher values, while lighter shades indicate lower values. Right: heat map of Ms values in Capitol Hill. Reds indicate higher Ms values, while blues indicate relatively lower Ms Values.

Figure 9:Left: Map of Ms values in Duwamish Valley. Darker blues indicate higher values, while lighter shades indicate lower values. Right: Heat map of Ms values in Duwamish Valley. Reds indicate higher Ms values, while blues indicate relatively lower Ms Values.

Fourier Transforms

Fourier transform results describe the different shapes of the hysteresis loops that can be produced by mixtures of magnetic phases with different Hc, Ms, Mr values. There were three general shapes that the hysteresis loops had – pseudo-single domain (PSD), single domain with small Ms, horizontal line (paramagnetic only), and SD/SP magnetite based on the Tauxe et al 1996 interpretations of hysteresis loops (See Appendix VI.7). Most of the samples had positive Ms and Mr values, but some of them had negative Mr, Ms, or a combination of both (Figure 10, f). The samples that had these negative values had such a small magnetic signal that the magnetometer was not able distinguish the result from base-level noise. These samples occur throughout the Duwamish/ South Beacon Hill and Capitol Hill areas (Figure 11).

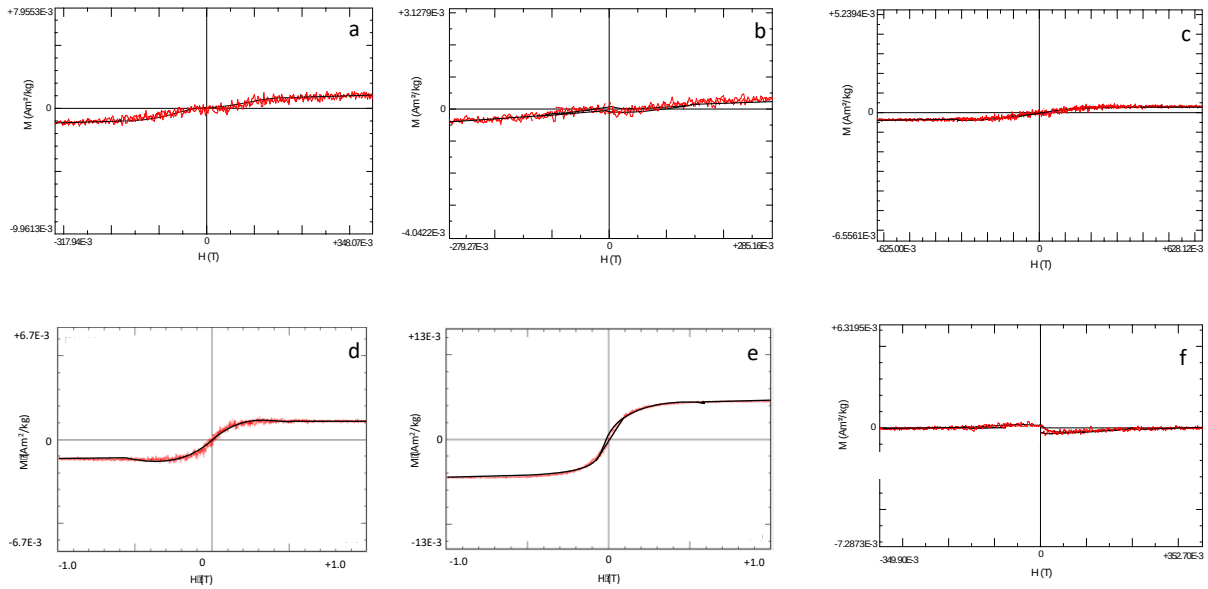

Figure 10: Representative hysteresis loops of the six types of hysteresis results traced in black to highlight the overall shapes . A) small Ms, b) SD/SP c) horizontal d) ends dip toward zero, e) PSD, f) diamagnetic center.

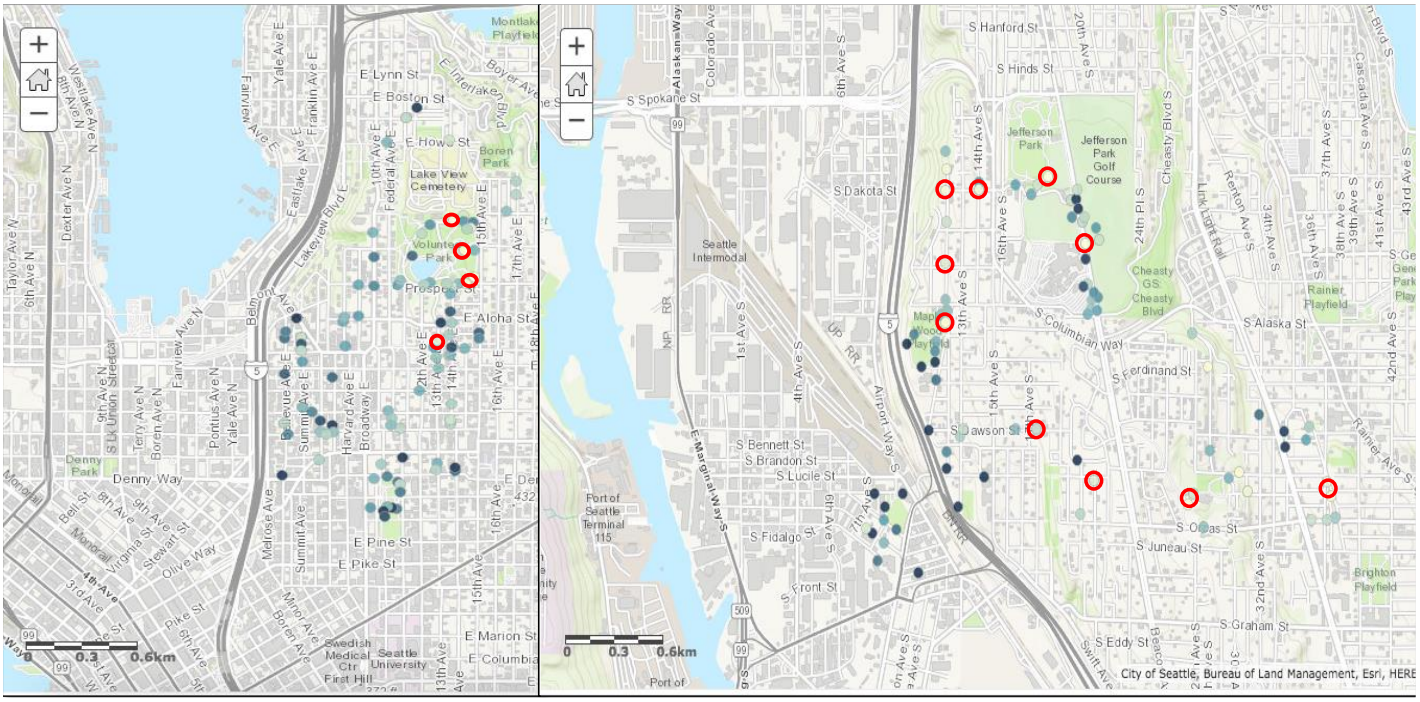

Figure 11: Ms value maps with red circles denoting samples that have Ms, Mr, below detection level.

Magnetic Susceptibility (See Appendix II)

The susceptibility readings for some of the samples were too low or negative because the Kappabridge instrument has a sensitivity of 1 x 10^{-7} SI, while some of the susceptibility values are less than that. The Bartington that was used for the high-school-collected samples has a lower sensitivity – 2 x 10^{-6} – but a quicker operation time than the Kappabridge. Although the sensitivities of the two instruments used are not fine enough for some of the samples, most of the samples were had high enough susceptibility to accurately assess, and provide an overall description of the Seattle air quality. Southern Seattle susceptibility readings range from 4.05x10^{-11} to 1.38x10^{-7} m^3/kg , with higher values closer to industrial land and on busy traffic roads. Capitol Hill susceptibility readings range between 5.45x10^{-11} and 6.28x10^{-8} m^3/kg, with

higher values located near the I-5 highway and heavily-trafficked roads (Figure 12).

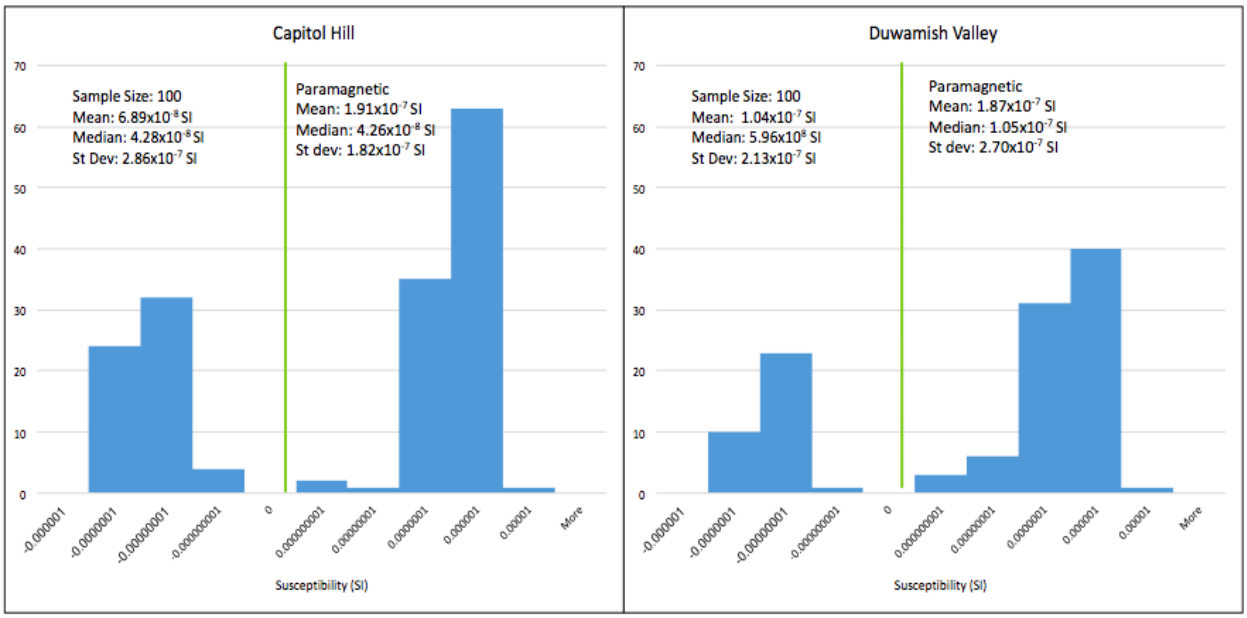

Figure 12: Histograms of susceptibility values of Duwamish Valley samples and Capitol Hill samples, respectively with sample size, mean, median, and standard deviation values. Paramagnetic mean, median, and standard deviation were separated from the diamagnetic data to reflect the particulate matter content.

Based on a Pearson Correlation 2-tailed analysis at the 0.01 level, the susceptibility and Ms values have a significant correlation (Figure 13).

Correlations

		Ms (mAm^2/kg)	Mass Susceptibilty (m^3/kg)
Ms (mAm^2/kg)	Pearson Correlation	1	.999**
	Sig. (2-tailed)		.000
	N	204	204
Mass Susceptibilty (m^3/kg)	Pearson Correlation	.999**	1
	Sig. (2-tailed)	.000	
	N	204	204

**. Correlation is significant at the 0.01 level (2-tailed).

Figure 13: Two-tailed Pearson correlation analysis of Ms values and susceptibility values.

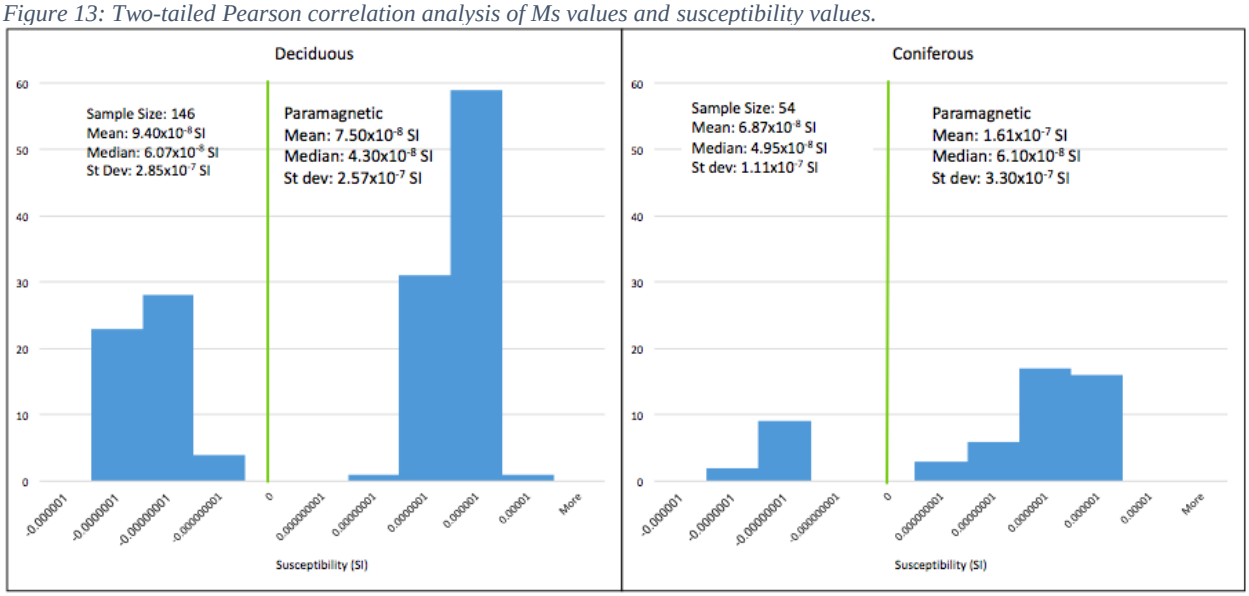

Figure 14: Histograms of susceptibility values of deciduous versus coniferous samples with sample size, mean, median, and standard deviation values. Paramagnetic mean, median, and standard deviation were separated from the diamagnetic data to reflect the particulate matter content.

Parks in both southern Seattle and Capitol Hill had lower susceptibilities, except Cal Anderson Park in Capitol Hill. Deciduous and coniferous trees that were collected next to each other (less than 1 meter apart) often indicated different susceptibilities (Figure 14), unlike the Ms values. Based on Pearson 2-tailed test, the susceptibility and the type of leaf are not significantly

correlated on the 0.01 level (Figure 15). A paired t-test (null hypothesis $\mu=0$) of all of the coniferous needles and deciduous leaves that grew near each other revealed that the susceptibility values are not significantly different, with a p-value of 0.823. Susceptibility values vary with spatial variation (Figures 16, 17).

Correlations

		Type	Mass Susceptibilty (m^3/kg)
Type	Pearson Correlation	1	-.057
	Sig. (2-tailed)		.420
	N	201	201
Mass Susceptibilty (m^3/kg)	Pearson Correlation	-.057	1
	Sig. (2-tailed)	.420	
	N	201	204

Figure 15: Two-tailed Pearson correlation analysis of susceptibility versus type of leaf (deciduous or coniferous).

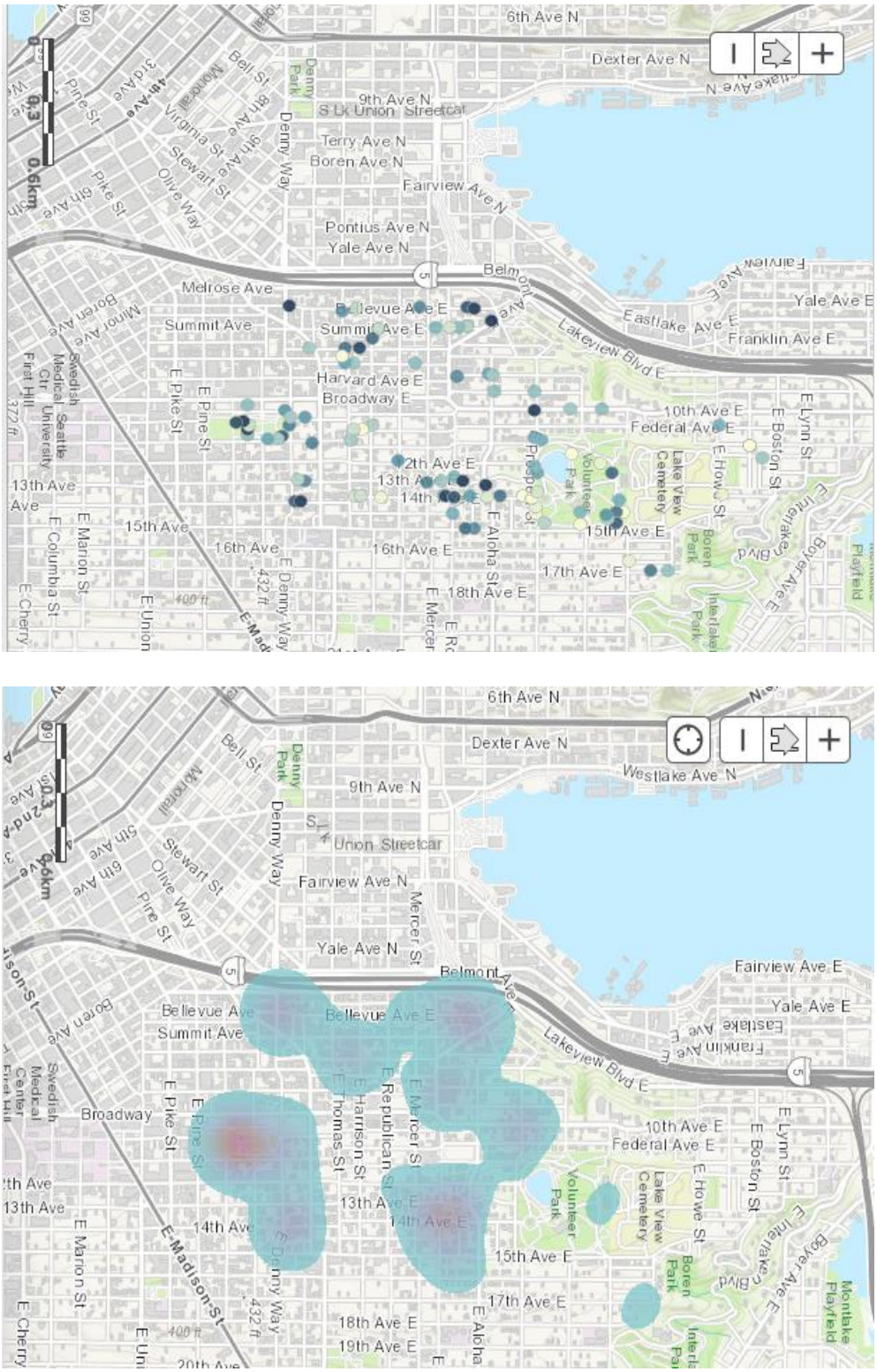

Figure 16: Left: Map of susceptibility in Capitol Hill. Darker blues indicate higher values, while lighter shades indicate lower values. Right: Heat map of susceptibility in Capitol Hill. Reds indicate higher susceptibility values, while blues indicate lower values.

Figure 17: Left: Map of susceptibility in Duwamish Valley. Darker blues indicate higher values, while lighter shades indicate lower values. Right: Heat map of susceptibility in Duwamish Valley. Reds indicate higher susceptibility values, while blues indicate lower values.

SIRM (See Appendix IV)

Samples that fit the criteria of high enough Ms values (> 2.0 mAm^2/kg), from different geographical locations, and had a variety of hysteresis shapes were analyzed using SIRM methods and SEM imaging (Figure 18, Figure 19). SIRM results contribute to the analysis of grain composition based on if the magnetic moment changes with increase in magnetic field. The cryogenic magnetometer readings were consistent and produced reliable results. In a magnetic field of 1 T, southern Seattle samples had magnetic moments around 1.99 Am^2; while at 300 mT, the same samples had magnetic moments of 1.89 Am^2. Samples closer to the industrial site had an increase of magnetic moment from 300 mT to 1 T. In a magnetic field of 1 T, Capitol Hill samples had around 2.00 Am^2 magnetic moment; and at 300 mT magnetic moment either stayed about the same or decreased (See Appendix IV). The source samples and the leaf samples have about a 1:1 ratio of magnetic moment values compared at 300 mT and 1 T (Figure 20), this indicates both sets of materials have similar magnetic properties.

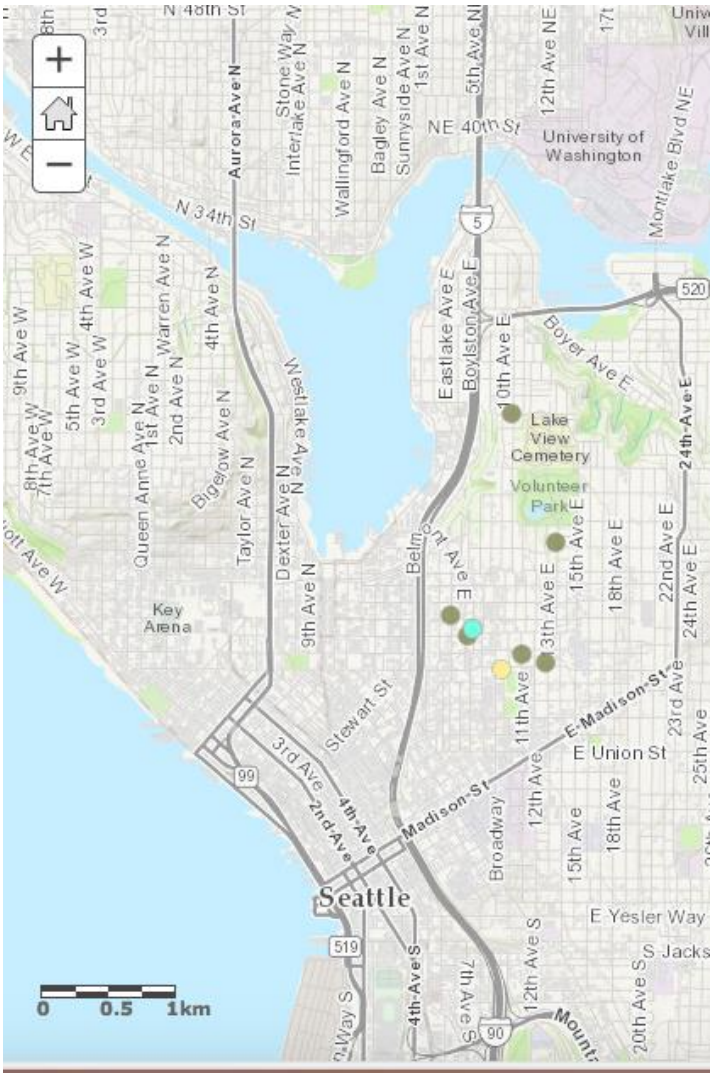

Figure 18: Locations in Capitol Hill of samples analyzed using SIRM and/or SEM. Blue represents samples that were used for both SIRM and SEM analyses. Green means that they only were used for SIRM. Yellow samples were only used in the SEM.

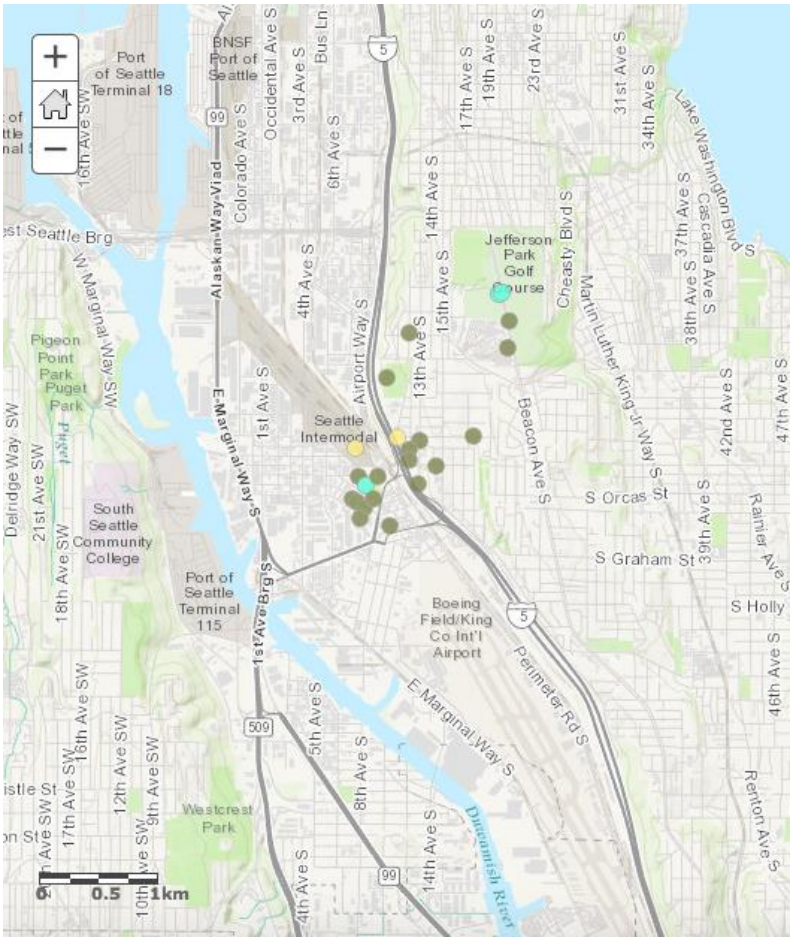

Figure 19: Locations of samples in the Duwamish Valley that were used in SIRM and/or SEM analyses.

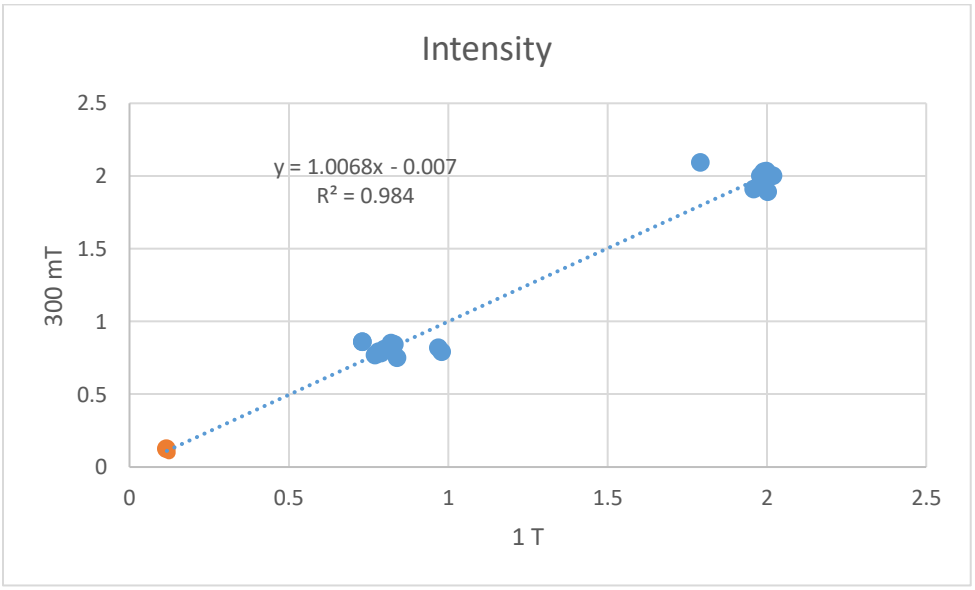

Figure 20: Graph of intensities measured with 300 mT and 1 T magnetic fields of samples and sources, where orange points represent the sources (diesel and gas-powered) and blue points are the samples.

Particle Morphology

SEM results provided back-scatter imaging and EDS spectrum analyses. The back-scatter imaging had allowed for morphological analysis of the magnetic and non-magnetic grains as well as of the leaf surfaces. The EDS spectrum provided chemical analyses of grain compositions. The SEM was able to image and chemically analyze all of the grains that were larger than about 2 microns in diameter, which all of the grains were. The Au-Pd coating on the leaves created a dust that can be seen in the images as flat, flaky tiny particles. Iron-rich particles on surfaces of samples tend to be spherical to cubic and about 10 microns in diameter (Figure 21), which is consistent with PM_{10} size and shape. Particles tend to collect in the microscopic, concave-lengthwise grooves in the coniferous needles (Figure 22) and near veins and in concave surfaces on deciduous leaves (Figure 23). The amount of particles on a sample's surface correlates to the Ms value of that sample, while the concentration of Fe correlates to the susceptibility (Table 2).

Table 2: Particle sizes, Fe content, Ms values, and susceptibility values of samples imaged in the scanning electron microscope.

Particle Sample	Diameter (microns)	Fe content	Ms (mAm^2/	m^3/kg)
leaf34e	10	FeTi	10.66	1.29E-09
leaf34d	25	60% Fe		
leaf34a	10	60% Fe		
leaf34b	20	small amount of Fe		
leaf34c	25	small amount of Fe		
leaf34	25	copper		
leaf32b	40	85% Fe	0.776	1.95E-07
leaf32	15	small amount of Fe		
leaf76dd2	9	85% Fe	48.19	3.018E-06
leaf76dd1	7	88% Fe		
leaf76dc	30	small amount of Fe		
leaf76db	5	70% Fe		
leaf76a	20	small amount of Fe		
leaf76d	8	85% Fe		
leaf82ca1	10	small amount of Fe	1.247	1.23E-07
leaf82ca	10	70% Fe		
leaf92c	21	70% Fe	1.069	2.96E-07
leaf92	35	small amount of Fe		
leaf99cb	30	FeTi	5.875	8.04E-10
leaf99ca2	11	93% Fe		
leaf99ca1	12	FeTi		
leaf99c	24	small amount of Fe		
leaf4a	7	60% Fe	3.776	3.68E-07
leaf4b	10	small amount of Fe		
Industrial 2	10	60% Fe	576.6	0.0000737
Industrial1	30	70% Fe		
Industrial 3	15	50% Fe		
Deisel4	5	small amount of Fe	1.468	4.32E-07
Deisel3	4	small amount of Fe		
Deisel2	3	small amount of Fe		
Deisel1	7	small amount of Fe		
Car3	6	small amount of Fe	16.13	2.49E-06

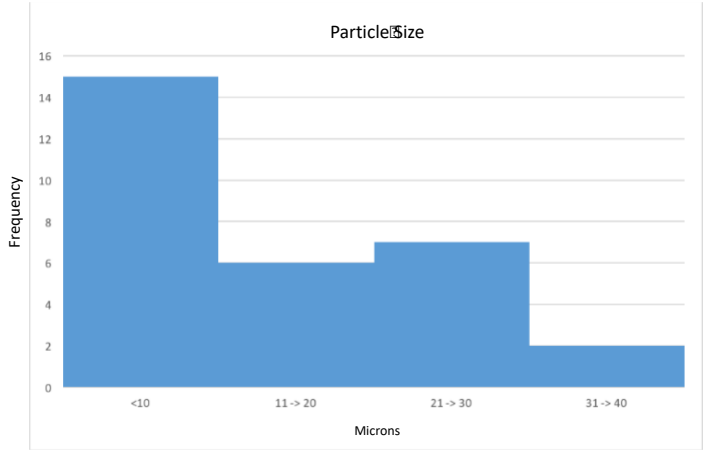

Figure 21: Distribution of grain size of Fe-containing particles on leaf samples imaged using the scanning electron microscope.

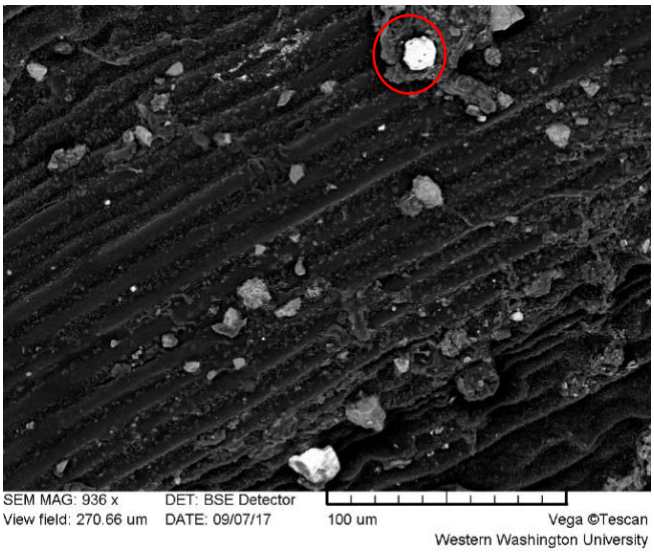

Figure 22: SEM-BSE image of sample CH99 conifer needle from Boylson Avenue in Capitol Hill with Fe-rich particulate in the top right corner.

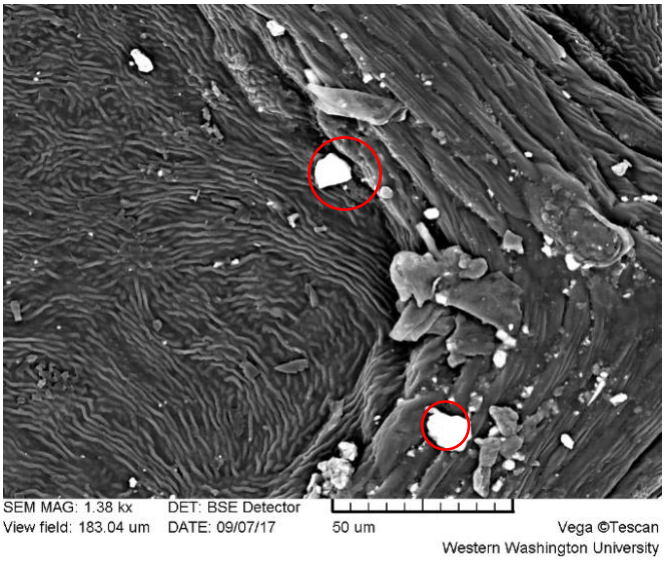

Figure 23: SEM-BSE image of sample CH82 deciduous leaf from E Denny Way near Cal Anderson Park in Capitol Hill with Fe-rich particulates in the bottom right and top center.

Chemical Characteristics

The Fe-rich particles have anywhere from 60% to 85% Fe (Figure 24), while some of the other particles either have Ca-Al-Si assemblages with around 10% to 15% Fe (Figure 25). Some of the metallic particles have Ti-Fe composition.

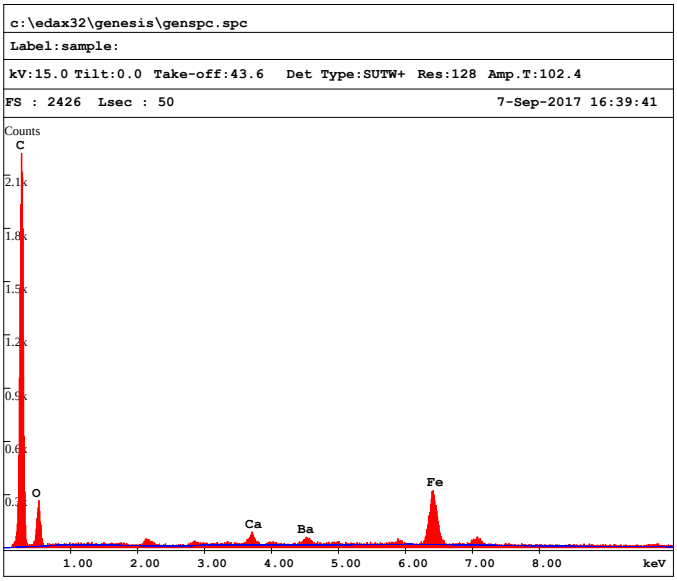

EDAX ZAF Quantification (Standardless)
Oxides
SEC Table : Default

Element	Wt %	Mol %	K-Ratio	Z	A	F
CaO	5.16	6.87	0.0390	1.0595	0.9659	1.0317
BaO	9.85	4.80	0.0762	0.7850	1.0308	1.0671
FeO	84.99	88.33	0.6311	0.9638	0.9912	1.0000
Total	100.00	100.00				

Element	Net Inte.	Bkgd Inte.	Inte. Error	P/B
CaK	11.00	3.84	5.56	2.86
BaL	6.66	3.94	8.10	1.69
FeK	63.42	5.04	1.91	12.58

Figure 24: Elemental analysis of highly Fe-rich particulate from sample CH99.

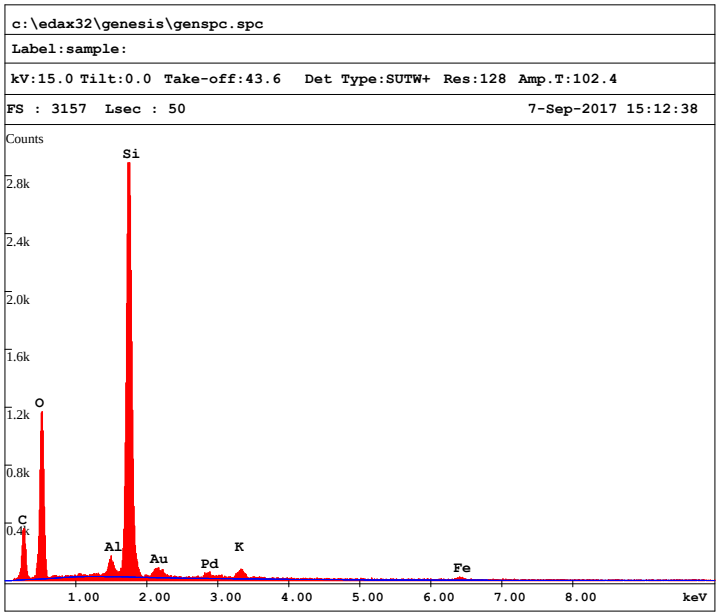

EDAX ZAF Quantification (Standardless)
Element Normalized
SEC Table : Default

Element	Wt %	At %	K-Ratio	Z	A	F
O K	35.31	49.80	0.1449	1.0364	0.3957	1.0006
AlK	2.26	1.89	0.0190	0.9599	0.8535	1.0255
SiK	56.68	45.53	0.5047	0.9847	0.9039	1.0004
K K	2.62	1.51	0.0225	0.9340	0.9165	1.0006
FeK	3.13	1.27	0.0268	0.8594	0.9967	1.0000
Total	100.00	100.00				

Element	Net Inte.	Bkgd Inte.	Inte. Error	P/B
O K	119.00	1.42	1.31	83.80
AlK	17.36	4.48	4.18	3.87
SiK	416.16	4.58	0.70	90.86
K K	11.02	2.86	5.25	3.85
FeK	4.12	0.84	8.27	4.90

Figure 25: Elemental analysis of a particulate low in Fe from sample CH82.

Non-magnetic PM characterization

Most of the particulate matter under the microscope is non-metallic and is composed of alkali and alkaline elements, with some traces of other elements. They are more abundant than the metallic particles.

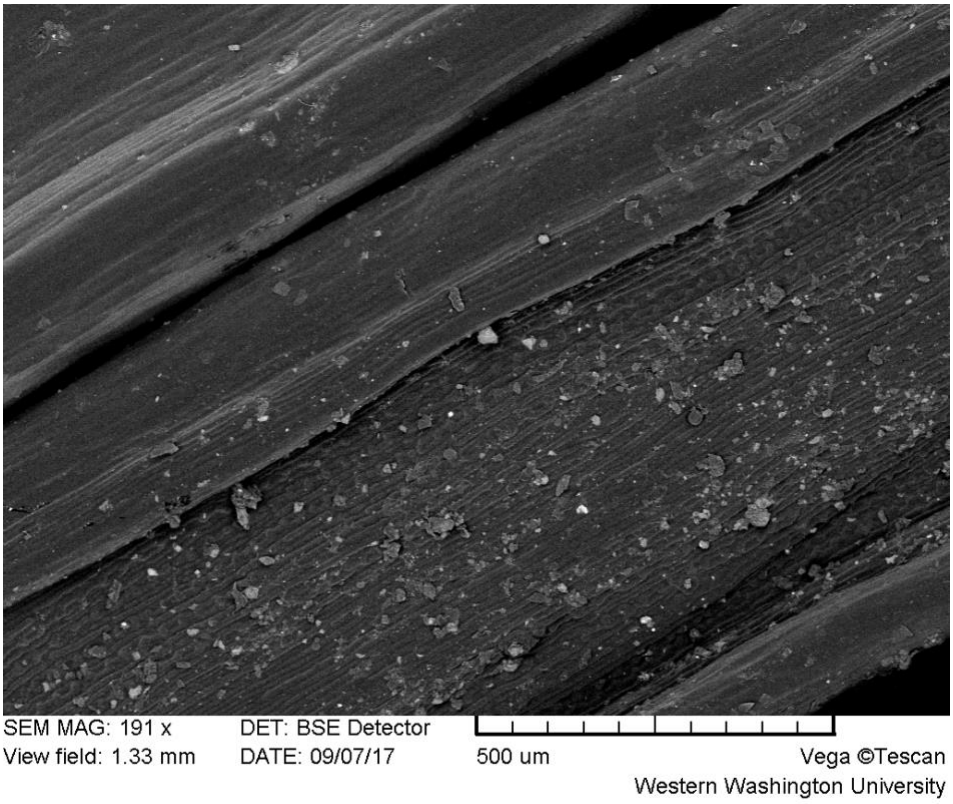

Figure 26: Wide view of all of the particulate matter collected on the surface of a coniferous needle, sample CH99.

Most of the non-metallic particles are ellipsoid-shaped with 20-micron length and 10-micron width gathered in clusters that often have some metallic particles in them (Figure 26).

Source Samples' Characteristics

Diesel Exhaust

Diesel exhaust was collected from a diesel vehicle's exhaust pipe. For the scope of this research, only one sample was used. The hysteresis values (Figure 27) are as follows: Hc = 13.20 mT, Mr = 543.8 $\mu Am^2/kg$, Ms = 1.468 mAm^2/kg, with a susceptibility of $973.7x10^{-9}$ SI. Compared to a study that found average Hc values of 8-11 mT and low susceptibility (Sagnotti et al 2009), our findings are similar. At 300 mT, magnetic moment was 0.478 Am^2 and at 1 T was -0.288 Am^2. SEM imaging exposes Fe-containing particles that are less than 10 μm in diameter

(Figure 28). EDAX analysis shows that most of the exhaust was soot with a small amount of Fe (3-21% Fe in Fe-containing particles) (Figure 29). Other elements in the particles were Nb, S, P, Ca, Si, and Al.

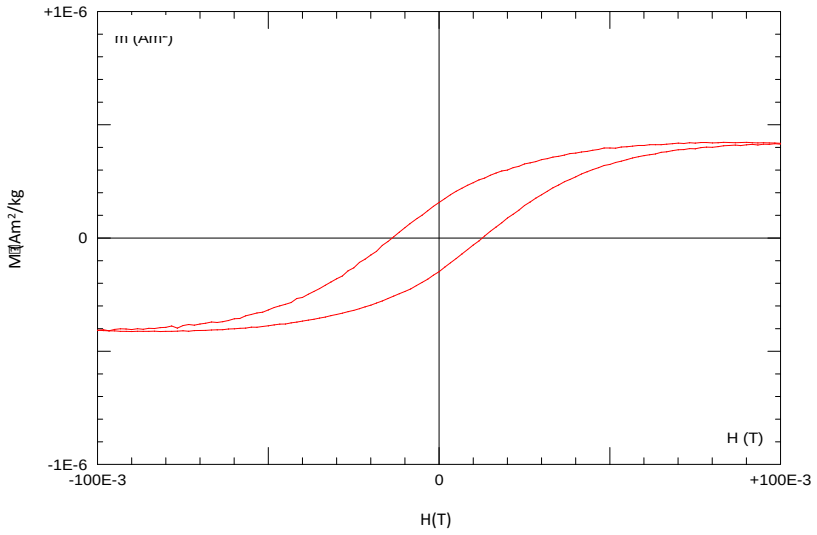

Figure 27: Hysteresis loop of the diesel exhaust.

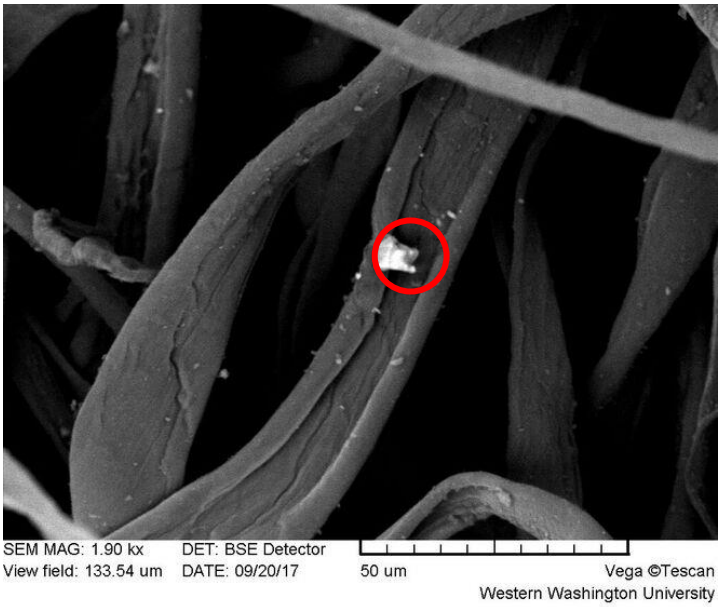

Figure 28: SEM-BSE image of Fe-containing particulate from the diesel exhaust.

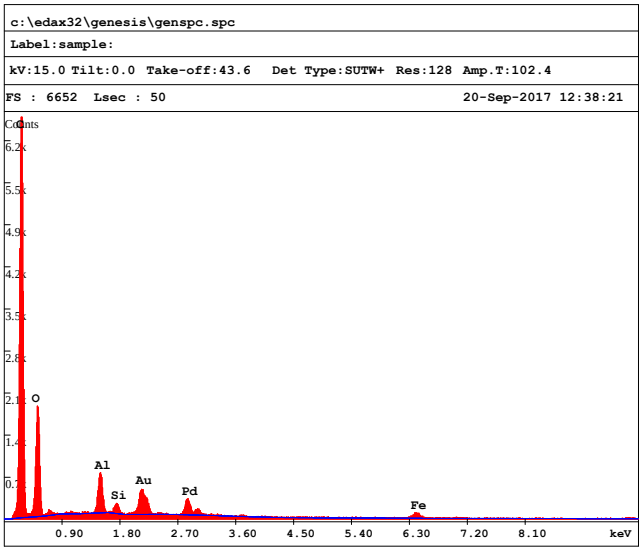

EDAX ZAF Quantification (Standardless)
Element Normalized
SEC Table : Default

Element	Wt %	At %	K-Ratio	Z	A	F
O K	52.35	70.78	0.3433	1.0504	0.6238	1.0008
AlK	20.35	16.31	0.1431	0.9732	0.7216	1.0016
SiK	6.08	4.68	0.0429	0.9988	0.7075	1.0003
FeK	21.23	8.22	0.1858	0.8722	1.0036	1.0000
Total	100.00	100.00				

Element	Net Inte.	Bkgd Inte.	Inte. Error	P/B
O K	186.98	4.74	1.06	39.45
AlK	86.66	16.14	1.78	5.37
SiK	23.48	16.18	4.50	1.45
FeK	18.92	3.64	3.83	5.20

Figure 29: Elemental analysis of the Fe-containing particle in the diesel.

Car Engine Valve

The combustion by-products scraped from a car exhaust manifold valve from a gas-powered engine had the following hysteresis properties (Figure 30): Hc = 6.997 mT, Mr = 1.472 mAm^2/kg, Ms = 16.13 mAm^2/kg and a susceptibility of $6.351x10^{-6}$ SI. At 300 mT, magnetic moment of 0.0536 Am^2 and at 1 T was -0.797 Am^2. SEM imaging reveals Fe-containing particles that are ~15 μm in diameter (Figure 31). EDAX analysis showed little Fe (~3% Fe) in metallic particles (Figure 32). Most of the particulates were made of Nb, Pb, Ca, Si, S, P, Na, and Zn.

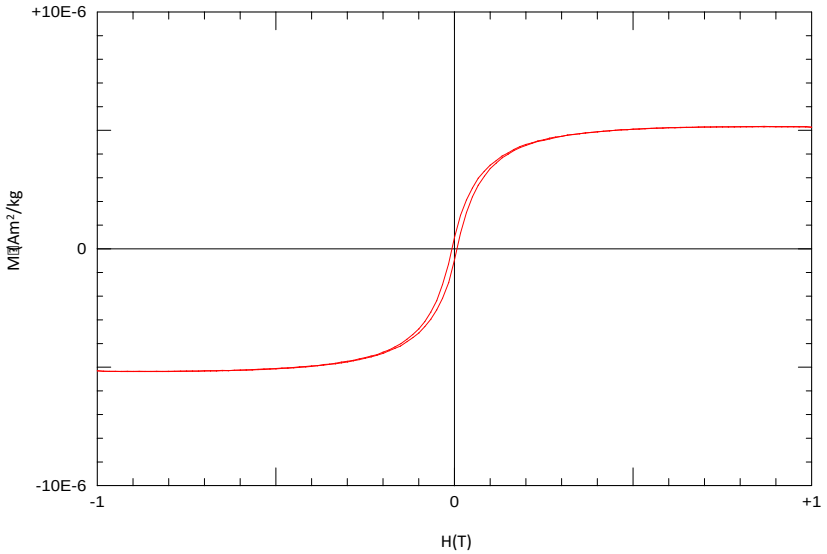

Figure 30: Hysteresis loop of car valve exhaust.

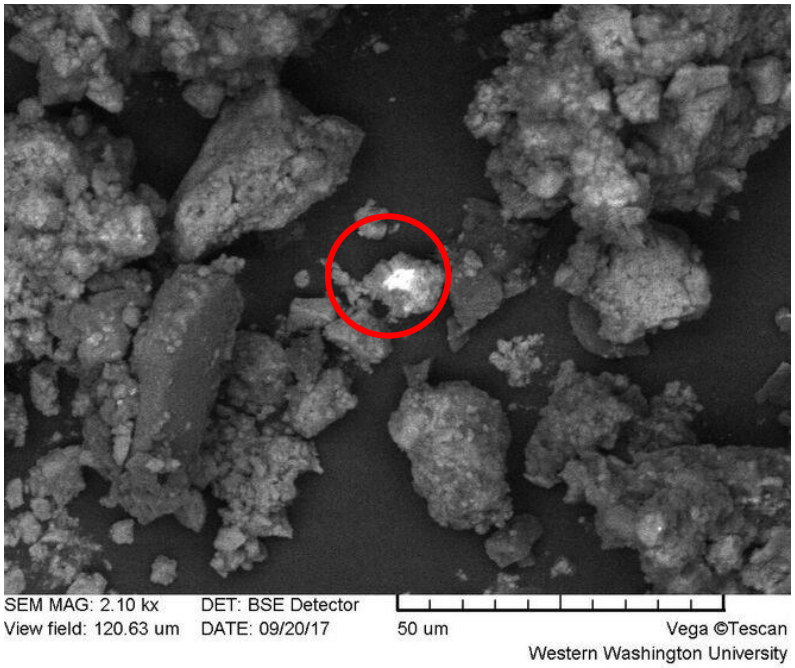

Figure 31: SEM-BSE image of car valve exhaust with Fe-containing particle in the center.

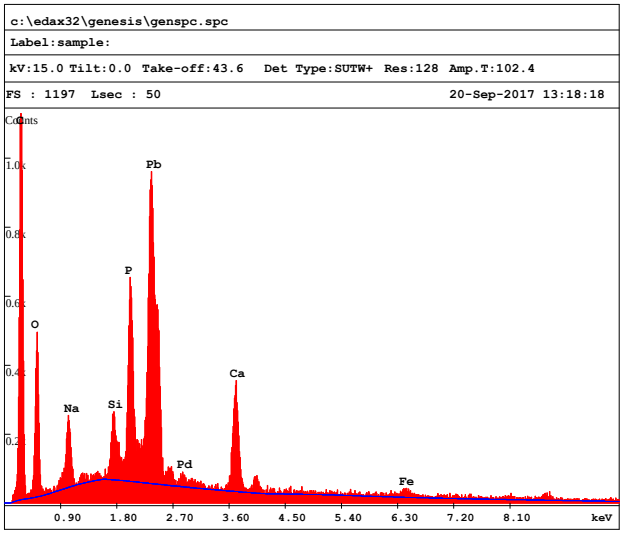

EDAX ZAF Quantification (Standardless)
Element Normalized
SEC Table : Default

Element	Wt %	At %	K-Ratio	Z	A	F
O K	15.27	44.69	0.0443	1.2069	0.2404	1.0002
NaK	3.74	7.61	0.0185	1.1234	0.4401	1.0007
SiK	3.06	5.10	0.0277	1.1950	0.7558	1.0040
P K	9.94	15.04	0.0927	1.1441	0.8137	1.0011
PbM	54.03	12.21	0.4403	0.8023	1.0152	1.0002
CaK	11.02	12.88	0.1033	1.1289	0.8301	1.0004
FeK	2.94	2.46	0.0297	1.0526	0.9586	1.0021
Total	100.00	100.00				

Figure 32: Elemental analysis of car exhaust Fe-containing particle.

Cluster Analysis

Based on dendrogram clustering patterns of variables Hc, Fourier Transforms, and SIRM ratios, there are three distinct clusters that each have a source (car or diesel) associated with them (Figures 33, 35, 37).

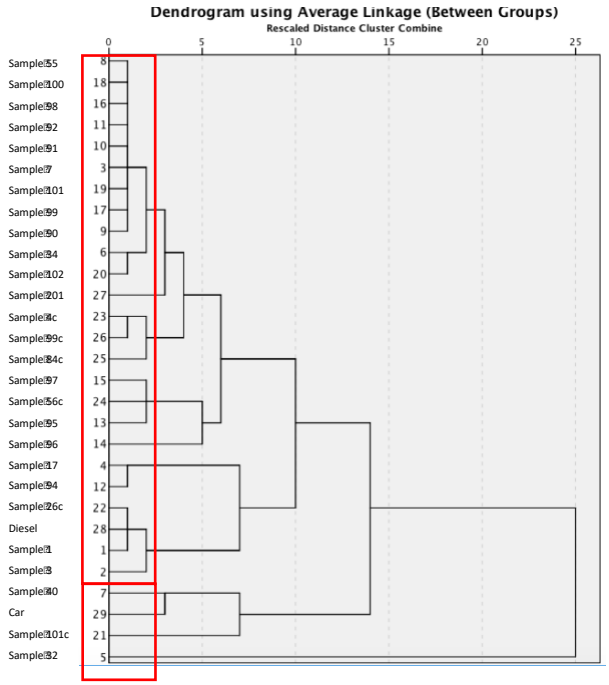

Figure 33: Dendrogram of Hc, SIRM, and Fourier Transforms for all leaf samples and the diesel and gas-fueled car exhaust samples.

Maps were made (Figures 34, 36, 38) to track the locations of the source-types of pollutants by color-coding the samples that were grouped in the same cluster as each of the sources. The maps that depict locations where each of the different source-based data clusters are found can be used to better understand where the particulates measured on samples originated from. Each source sample is in one of the clusters and is color-coded in the map to display the spatial variability of the source of the airborne PM. For example, if a sample is in the same cluster as one of the sources, the dot on the map representing that sample is the same color assigned to the source.

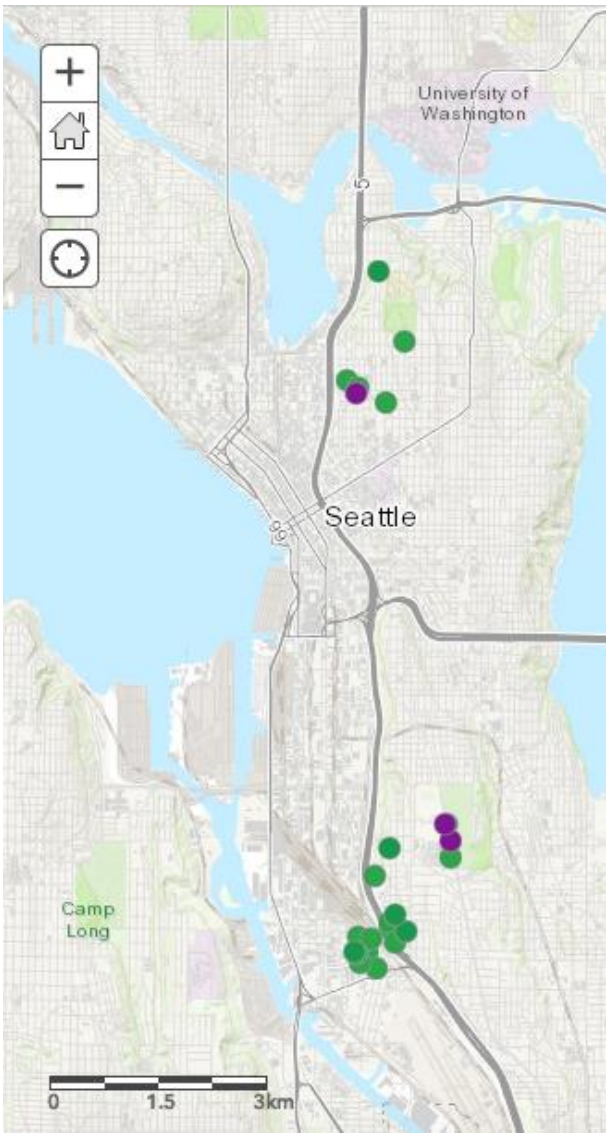

Figure 34: Map of pollutant sources based on Hc, Fourier Transforms, and SIRM ratio values. Green signifies diesel source, purple is car source.

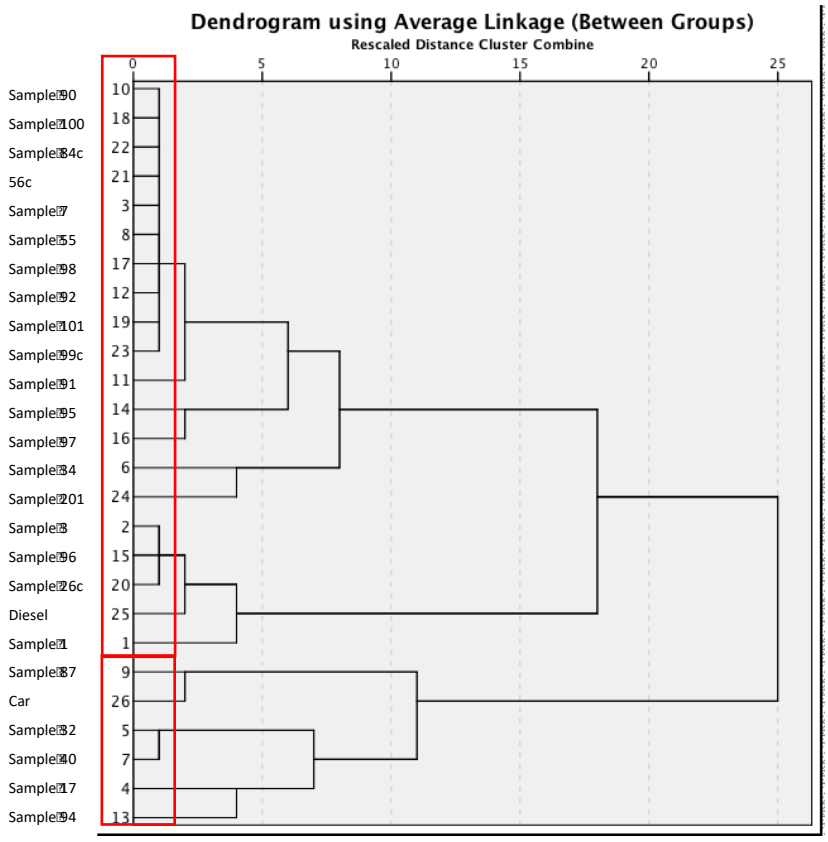

Figure 35: Dendrogram of SIRM, Fourier Transforms, and susceptibility for all leaf samples and the diesel and gas-fueled car exhaust samples.

.

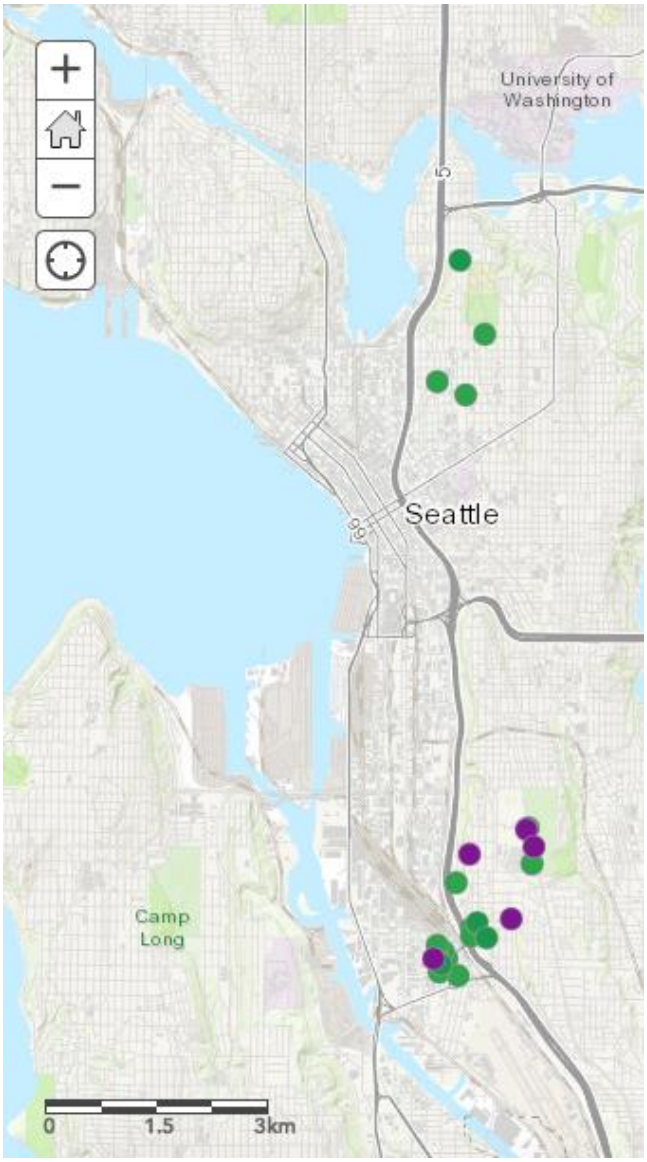

Figure 36: Map of pollution sources based on SIRM, Fourier Transforms, and susceptibility.

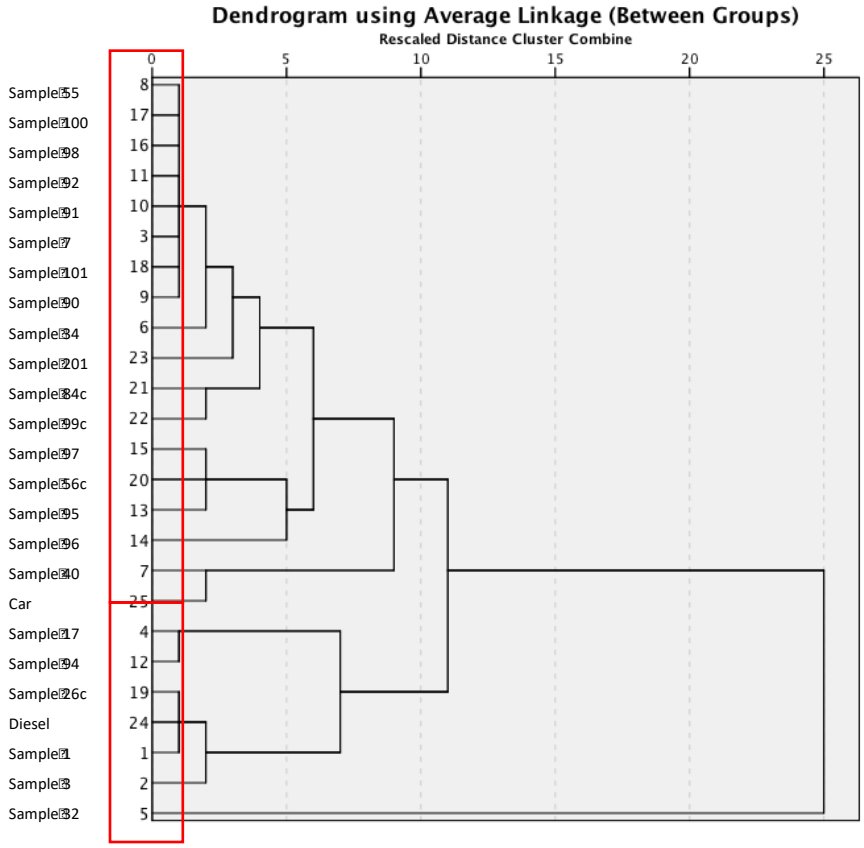

Figure 37: Dendrogram of susceptibility, SIRM, Fourier Transforms, and Hc for all leaf samples and the diesel and gas-fueled car exhaust samples.

.

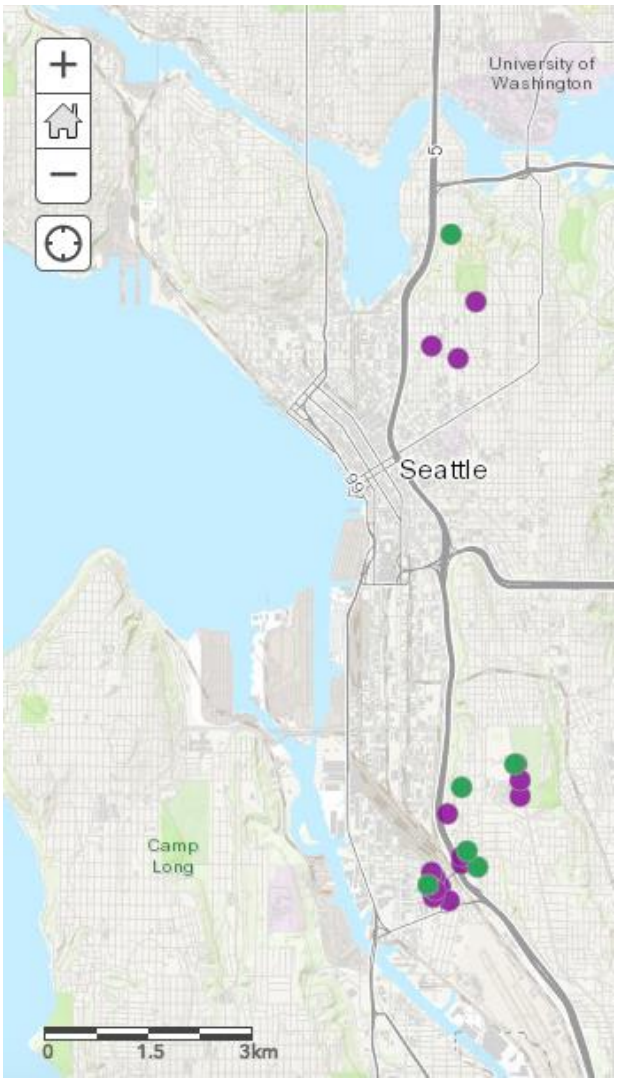

Figure 38: Map of pollutant source based on Fourier Transforms, SIRM, susceptibility, and Hc.

PM Abundance with Distance from Source

In order to better understand spatial correlations of distance from source and PM concentrations, distance from presumed road sources and Ms values were compared. This method provides more information on source identification and spatial variation of exposure levels, as well as inform possible mitigation measures.

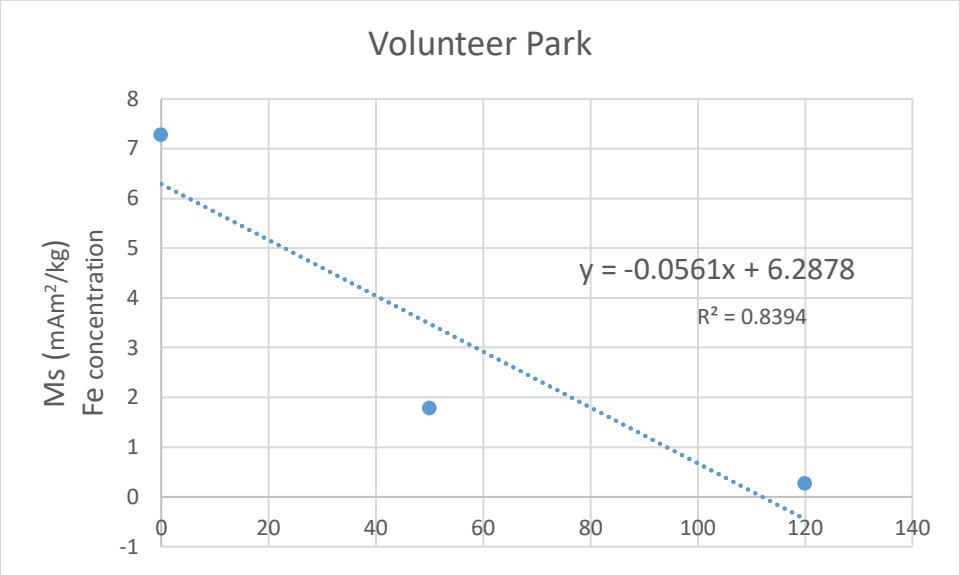

Figure 39: Relationship of distance from source (traffic) and amount of PM in Volunteer Park in Capitol Hill.

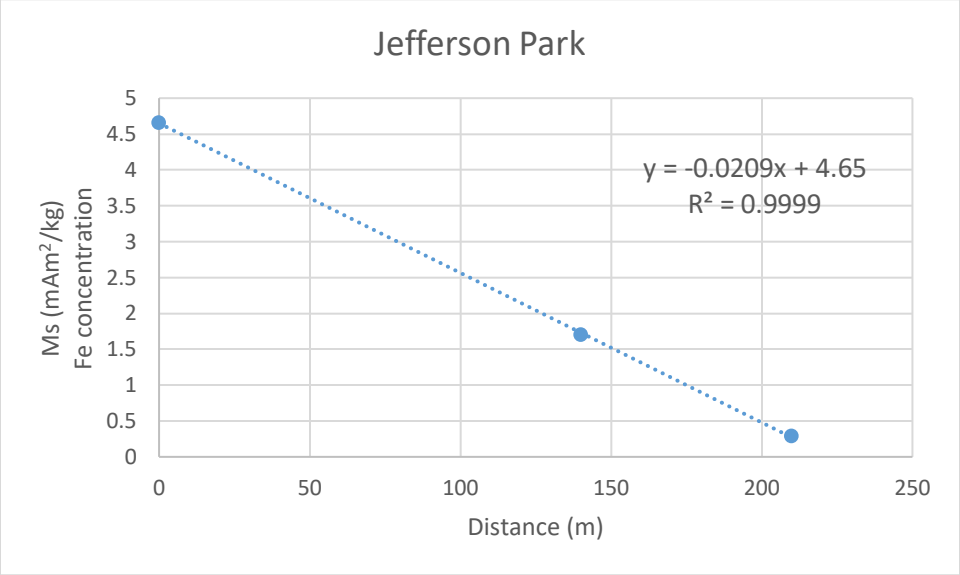

Figure 40: Relationship between distance from source and amount of PM in Jefferson Park and Golf Course in south Seattle next to Beacon Avenue.

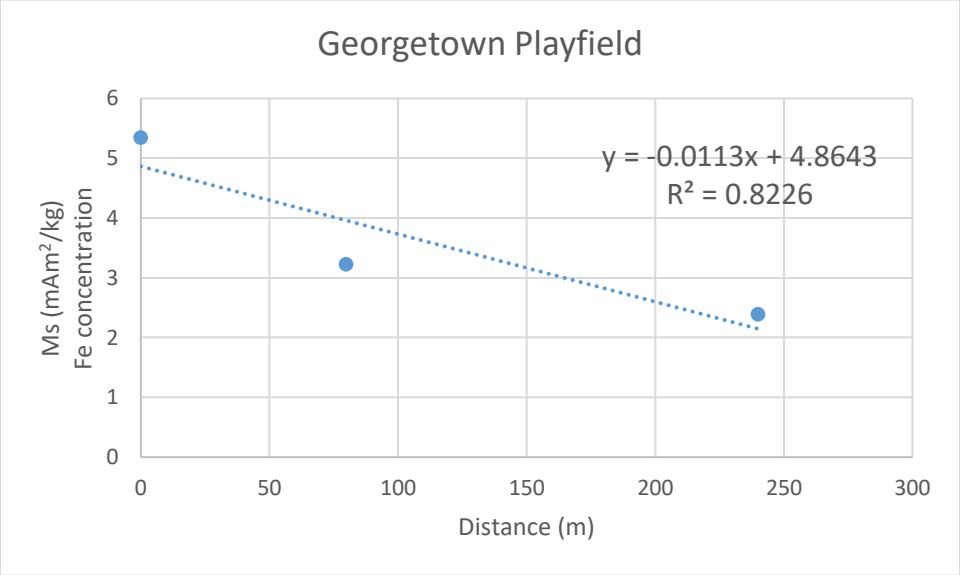

Figure 41: Relationship between distance from source and amount of PM in Georgetown Playfield in south Seattle.

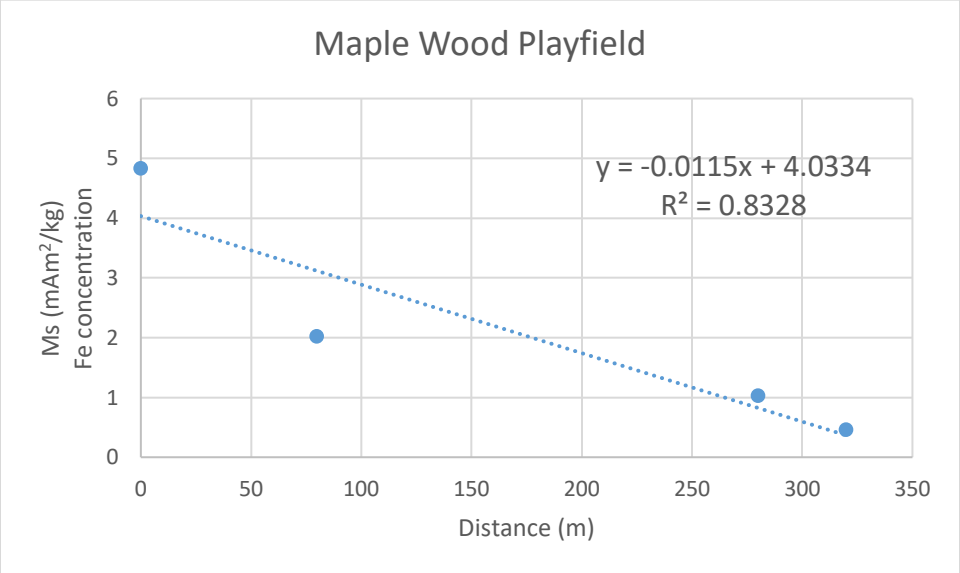

Figure 42: Relationship between distance from source and amount of PM in Maple Wood Playfield near I-5 highway in Duwamish Valley.

In general, as distance from the presumed source increases, the Ms value decreases, which means that the Ms values are recording the PM levels in the air and not other background signals, such as regional PM sources, and makes it less likely that these variations track Fe content of the plant material itself unless the soil has a similar variation. Because the Ms value is recording the PM

levels, we can use the Ms levels to indicate the rate of pollution mitigation with distance from potential source.

As the samples were collected farther into Volunteer Park (Figure 39) from the 15th Ave, the Ms decreased at a rate of ~1 mAm_2/kg per 15 meters. The PM levels would decrease to background levels around 100 meters from the road source.

Samples collected at Jefferson Park and Golf Course (Figure 40), which had a moderate amount of trees, has a decreasing Ms with distance rate of 1 mAm^2/kg per 47.9 meters. The pollution would degrade to zero around 222.9 meters away from the presumed source.

Samples collected at playing fields, Maple Wood and Georgetown (Figures 41, 42), with less and smaller trees than Volunteer Park had a rate of decrease of Ms values of 1 mAm^2/kg per 72.6 meters. The source pollution would reduce to zero at 322 to 372 meters from the source.

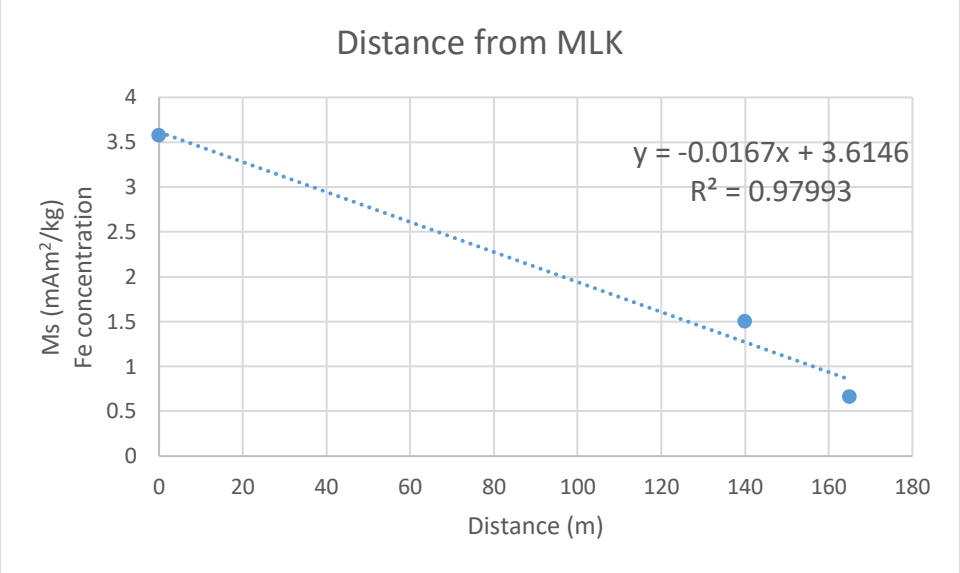

Figure 43:Relationship between distance from source and amount of PM near the high-traffic Martin Luther King Jr Way S in Duwamish Valley.

Distance from presumed source was also compared to Ms values near the high-traffic (Figure 43), low foliaged Martin Luther King Jr Way S. The rate of decrease of Ms values for MLK Jr Way S was 1 mAm^2/kg per 58.56 meters. The source pollution reduced to zero at 213.71 meters

from the street. Like the low foliage Maple Wood and Georgetown playfields, this area also has a lower rate of reduction of pollution as distance from presumed source increases compared to the higher foliage parks.

As the amount of traffic per day on a road increases, the Ms value of the leaves within 100 meters of increases (Figure 44). Although I-5 in Capitol Hill and in Duwamish Valley has about the same amount of traffic per day, the Duwamish Valley average Ms value is higher.

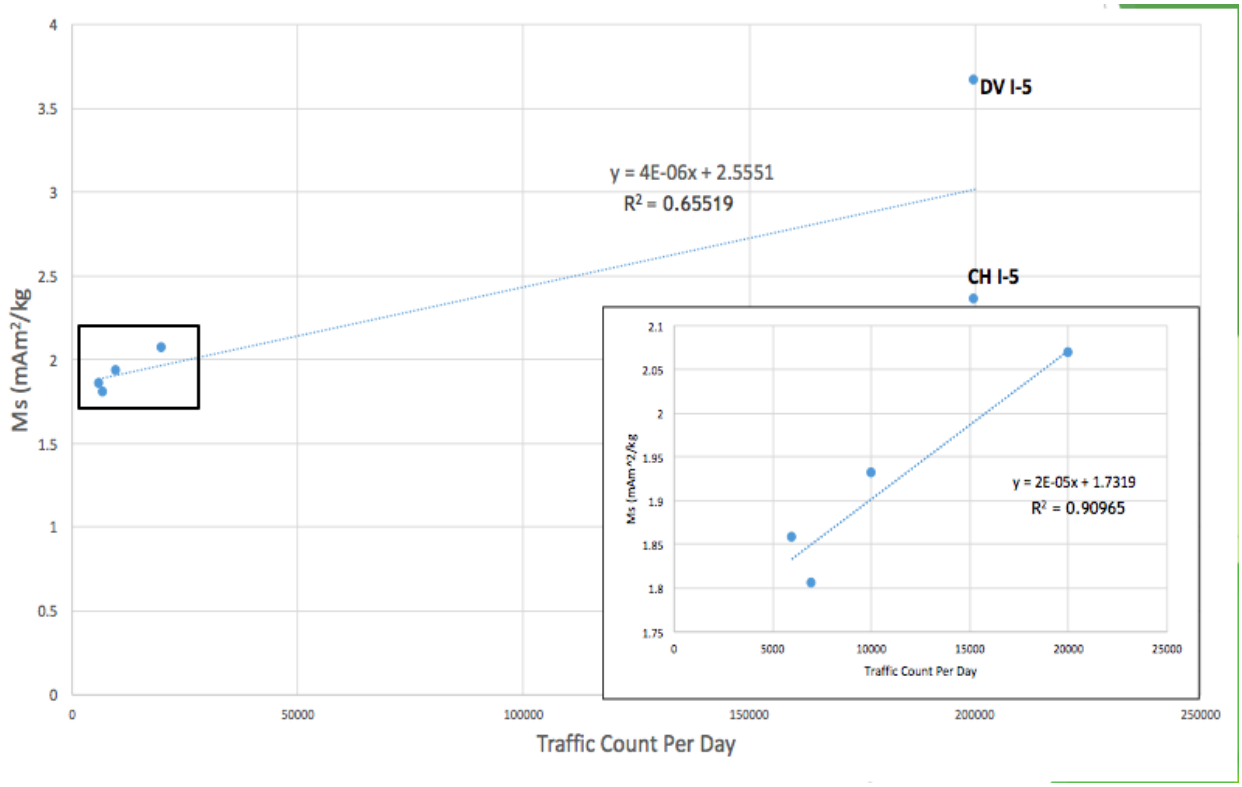

Figure 44: Plot of the average Ms value (average of 3-10 samples per road) of leaves within 100 meters of the highest density traffic roads in Capitol Hill and Duwamish Valley inset with zoomed-in plot of the the lower four most trafficked roads.

The rate that the Ms value increases in relation to an increase in the amount of daily traffic on roads in the Capitol Hill area is lower than the rate of the increase of the Ms values in relation to an increase in traffic density in the southern Seattle location (Figure 45).

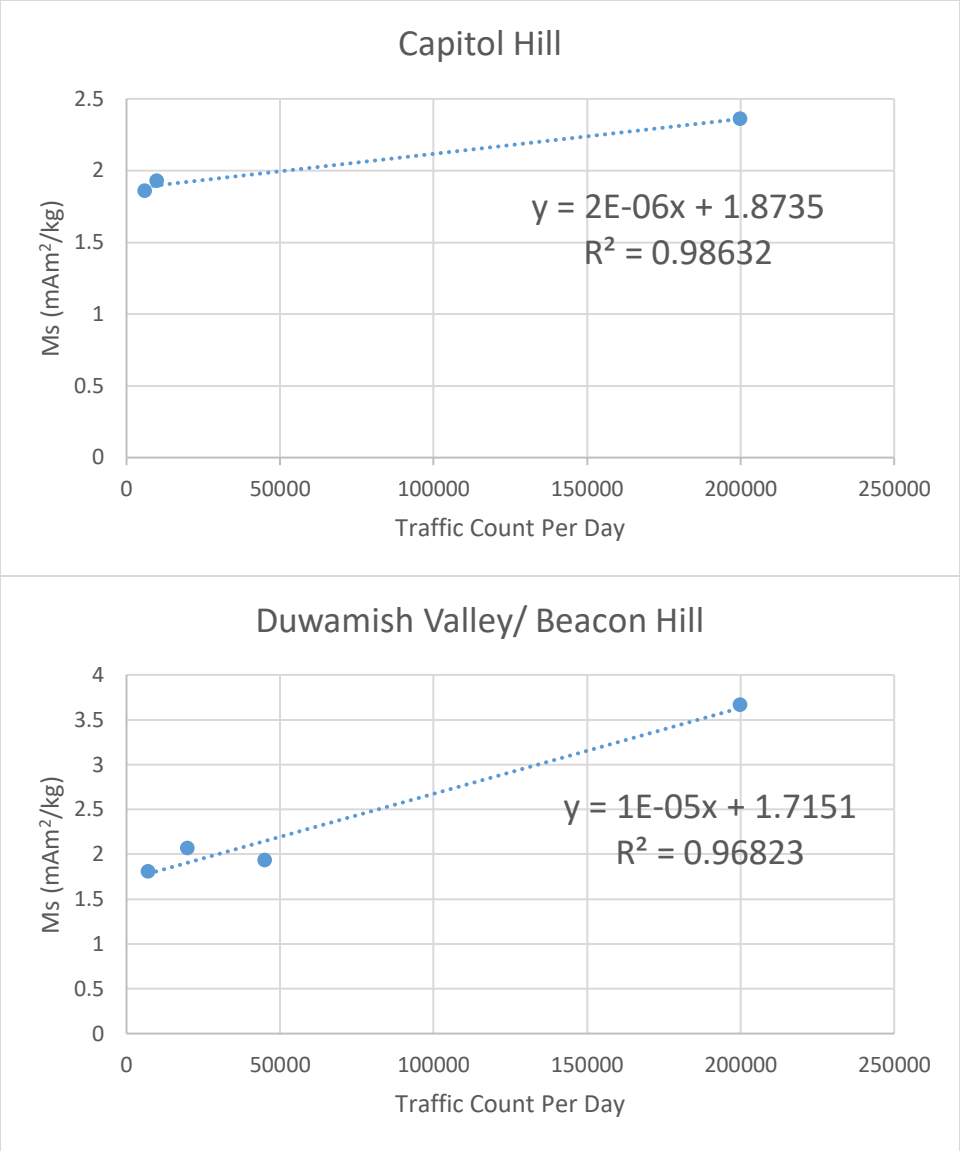

Figure 45: Top: Traffic count per day versus the Ms value on highest traffic roads in Capitol Hill. Bottom: Traffic count per day of highest traffic roads in the southern Seattle site.

Discussion

Magnetic Properties of Deciduous Versus Conifers

The hysteresis properties of the samples in Capitol Hill are more homogenous than those properties in the Duwamish Valley/ South Beacon Hill samples, meaning southern Seattle has more of a mixture of metallic particle size and Fe content. The Ms values for all conifers is slightly more variable than that of the deciduous leaves but not significantly. If the former is the case, then the deciduous results are more reliable for the time of year, while the coniferous

results could be an average of the whole year. If the latter is the case, then more research would have to be done on the morphology of the leaf surface structure and the associated particulates. Susceptibility values are higher on average and more consistent in the Duwamish Valley/ South Beacon Hill area than in Capitol Hill, indicating that the pollution is higher and has a more consistent particulate size. Susceptibility for all conifers non-significantly has a larger range than that of all deciduous leaves. The former would mean that the conifer values reflect the year-round average while the deciduous values relate to the time of their sampling. The latter would mean that there would need to be more research on the morphology of the leaf surfaces. The Ms and susceptibility values significantly correlate, which means that both processes can be used to evaluate the spatial particulate matter variability. This correlation allows for the use of just susceptibility because it takes less time and evaluates all particulate matter, not just metallic. The susceptibility correlates with particulate size and amount of a particulates, while the Ms correlates with the concentration of Fe in a particulate and the amount of Fe-rich particulates.

Few coniferous trees naturally grow next to deciduous trees in the study area, which made it difficult to compare the results of each type of tree with one another. However, there were a few instances where there was a coniferous tree next to a deciduous tree. On Beacon Ave near the Jefferson Park Community Center, the conifer has higher Ms and susceptibility values than the deciduous leaf. Another set of leaves south on Beacon Ave have the same pattern. A deciduous tree near each other on 14th Ave S has higher magnetic values than its coniferous counterpart. Patterns show that comparing deciduous and coniferous leaves can give different results.

Origins of PM – Diesel versus Non-Diesel Emissions

Traffic flow maps from the Seattle Department of Transportation superimposed on the Ms value maps of Capitol Hill and Duwamish Valley/ South Beacon Hill compare the Ms values to the amount of traffic near those values (Figures 46, 47). In a 2009 study, the car brake samples had a Hc value of 4.5-6.5 mT (Sagnotti et al 2009), which is close to our findings.

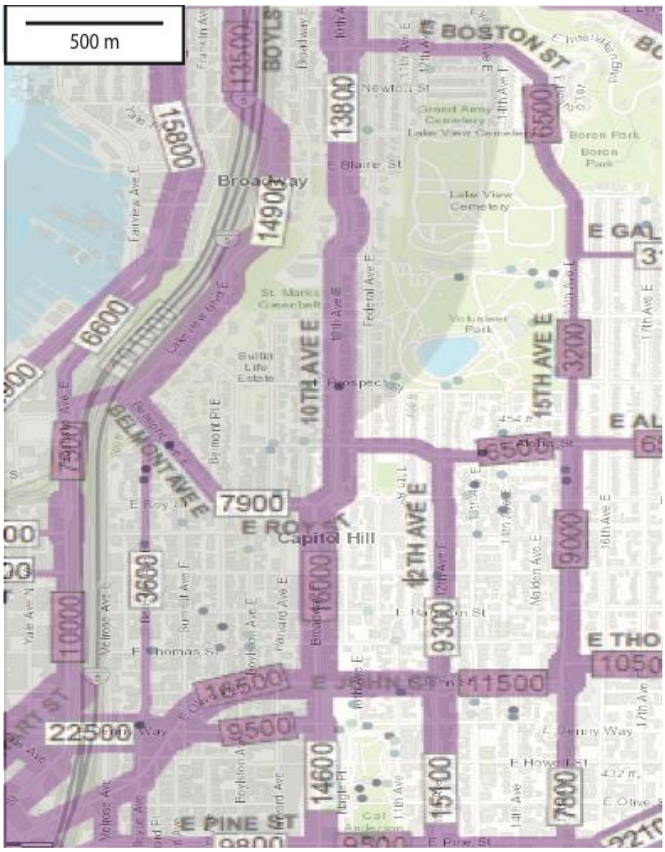

Figure 46: Traffic flow map superimposed with the Ms value map in Capitol Hill. The thicker the purple line is, the more daily traffic volume on that roadway.

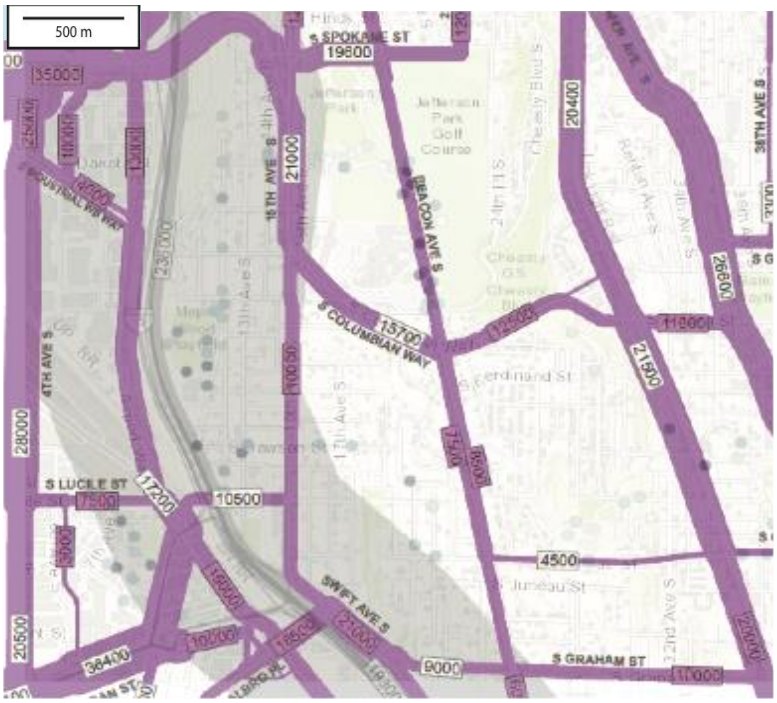

Figure 47: Traffic flow map superimposed on the Ms values map in Duwamish Valley.

In addition, the relationship between Ms value and traffic count per day tells how likely pollution is coming from a diesel or a car source because diesel-powered vehicles produce 100 times more PM than non-diesel vehicles (Maher et al 2008, Sagnotti et al 2009). Because the rate of Ms value/traffic per day is higher in the southern Seattle site than in Capitol Hill, we can infer that there are more diesel emissions in southern Seattle most likely due to the diesel trucks travelling through and there is a diesel-emitting rail yard in the industrial area. Additionally, the Mr values, which determine the amount of $PM_{2.5}$, are higher in the Capitol Hill area, we can infer the pollution source to be gas-powered vehicles because gas-powered vehicles emit more $PM_{2.5}$ than diesel engines by several orders of magnitude (Hoden & Barnard 2004, Maher et al 2008).

Samples collected near the industrial land in southwest Seattle had higher Ms and susceptibility values. To evaluate if the higher rates were due to car emissions diesel emissions on those streets, we compared the hysteresis values of the gasoline-powered car valve exhaust, the diesel exhaust, and the leaf samples were nearest to the sources (Figures 47, 48, 49). The

sample from the diesel exhaust had the higher coercivity compared to that of the car valve dust sample (Figure 48).

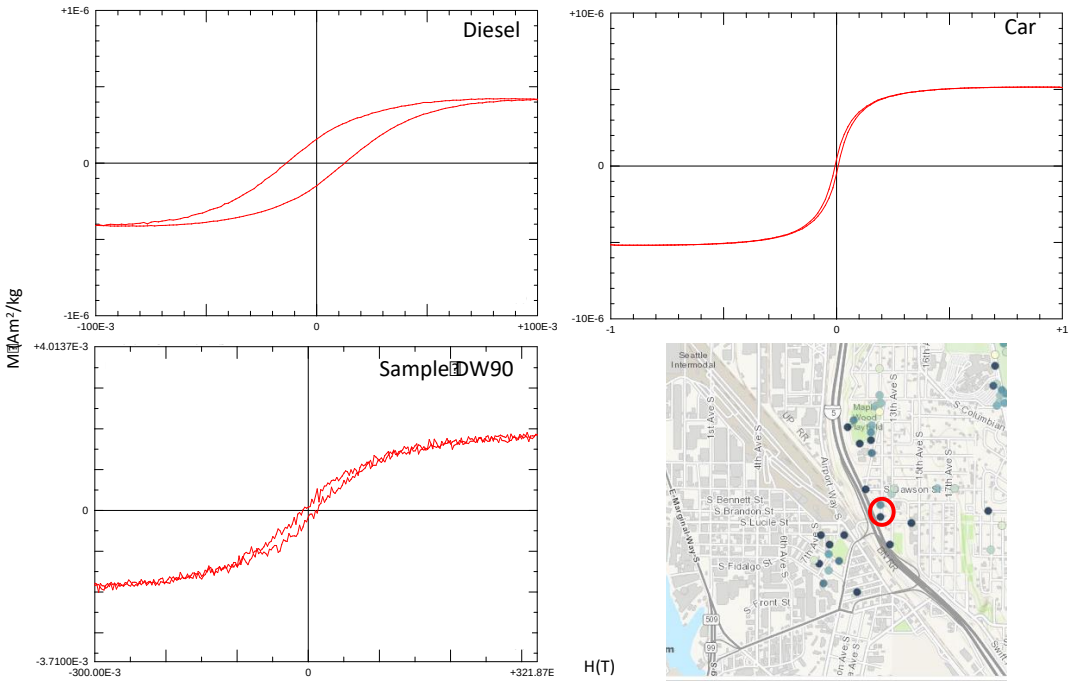

Figure 48: Hysteresis loop of sample east of the industrial area in Duwamish Valley.

The magnetic intensity of sources and leaf samples do not change significantly between a 300 mT magnetic field and a 1 T magnetic field, which means that the samples have primarily magnetite compositions.

In order to gauge the amount of PM, we used the Ms and susceptibility values of the leaf samples, while we used the Hc and IRM values to gauge the different sources. We compare the Ms and susceptibility values to the amount of potential sources such as diesel and gas-powered exhaust. We focused in on the most trafficked roads, including highway I-5, and bus routes that go through Capitol Hill and Duwamish Valley. The most trafficked roads in Seattle generally have about 10, 000 cars per average week day, while I-5 in the Seattle area has about ten times that amount of traffic. The buses repeat the bus routes on average every 20 minutes throughout Seattle.

Although Beacon Ave (See Appendix VI.8) is far away from the industrial land and is surrounded by Jefferson Park, it has high susceptibility and Ms values. Compared to the hysteresis properties of the three sources, most of the samples collected on Beacon Ave are most similar to the car valve, with some more similar to the diesel exhaust. Beacon Ave is one of the streets in the southern Seattle area with the highest daily traffic counts (~10,000 cars/day) and bus route 36 (Figure 49) goes down Beacon Ave.

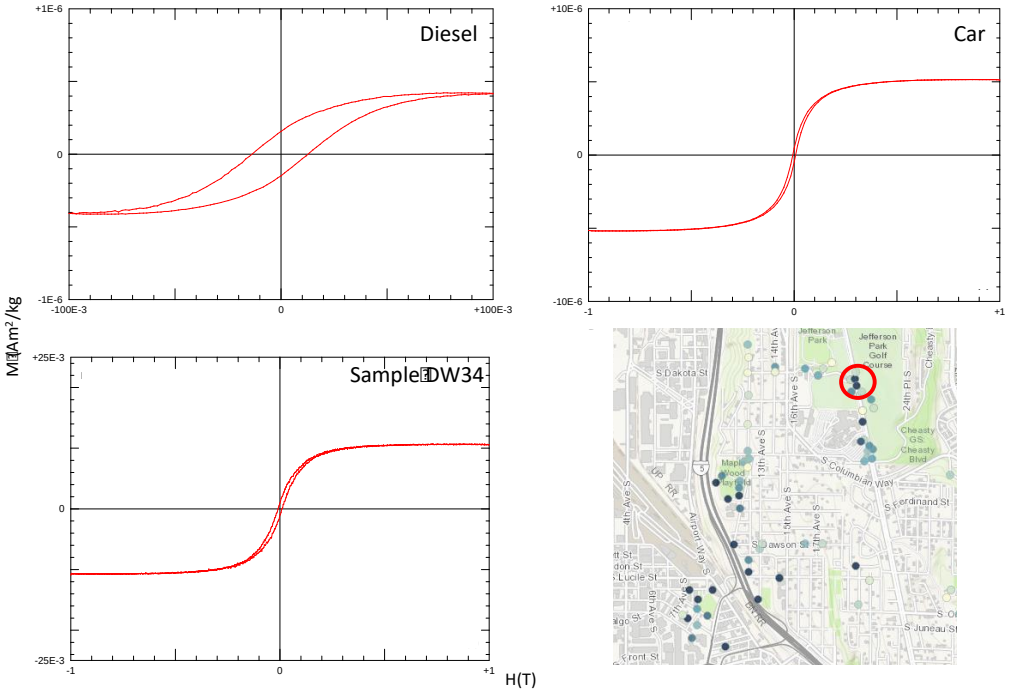

Figure 49: Hysteresis loop of sample from Beacon Avenue in south Seattle.

Similar to Beacon Ave, Martin Luther King Jr Way S is far from the industrial area but has high magnetic values. It has most similar hysteresis properties to the car exhaust, which aligns with the high rates of traffic (~50,000 cars/day) and is on bus route 106 (See Appendix VI.9).

In Capitol Hill, the samples with the highest magnetic values correspond with the streets with the highest traffic volumes (E John St, 10th Ave E, 15th Ave E, and Belmont Ave E). In

addition to the high traffic, E John St and 15th Ave have bus routes, with E John St having Routes 8, 10, 43 and 15th Ave having Route 10 (See Appendix VI.10).

Parks

Two parks in Capitol Hill were sampled, Volunteer Park (~1.6 km^2) and Cal Anderson Park (~0.3 km^2). Samples in Volunteer Park on average had lower magnetic values than those in Cal Anderson Park. Because Volunteer Park has more greenery than Cal Anderson Park, there is less PM in the air. Additionally, Cal Anderson Park is just south of E John St, which is heavily trafficked and has multiple bus routes. Most of the samples in Cal Anderson Park have hysteresis similar to the diesel exhaust, while most samples in Volunteer Park have car valve magnetic signatures (Figure 50).

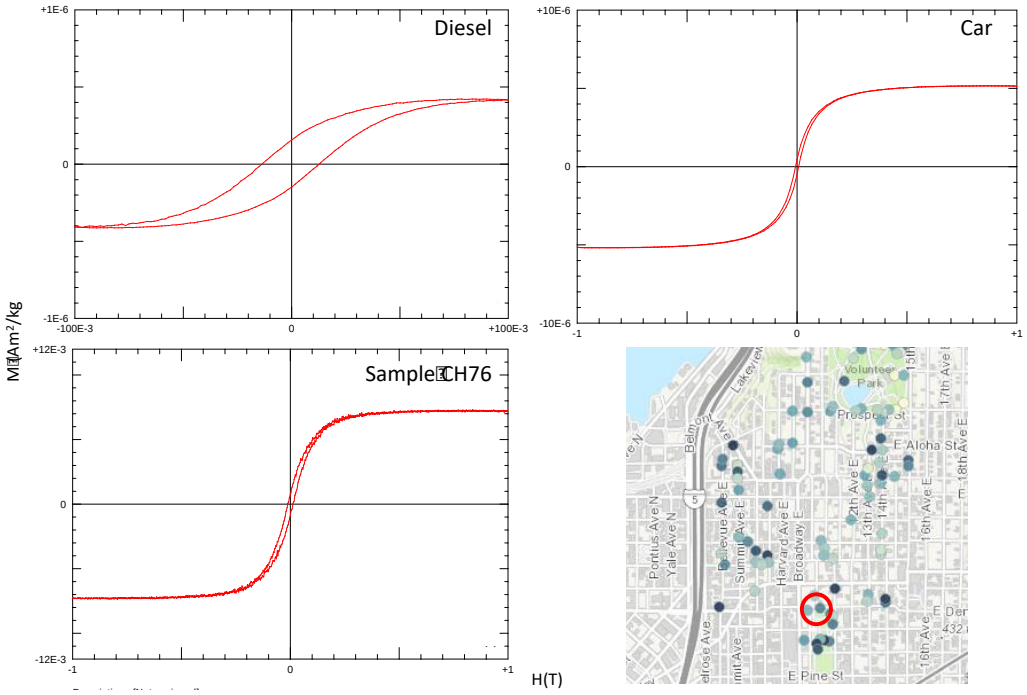

Figure 50: Hysteresis loop of sample collected in Cal Anderson Park in Capitol Hill.

In the Maple Wood Playfield just east of I-5, the samples closer to I-5 have hysteresis signatures comparable to the car valve and diesel exhaust. The samples farther into the park away from the highway have lower magnetic values, which suggests that the greenery decreases the amount of

PM in the air. Maple Wood Playfield, which is the closest sampled park to I-5 has higher Ms values than the other parks, which suggests that the I-5 traffic exhaust contributes to the Maple Wood Playfield PM. However, the susceptibility values for Maple Wood Playfield are on average similar to the other parks sampled. There was no pattern correlating the distance from I-5 to the amount of PM in the parks, which means I-5 pollution is not the main source of pollution for these parks.

Based on cluster analysis using variables that describe composition and the particle morphology of the sources of the PM, such as Hc, Fourier transforms of hysteresis loop shape, susceptibility, and SIRM, small spatial variations emerge within the overall patterns described above. Most of the leaf samples that have magnetic properties that are consistent with the diesel-source cluster do occur in bus routed streets, and most of the leaf samples that have magnetic properties that are consistent with the gas-powered cluster are found in high trafficked areas. Based on the cluster analysis source maps, both Capitol Hill and Duwamish Valley/ South Beacon Hill have a mixture of diesel and gas-fueled emissions. Another notable pattern is that the Beacon Avenue PM comes from all three sources, while the other bus route streets have mostly traffic-derived signatures.

Conclusions

Overall, we found that leaves can be used as dependable biomonitors of airborne PM, as other studies in the past have concluded. Further, we have found that Ms and susceptibility values both have similar results, which means that susceptibility is a reliable, quick, and easy method for characterizing PM, including non-metallic PM. SIRM and Hc are useful for characterizing the composition and concentration of metallic particles on leaf surfaces. Furthermore, Ms values correlate to the amount of PM as distance increases from the presumed

source, which provides a glance at possible mitigation techniques, such as adding more foliage closer to roadsides. Lastly, coniferous and deciduous leaves have similar magnetic properties, which means that either or both can be used as biomonitors. Although the coniferous leaves stay throughout the year while the deciduous leaves are seasonal, the data suggest that each leaf type has similar magnetic readings, which means that future studies can use either or both types of leaves.

Based on magnetic readings, chemical analysis, and spatial analysis, this study corroborates past studies that have stated that Seattle has more pollution issues in the southern region (Abel and White 2011, Abel and White 2014, which then contributes to worse health effects, such as respiratory and cardiovascular issues (Shwartz et al 1993, Gould & Cummings 2013). As a part of this study, community science played a role in assessing the air pollution distribution in southern Seattle. The samples that the high school students collected augmented the study while additionally providing a gateway for students and other community members to participate in the science happening in their backyard. There were some setbacks with community science – some of the samples collected were either not the intended type of leaf, were mislabeled, or did not have coordinates linked to them. Future studies using community science can improve our model in order to increase sample-collecting success.

Though the leaf magnetic particulates had varying sizes, most were around 10 microns in diameter, which is detrimental to health. The magnetic particles in the diesel and car valve were consistently small (3-7 microns). Magnetic particulates on leaves were around 80% Fe, while magnetic particles in diesel (~3-21%) and car valve (~3). Because the leaves had variable-sized particulates, they must be a mixture of the sampled sources. The magnetic particles on the leaves

had higher concentrations of Fe because they were an aggregate of multiple Fe-containing sub-particles from the sources.

Traffic sources are localized to the road sides and extend about 100-370 meters into parks depending on the amount of foliage. Samples collected long bus routes have more diesel signatures, while non-bus route roads have car signatures. Near high-traffic roads, PM begins to decrease within ten meters from the road and decreases more rapidly with more foliage. Capitol Hill's PM is a mixture of car traffic and bus route traffic based on the high Mr values and some of the Ms values near bus routes. The parks in both areas help reduce the amount of PM, but the more abundant and larger trees seem to allow for more pollution mitigation. The PM levels are higher in the southern Seattle site than in Capitol Hill based on the higher counts of high Ms and susceptibility values. Most likely the higher amount of airborne PM pollution in southern Seattle is due to the industrial landscape that has more diesel traffic, which produces more PM than a non-diesel source by orders of magnitudes.

Biomonitoring is a beneficial and low-cost process that empowers community scientists and determines sources more precisely than current air monitoring stations. Because biomonitoring occurs at ground level and near roads, we can assess which streets and industrials areas have higher amounts of PM instead of relying on air monitors that report the pollution of a larger area. Biomonitoring allows for the characterization of distinct particles in order to assess the composition of these particles to determine source and how potentially dangerous they are to human health. Biomonitoring in addition to modern air monitors would improve the air monitoring system of Seattle. Because Ms and susceptibility values significantly correlate, susceptibility can be used instead of hysteresis because it is more time efficient and reflects all PM rather than just magnetic PM.

Future projects would augment the findings of this research. For example, a more extensive data set of the magnetic properties and compositions of the pollution sources could be collected and refined so that it can be compared to those properties of the collected leaves. Soil samples or other leaf-type samples could be collected near the industrial site so that more information could be known about the industrial area. More spatial coverage of the sample sites could be accomplished if more leaf types and soils were incorporated in the study. Lastly, more sample sites throughout Seattle would improve the overall spatial variation mapping of biomonitored air pollution in Seattle.

References

Abel, T.D. and White, J., 2015. Gentrified sustainability: inequitable development and Seattle's skewed riskscape. Interdisciplinary Environmental Review, 16(2-4), pp. 124-157.

Abel, T.D. and White, J., 2011. Skewed riskscapes and gentrified inequities: environmental exposure disparities in Seattle, Washington. American journal of public health, 101(S1), pp.S246-S254.

Abel, Troy, Jonah White, and Stacy Clauson. "Risky Business: Sustainability and Industrial Land Use across Seattle's Gentrifying Riskscape." *Sustainability* 7, no. 12 (2015): 15718-5753.

Ancuceanu, Robert, Mihaela Dinu, Marilena Hovaneţ, Adriana Anghel, Carmen Popescu, and Simona Negreş. "A Survey of Plant Iron Content—A Semi-Systematic Review." *Nutrients*7, no. 12 (2015): 10320-0351.

Bernard, Sara. "Largest Green Wall in Seattle Takes Shape in Georgetown." Seattle Weekly. October 26, 2016. Accessed May 16, 2017. http://www.seattleweekly.com/news/largest-green-wall-in-seattle-takes-shape-in-georgetown/.

Brook, R. D., S. Rajagopalan, C. A. Pope, J. R. Brook, A. Bhatnagar, A. V. Diez-Roux, F. Holguin, Y. Hong, R. V. Luepker, M. A. Mittleman, A. Peters, D. Siscovick, S. C. Smith, L. Whitsel, and J. D. Kaufman. "Particulate Matter Air Pollution and Cardiovascular Disease: An Update to the Scientific Statement From the American Heart Association." *Circulation*121, no. 21 (2010): 2331-378.

Cakmak, Sabit, Robert Dales, Lisa Marie Kauri, Mamun Mahmud, Keith Van Ryswyk, Jennifer Vanos, Ling Liu, Premkumari Kumarathasan, Errol Thomson, Renaud Vincent, and Scott Weichenthal. "Metal Composition of Fine Particulate Air Pollution and Acute Changes in Cardiorespiratory Physiology." *Environmental Pollution*189 (2014): 208-14.

Curtis, Luke, William Rea, Patricia Smith-Willis, Ervin Fenyves, and Yaqin Pan. "Adverse Health Effects of Outdoor Air Pollutants." *Environment International* 32, no. 6 (August 2006): 815–30.

Donovan, Geoffrey H., Sarah E. Jovan, Demetrios Gatziolis, Igor Burstyn, Yvonne L. Michael, Michael C. Amacher, and Vicente J. Monleon. "Using an epiphytic moss to identify previously unknown sources of atmospheric cadmium pollution." Science of The Total Environment 559 (2016): 84-93.

Dunlop, David J., and Özden Özdemir. *Rock Magnetism Fundamentals and Frontiers*. Cambridge: Cambridge Univ. Press, 1997.

EPA. Environmental Protection Agency. 2016. "Particulate Matter (PM) Pollution." Web.

Environmental Science Associates, “Air Quality.” *Air Quality | ESA*, www.esassoc.com/services/air-quality.

Environmental Protection Agency (EPA). 2001. National Priorities List for Uncontrolled Hazardous Waste Sites. *Federal Register* 66(178): 47583-47590.

Gatziolis, Demetrios, Jovan, Sarah, Donovan, Geoffrey, Amacher, Michael, and Monleon, Vicente. “Elemental Atmospheric Pollution Assessment Via Moss-Based Measurements in Portland, Oregon.” *United States Department of Agriculture.* June 2016.

Gould, Linn, and BJ Cummings. 2013. “Duwamish Valley Cumulative Health Impacts Analysis: Seattle, Washington.” Just Health Action and Duwamish River Cleanup Coalition/Technical Advisory Group.

Hansard, R., Maher, B.A., Kinnersley, R., “Biomagnetic monitoring of industryderived particulate pollution.” *Environmental Pollution* 159, (2011): 1673-1681.

Hodan, William, and William Barnard. "Evaluating the Contribution of PM2.5 Precursor Gases and Re-entrained Road Emissions to Mobile Source PM2.5 Particulate Matter Emissions" EPA. 2004.

Hofman, Jelle, Wouter Lefebvre, Stijn Janssen, Ruben Nackaerts, Siegmund Nuyts, Lars Mattheyses, and Roeland Samson. “Increasing the Spatial Resolution of Air Quality Assessments in Urban Areas: A Comparison of Biomagnetic Monitoring and Urban Scale Modelling.” *Atmospheric Environment* 92 (August 2014): 130–40.

Kardel, F., K. Wuyts, M. Babanezhad, U.W.A. Vitharana, T. Wuytack, G. Potters, and R. Samson. “Assessing Urban Habitat Quality Based on Specific Leaf Area and Stomatal Characteristics of Plantago Lanceolata L.” *Environmental Pollution* 158, no. 3 (March 2010): 788–94.

Kardel, F., K. Wuyts, B.A. Maher, R. Hansard, and R. Samson. “Leaf Saturation Isothermal Remanent Magnetization (SIRM) as a Proxy for Particulate Matter Monitoring: Inter-Species Differences and in-Season Variation.” *Atmospheric Environment* 45, no. 29 (September 2011): 5164–71.

Kaur, S., M. J. Nieuwenhuijsen, and R. N. Colvile. 2005. Pedestrian exposure to air pollution along a major road in Central London, UK. *Atmospheric Environment* 39(38): 7307-7320.

Kessler, Rebecca. 2013. “Green Walls Could Cut Street-Canyon Air Pollution.” *Environmental Health Perspectives* 121(1): A14–A14 (April 27, 2016).

Knibbs, Luke D., Tom Cole-Hunter, and Lidia Morawska. 2011. A review of commuter exposure to ultrafine particles and its health effects. *Atmospheric Environment* 45(16): 2611-2622.

Koenig, Jane Q. "Health Effects of Indoor Air Pollution." *Health Effects of Ambient Air Pollution*, 2000, 195-212.

Kumar, Prashant, Lidia Morawska, Claudio Martani, George Biskos, Marina Neophytou, Silvana Di Sabatino, Margaret Bell, Leslie Norford, and Rex Britter. 2015. The Rise of Low-Cost Sensing for Managing Air Pollution in Cities. *Environment International* 75: 199–205.

Larson, Selena. "Google Uses Street View Cars to Collect Pollution Data." CNNMoney. Accessed April 25, 2018. http://money.cnn.com/2017/06/05/technology/google-street-view-edf-air-quality-oakland/index.html.

Lehndorff, E., and L. Schwark. "Biomonitoring of air quality in the Cologne Conurbation using pine needles as a passive sampler—Part II: polycyclic aromatic hydrocarbons (PAH)." Atmospheric Environment 38, no. 23 (2004): 3793-808.

Lin, Mei, Yue Chen, Richard T. Burnett, Paul J. Villeneuve, and Daniel Krewski. "The Influence of Ambient Coarse Particulate Matter on Asthma Hospitalization in Children: Case-Crossover and Time-Series Analyses." *Environmental Health Perspectives*110, no. 6 (2002): 575-81.

Madejon, P., T. Maranon, and J. Mmurillo. "Biomonitoring of Trace Elements in the Leaves and Fruits of Wild Olive and Holm Oak Trees." *Science of The Total Environment* 355, no. 1-3 (2006): 187-203.

Maher, B.A., C. Moore, and J. Matzka. “Spatial Variation in Vehicle-Derived Metal Pollution Identified by Magnetic and Elemental Analysis of Roadside Tree Leaves.” *Atmospheric Environment* 42, no. 2 (January 2008): 364–73.

Maher, Barbara A., Imad AM Ahmed, Brian Davison, Vassil Karloukovski, and Robert Clarke. “Impact of Roadside Tree Lines on Indoor Concentrations of Traffic-Derived Particulate Matter.” *Environmental Science & Technology* 47, no. 23 (2013): 13737–13744.

Matzka, J, and B.A Maher. “Magnetic Biomonitoring of Roadside Tree Leaves: Identification of Spatial and Temporal Variations in Vehicle-Derived Particulates.” *Atmospheric Environment* 33, no. 28 (December 1999): 4565–69.

Mitchell, R., B.A. Maher, and R. Kinnersley. “Rates of Particulate Pollution Deposition onto Leaf Surfaces: Temporal and Inter-Species Magnetic Analyses.” *Environmental Pollution* 158, no. 5 (May 2010): 1472–78.

National Science and Technology Council (NSTC). 2013. Air Quality Observation Systems in the United States. Committee on Environment, Natural Resources, and Sustainability. https://www.whitehouse.gov/sites/default/files/microsites/ostp/NSTC/air_quality_obs_2013.pdf (Accessed April 22, 2015).

“Northwest Clean Air Agency.” *North West Clean Air*, nwcleanairwa.gov/air-quality-center/.

Pattinson, Woodrow, Ian Longley, and Simon Kingham. 2014. Using mobile monitoring to visualise diurnal variation of traffic pollutants across two near-highway neighbourhoods. *Atmospheric Environment* 94: 782-792.

Park, Tania Tam et. al. 2014. *High Impacted Communities.* Seattle, WA: *Puget Sound Clean Air Agency.*

Puget Sound Clean Air Agency (PSCAA). 2016. *Air Quality in the Duwamish Valley 2016 Overview.* Seattle, WA.

Rai, P.K., Chutia, B.M. and Patil, S.K., 2014. Monitoring of spatial variations of particulate matter (PM) pollution through bio-magnetic aspects of roadside plant leaves in an Indo-Burma hot spot region. *Urban Forestry & Urban Greening*, 13(4): 761-770.

Ristovski, Zoran D., Branka Miljevic, Nicholas C. Surawski, Lidia Morawska, Kwun M. Fong, Felicia Goh, and Ian A. Yang. "Respiratory health effects of diesel particulate matter." Respirology 17, no. 2 (2012): 201-12.

Sagnotti, Leonardo et al. 2009 "Compositional, Morphological, and Hysteresis Characterization of Magnetic Airborne Particulate Matter in Rome, Italy." *Geochemistry Geophysics* Geosystems 10.8.

Sant'Ovaia, Helena, Maria João Lacerda, and Celeste Gomes. 2012. Particle pollution–An environmental magnetism study using biocollectors located in northern Portugal. Atmospheric environment 61: 340-349.

Schwartz, Joel, et al. 1993. "Particulate Air Pollution and Hospital Emergency Room Visits for Asthma in Seattle", *American Review of Respiratory Disease* 147 (4): 826-831.

Schulte, Jill K, Assaf P Oron, Joel Kaufman, Julie Fox, Sheryl Magzamen, Nancy Beaudet, and Timothy Larson. 2013. *Diesel Exhaust Exposure in the Duwamish Study (DEEDS):* Technical Report. Seattle, WA: University of Washington School of Public Health, Department of Environmental Health Sciences.

Schulte, J.K., Fox, J.R., Oron, A.P., Larson, T.V., Simpson, C.D., Paulsen, M., Beaudet, N., Kaufman, J.D. and Magzamen, S., 2015. Neighborhood-scale spatial models of diesel exhaust concentration profile using 1-nitropyrene and other nitroarenes. Environmental science & technology, 49(22), pp.13422-13430.

"Seattle Department of Transportation 2017 TRAFFIC REPORT." Seattle Department of Transportation. Accessed April 25, 2018. www.seattle.gov/Documents/Departments/SDOT/About/DocumentLibrary/Reports/2017_Traffic_Report.pdf&p=DevEx.LB.1,5065.1.

Snyder, Emily G, et al. 2013. “The Changing Paradigm of Air Pollution Monitoring.” Environmental Science & Technology 47 (20).

Strum, M. and Scheffe, R., 2016. National review of ambient air toxics observations. *Journal of the Air & Waste Management Association*, *66*(2), pp.120-133.

Szönyi, Michael, Leonardo Sagnotti, and Ann M. Hirt. 2007. “On Leaf Magnetic Homogeneity in Particulate Matter Biomonitoring Studies.”*Geophysical Research Letters* 34(6): L06306.

Tan, Pang Ning, Michael Steinbach, and Vipin Kumar. *Introduction to Data Mining*. Boston: Pearson, 2005.

Tauxe, Lisa, H. Neal Bertram, and Christian Sebrino. 2002. “Physical interpretation of hysteresis loops: Micromagnetic modeling of fine particle magnetite.” *Geochemistry Geophysics Geosystems* 3 (10).

Tauxe, L., T. A. T. Mullender, and T. Pick. "Potbellies, Wasp-waists, and Superparamagnetism in Magnetic Hysteresis." *Journal of Geophysical Research: Solid Earth*101, no. B1 (1996): 571-83.

Urbat, M, E Lehndorff, and L Schwark. "Biomonitoring Of Air Quality In The Cologne Conurbation Using Pine Needles As A Passive Sampler—Part I: Magnetic Properties". Atmospheric Environment 38.23 (2004): 3781-3792.

U.S. Congress. Committee on Interstate and Foreign Commerce. *Clean Air Act Amendments of 1977: Hearings before the Subcommittee ... Ninety-fifth Congress, First Session on H.R. 4151 and H.R. 4758, Bills to Amend the Clean Air Act, and for Other Purposes, H.R. 4444 (and All Identical Bills) Bills to Amend the Clean Air Act to Establish Certain Motor Vehicle Emission Standards, and for Other Purposes (and All Additional Bills Pertaining to the Amendment of the Clean Air Act), March 8, 9, 10, 11, and April 18, 1977*. Cong. Washington: U.S. Govt. Print. Off., 1978.

Zeger, Scott L., Francesca Dominici, Aidan McDermott, and Jonathan M. Samet. “Mortality in the Medicare Population and Chronic Exposure to Fine Particulate Air Pollution in Urban Centers (2000–2005).” *Environmental Health Perspectives* 116, no. 12 (August 12, 2008): 1614–19.

Zhang, Chunxia, Baochun Huang, Zhenyu Li, and He Liu. "Magnetic Properties of High-road-side Pine Tree Leaves in Beijing and Their Environmental Significance." Chinese Science Bulletin 51, no. 24 (2006): 3041-052.

Appendices

Appendix I – Hysteresis Properties

DW

Sample	Mass (g)	Hc (mT)	Mr (μAm^2/kg)	Ms (mAm^2/kg)	Ms/Mr
1	0.0571	11.41	106	1.218	-0.01149056
2	0.0783	6.875	127.8	3.832	0.029984351
3	0.0717	15.48	69.05	0.6753	0.00977987
4	0.0791	9.306	345	3.776	0.010944928
5	0.0835	8.847	228.6	2.351	0.010284339
6	0.0855	14.13	38.18	1.266	-0.03315872
7	0.0772	10.11	149.4	2.019	0.013514056
8	0.0861	9.579	416.4	4.835	0.011611431
9	0.0665	11.73	357	3.865	0.010826331
10	0.0776	15.21	529.9	4.429	0.008358181
11	0.0599	8.917	156.8	1.873	-0.01194515
12	0.0661	8.587	57.71	1.032	0.017882516
13	0.0694	18.47	96.14	0.4572	-0.00475556
14	0.0879	7.468	114.6	0.9748	0.008506108
15	0.0897	10.54	-230.2	-0.4389	0.001906603
16	0.0848	10.21	82.55	0.9745	0.011804967
17	0.0855	32.68	-177.8	0.05456	-0.00030686
18	0.0801	3.192	298.8	0.2664	0.000891566
19	0.095	4.279	-79.18	-0.2337	0.002951503
20	0.0608	105.7	314	0.2121	0.000675478
21	0.0675	11.53	122.8	1.005	0.008184039
22	0.0595	4.874	229	1.739	0.007593886
23	0.0648	10.86	-357.3	-0.8633	0.002416177
24	0.0701	-22.52	-153.4	-0.09984	0.000650847
25	0.0757	4.608	129.9	1.55	0.011932256
26	0.0653	11.67	201.6	2.472	-0.01226190
27	0.0785	8.124	27.17	1.398	0.051453809
28	0.0759	12.59	-377	-1.116	0.002960212
29	0.0715	-3.624	142.8	0.282	-0.00197479
30	0.0787	11.11	47.54	1.757	0.036958351
31	0.0848	8.792	143.4	1.874	0.01306834
32	0.0551	0.9021	245.6	0.7763	-0.00316083
33	0.0699	-1.83	68.88	0.36	0.005226481
34	0.0774	9.285	976.6	10.66	0.010915421

35	0.0664	8.775	476	5.057	0.01062395
36	0.0639	9.421	500.1	4.657	0.009312138
37	0.0631	-8.32	333.2	0.4534	-0.00136074
38	0.0639	5.968	-323.3	-0.8363	0.002586762
39	0.0794	-8.485	11.22	0.4453	0.039688057
40	0.0513	8.322	234.7	0.8836	-0.00376480
41	0.0749	13.68	-408.1	-0.5984	0.001466307
42	0.0737	-24.53	125.4	0.04511	0.000359729
43	0.0809	-11.82	32.97	0.2949	0.008944495
44	0.0724	8.013	22.75	1.696	-0.07454945
45	0.0886	11.59	193	0.3554	-0.00184145
46	0.0767	5.569	93.6	1.457	0.015566239
47	0.0846	8.588	353.4	3.224	0.009122807
48	0.0711	0.2431	47.19	0.5306	-0.01124390
49	0.0737	15.89	103.9	0.88953	0.008561405
50	0.0725	4.206	168.6	0.8124	-0.00481850
51	0.0777	10.82	112.3	1.307	0.011638468
52	0.0741	3.583	177.9	1.532	0.00861158
53	0.0635	8.09	53.87	1.75	-0.03248561
54	0.0776	7.234	76.57	1.898	0.024787776
55	0.073	9.391	186.6	2.85	0.015273312
56	0.0496	-3.837	191.4	0.684	0.003573668
57	0.0634	-18.77	-184	-0.3705	0.002013587
58	0.0626	7.088	18.21	1.179	-0.06474464
59	0.0629	1.342	33.54	1.21	-0.03607632
60	0.0468	-56.67	501.7	0.7774	0.001549532
61	0.0693	10.26	54.3	2.414	0.044456722
61	0.0761	9.034	222.2	1.499	0.006746175
62	0.0862	10.69	111.8	0.6588	0.005892665
63	0.0836	8.17	345.1	3.583	0.010382498
64	0.0558	7.313	467.6	3.126	0.006685201
66	0.0675	23.32	28.04	0.6567	0.023420114
67	0.0494	-38.42	-689	-0.07737	0.000112293
68	0.0831	-22.74	-251.9	-0.2505	0.000994442
69	0.0707	-10.9	165.4	0.393	-0.00237605
70	0.0841	4.104	46.32	0.7575	-0.01635362
71	0.0757	7.958	34.69	0.451	0.013000865
72	0.0744	-11.6	184.9	0.288	-0.00155759
73	0.0745	17.78	55.51	0.7416	0.013359755
74	0.078	-63.02	60.13	0.121	0.002012307

75	0.0602	14.75	234	1.254	0.005358974
76	0.0747	11.31	32.17	0.93	0.028908921
78	0.0629	10.78	-294.1	-0.76	0.002584155
79	0.0574	12.86	-229.2	-1.206	0.00526178
80	0.0894	-4.283	13.04	0.2392	0.018343558
82	0.079	12.21	-125.3	-0.6246	0.004984836
83	0.0828	-0.1312	225.3	0.03045	-0.00013515
84	0.0677	2.194	46.53	0.5337	-0.01147001
85	0.0606	9.84	130.3	3.296	0.025295472
86	0.0668	93.62	-198.5	0.06704	-0.00033773
87	0.0888	-9.087	-106.3	0.3538	-0.00332831
88	0.0942	10.45	67.54	1.061	0.015709209
89	0.0624	-9.469	174.3	0.3634	-0.00208491
90	0.095	10.56	117.9	1.962	0.016641221
91	0.0949	9.303	530.5	5.353	0.010090481
92	0.076	9.143	174	3.234	0.018586207
93	0.0705	7.523	158.6	1.577	0.009943253
94	0.0553	42.37	314	0.101	-0.00032165
95	0.0751	6.054	307	5.446	0.017739414
96	0.0743	4.507	14.25	1.092	0.076631579
97	0.0648	5.032	192.1	2.258	0.011754295
98	0.0706	9.574	749.4	10.35	0.013811049
99	0.0803	10.11	472.6	5.595	0.011838764
100	0.0653	9.273	179.5	2.392	0.013325905
101	0.0634	9.855	265.9	3.418	0.012854457
102	0.0824	9.52	299.7	4.335	0.014464464
CH					
1	0.0779	7.216	204	4.485	0.021985294
2	0.0848	10.18	151.5	1.978	0.013056106
3	0.0792	4.42	119.1	0.4758	0.003994962
4	0.0673	12.58	249.2	1.14	0.004574639
5	0.0696	7.423	138.8	2.611	0.018811239
6	0.0766	8.732	350	2.43	0.006942857
7	0.0694	12.97	189.8	2.174	0.011454162
8	0.0566	1.802	43.22	4.166	-0.09639056
9	0.0769	5.593	47.1	0.6565	-0.01393842
10	0.08677	-1.782	11.5	0.3277	0.028495652
11	0.0703	9.111	142.9	2.876	0.020125962
12	0.0656	2.437	116.7	0.4618	-0.00395715

13	0.0872	9.758	135.2	1.601	0.011841716
14	0.071	12.98	112.9	2.077	0.018396811
15	0.0654	6.544	306.9	2.913	0.009491691
16	0.0619	1.657	33.46	0.954	0.028511656
17	0.0688	6.384	87.39	1.438	0.016454972
18	0.0803	8.005	152.7	1.435	0.009397511
19	0.0502	17.33	366.6	1.446	0.003944354
20	0.0681	14.94	146	1.121	0.007678082
21	0.0778	14.04	177.6	1.502	0.008457207
22	0.061	10.63	216.4	1.669	0.007712569
23	0.0755	8.849	154.3	2.053	0.01330525
24	0.0718	4.448	119.1	2.245	0.018849706
25	0.0665	-8.494	45.94	1.273	0.027710057
26	0.0619	13.4	20240	1.187	5.86462E-05
27	0.067	-3.906	38.48	0.509	-0.01322765
28	0.0616	2.017	143.9	0.491	-0.00341209
29	0.0919	9.742	208	4.573	0.021985577
30	0.0915	-8.56	25.25	0.1857	0.007354455
31	0.056	-2.216	326.1	1.004	0.00307881
32	0.0842	15.85	71.96	0.6359	0.008836854
33	0.0664	-3.126	133.9	0.5589	0.00417401
34	0.0591	55.44	40.01	0.1804	-0.00450887
35	0.0828	16.35	-81.64	-0.257	0.003147967
36	0.0795	17.4	155.3	1.777	0.01144237
37	0.0631	-7.414	6916	7.28	0.001052632
38	0.0837	9.251	200.4	2.156	0.010758483
39	0.0758	89.05	23.5	0.07148	0.003041702
40	0.0785	1.286	69.24	0.5514	0.007963605
41	0.0775	12.97	-123.4	-0.2856	0.002314425
42	0.0777	-0.4712	-93.57	-0.3107	0.003320509
43	0.0723	7.981	-107	-0.3401	0.003178505
44	0.0673	10.63	193.9	1.107	0.005709128
45	0.0646	-18.72	35.03	0.3425	-0.00977733
46	0.0793	10.48	132.1	0.5506	-0.00416805
47	0.0734	8.813	87.98	1.32	0.01500341
48	0.0653	16.86	82.94	0.653	0.007873161
49	0.0767	8.288	99.61	1.494	0.014998494
50	0.0647	9.432	170.1	1.014	0.005961199
51	0.0556	7.199	250	2.567	0.010268
52	0.0837	6.282	50.71	0.4413	-0.00870242

53	0.0801	12.12	182.7	1.805	0.009879584
54	0.067	7.868	107.4	1.211	0.011275605
55	0.0658	10.9	223.7	1.369	0.006119803
56	0.0674	5.737	145.2	2.767	0.019056474
57	0.0655	7.689	114.4	2.681	0.023435315
58	0.0714	6.025	219.1	2.106	0.009612049
59	0.0689	17.52	256.3	1.279	0.004990246
60	0.0748	4.727	55.07	0.8047	-0.01461231
61	0.0636	-0.3099	62.73	0.00508	-8.0982E-05
62	0.0885	9.253	9.051	0.9885	0.109214451
63	0.0648	15.42	263	0.889	0.003380228
64	0.0538	15.1	49.76	1.505	-0.03024517
65	0.0538	6.217	66.39	1.327	0.01998795
66	0.049	29.89	29.73	0.4647	-0.01563067
67	0.0588	8.67	79.4	1.145	0.014420655
68	0.0865	11.08	38.89	0.7492	0.019264592
69	0.0533	9.509	76.83	1.088	-0.01416113
70	0.0813	12.54	57.17	0.7646	0.013374147
71	0.0755	12.06	174.9	2.134	0.012201258
72	0.0656	12.8	252.2	2.362	0.009365583
73	0.053	-1.069	13	0.5102	-0.03924615
74	0.0613	13.95	321.3	2.285	0.007111734
75	0.0652	11.84	269.5	2.159	0.008011132
76	0.0817	12.31	822	7.24	0.008807786
77	0.0551	10.28	291	1.216	-0.00417869
78	0.0535	11.52	941.4	8.517	0.009047164
79	0.0737	11.84	405.8	2.906	0.007161163
81	0.0747	9.123	168.7	1.662	0.009851808
82	0.067	18.07	162.5	1.247	0.007673846
84	0.0557	13.84	405	3.74	0.009234568
85	0.0848	10.41	80.03	1.294	0.016168937
86	0.0665	-12.13	180	0.5723	0.003179444
87	0.0731	7.36	119.8	2.566	0.021419032
88	0.0815	9.559	410.5	3.658	0.008911084
89	0.0901	12.24	54.2	0.5818	-0.01073431
90	0.0761	3.223	50.41	0.2604	0.005165642
91	0.0783	0.7089	213.3	0.6377	0.002989686
92	0.0754	6.555	60.69	1.069	0.017614104
93	0.0704	8.89	350.6	2.962	0.008448374
94	0.0863	7.089	18.14	0.6646	0.036637266

95	0.0679	12.05	32.93	0.7741	-0.02350744
96	0.0545	11.91	782.8	4.117	0.005259325
97	0.0641	94.98	-21.14	0.02546	-0.00120435
98	0.0598	9.916	461	2.609	0.005659436
99	0.0812	11.89	686	5.875	0.00856414
100	0.0628	19.66	10.44	0.9764	-0.09352490
101	0.0666	6.676	4.8	0.5902	0.122958333
102	0.1036	10.41	30.02	0.6354	0.021165889
Industrial		8.62	68450	576.6	0.008423667
Diesel		13.2	543	1.468	0.002703499
Car		6.997	1472	16.13	0.01095788

Appendix II – Susceptibilities

DW	Lat	Long	Bulk Susceptibility (SI)	Mass Susceptibilty (m^3/kg)	Surface Area Susceptibilty/ m^3	
1	47.55333413	-122.314166	114.3E-09	1.02E-07	1.28E-06	d
2	47.55333413	-122.314166	1.101E-09	5.02E-10	6.28E-09	c
3	47.55531643	-122.316134	876E-09	1.38E-06	1.73E-05	d
4	47.55559286	-122.318736	263.7E-09	2.94E-07	3.68E-06	d
5	47.55803648	-122.318093	381.7E-09	1.92E-07	2.40E-06	c
6	47.55989906	-122.318095	407.6E-09	1.59E-07	1.99E-06	c
7	47.56023346	-122.319859	508.7E-09	1.76E-07	2.20E-06	c
8	47.55974224	-122.320477	1.415E-09	4.05E-10	5.06E-09	c
9	47.55864648	-122.319295	258.2E-09	4.06E-07	5.08E-06	d
10	47.55889169	-122.31816	369E-09	3.36E-07	4.20E-06	d
11	47.55940453	-122.318155	40.09E-09	4.88E-08	6.10E-07	d
12	47.56112071	-122.317747	86.75E-09	3.93E-08	4.91E-07	c
13	47.56138739	-122.317199	13.56E-09	5.87E-09	7.34E-08	c

14	47.56136915	-122.317159	186.3E-09	8.21E-08	1.03E-06	c
15	47.56082104	-122.317286	76.11E-09	2.72E-08	3.40E-07	c
16	47.56190994	-122.317311	21.72E-09	2.36E-08	2.95E-07	d
17	47.56368255	-122.317315	92.73E-09	3.98E-08	4.98E-07	c
18	47.56568878	-122.317262	127.7E-09	1.47E-07	1.84E-06	d
19	47.56718263	-122.317296	17.06E-09	6.26E-09	7.83E-08	c
20	47.56822584	-122.317203	-142.4E-09	-1.11E-07	-1.39E-06	d
21	47.56905414	-122.317285	-1.457E-09	-1.91E-09	-2.39E-08	d
22	47.56756234	-122.314579	129.5E-09	9.80E-08	1.23E-06	d
23	47.56724743	-122.314583	84.85E-09	4.00E-08	5.00E-07	c
24	47.56724743	-122.314583	92.87E-09	4.77E-08	5.96E-07	c
25	47.56743638	-122.311576	-65.03E-09	-6.33E-08	-7.91E-07	d
26	47.56697845	-122.310239	114E-09	2.78E-07	3.48E-06	d
27	47.56697845	-122.310239	223.1E-09	1.00E-07	1.25E-06	c
28	47.56785249	-122.308951	-59.34E-09	-5.74E-08	-7.18E-07	d
29	47.56747058	-122.309781	-64E-09	-9.58E-08	-1.20E-06	d
30	47.56587875	-122.306930	100.7E-09	1.30E-07	1.63E-06	d
31	47.56587875	-122.306930	452.6E-09	2.17E-07	2.71E-06	c
32	47.56669806	-122.307012	271.8E-09	1.56E-07	1.95E-06	c
33	47.56669806	-122.307012	-53.36E-09	-7.12E-08	-8.90E-07	d
34	47.56677654	-122.306599	2.712E-09	1.03E-09	1.29E-08	c
35	47.56677654	-122.306599	808.4E-09	7.71E-07	9.64E-06	d
36	47.5662984	-122.306393	295E-09	5.75E-07	7.19E-06	d

37	47.56590839	-122.305879	329.7E-09	1.34E-07	1.68E-06	c
38	47.5656845	-122.306055	-99.14E-09	-5.03E-08	-6.29E-07	c
39	47.5656845	-122.306055	-28.33E-09	-3.09E-08	-3.86E-07	d
40	47.56461239	-122.305830	36.84E-09	4.28E-08	5.35E-07	d
41	47.56461239	-122.305830	7.582E-09	2.80E-09	3.50E-08	c
42	47.56477649	-122.304698	-150.2E-09	-6.39E-08	-7.99E-07	c
43	47.56477649	-122.304698	-285.5E-09	-2.20E-07	-2.75E-06	d
44	47.56539923	-122.305009	43.59E-09	5.86E-08	7.33E-07	d
45	47.56720801	-122.306527	65.61E-09	3.27E-08	4.09E-07	c
46	47.5638567	-122.305853	79.31E-09	8.92E-08	1.12E-06	d
47	47.5638567	-122.305853	345.7E-09	2.60E-07	3.25E-06	d
48	47.56267686	-122.305669	98.7E-09	0.000000141	1.76E-06	d
49	47.56190992	-122.305321	65.61E-09	1.00E-07	1.25E-06	d
50	47.56142464	-122.305420	21.09E-09	2.91E-08	3.64E-07	d
51	47.56118284	-122.305609	5.249E-09	2.52E-09	3.15E-08	c
52	47.56140326	-122.304862	6.27E-09	8.40E-09	1.05E-07	d
53	47.5620415	-122.304761	-76.59E-09	-1.18E-07	-1.48E-06	d
54	47.56226893	-122.305170	333.7E-09	1.34E-07	1.68E-06	c
55	47.56255267	-122.30596	581.4E-09	2.72E-07	3.40E-06	c
56	47.56027604	-122.297074	-16.96E-09	-5.44E-08	-6.80E-07	d
57	47.55868446	-122.295779	-27.99E-09	-4.29E-08	-5.36E-07	d
58	47.55460742	-122.295621	-64.3E-09	-1.45E-07	-1.81E-06	d
59	47.55329335	-122.294097	-13.7E-09	-1.69E-08	-2.11E-07	d

60	47.55355786	-122.293216	-20.27E-09	-3.04E-08	-3.80E-07	d
61	47.55633707	-122.29157	353.4E-09	1.80E-07	2.25E-06	c
62	47.55511632	-122.287692	-32.37E-09	-5.59E-08	-6.99E-07	d
63	47.55479431	-122.289451	293.8E-09	2.58E-07	3.23E-06	d
64	47.55479431	-122.289451	223.9E-09	3.30E-07	4.13E-06	d
65	47.55555032	-122.289481	-25.51E-09	-3.92E-08	-4.90E-07	d
66	47.55575347	-122.287418	36.16E-09	6.25E-08	7.81E-07	d
67	47.55310812	-122.285978	-59.78E-09	-1.25E-07	-1.56E-06	d
68	47.55241302	-122.285616	39.36E-09	1.80E-08	2.25E-07	c
69	47.55138519	-122.285284	-38.2E-09	-7.00E-08	-8.75E-07	d
70	47.55138519	-122.285284	100.6E-09	5.32E-08	6.65E-07	c
71	47.55121855	-122.285978	172E-09	5.28E-08	6.60E-07	c
72	47.55122681	-122.287307	83.98E-09	9.23E-08	1.15E-06	d
73	47.5526448	-122.292524	12.69E-09	1.78E-08	2.23E-07	d
74	47.5526448	-122.292524	-185.6E-09	-1.11E-07	-1.39E-06	c
75	47.55092142	-122.296136	51.61E-09	5.54E-08	6.93E-07	d
76	47.55092142	-122.296136	101.9E-09	5.46E-08	6.83E-07	c
78	47.55197284	-122.297384	-108.2E-09	-4.83E-08	-6.04E-07	c
79	47.55250115	-122.296965	-154.8E-09	-1.45E-07	-1.81E-06	d
80	47.55250115	-122.296965	-70.13E-09	-2.58E-08	-3.23E-07	c
81	47.55109252	-122.305012	226.1E-09	8.79E-08	1.10E-06	d
82	47.55313594	-122.30515	-96.66E-09	-3.74E-08	-4.68E-07	c
83	47.55313594	-122.30515	-43.68E-09	-3.45E-08	-4.31E-07	d

84	47.55154087	-122.306242	160.8E-09	6.49E-08	8.11E-07	c
85	47.55416083	-122.306500	606.1E-09	2.16E-07	2.70E-06	c
86	47.55562067	-122.309843	190.4E-09	7.12E-08	8.90E-07	c
87	47.55562067	-122.309843	101E-09	6.98E-08	8.73E-07	d
88	47.55564929	-122.311611	71.29E-09	4.95E-08	6.19E-07	d
89	47.55565651	-122.315824	121.9E-09	8.55E-08	1.07E-06	d
90	47.55456708	-122.317221	170.1E-09	1.29E-07	1.61E-06	d
91	47.55253253	-122.323122	393.6E-09	3.71E-07	4.64E-06	d
92	47.55188894	-122.322319	139.5E-09	1.08E-07	1.35E-06	d
93	47.55125037	-122.32236	-15.6E-09	-1.48E-08	-1.85E-07	d
94	47.55083628	-122.323861	52.92E-09	2.13E-08	2.66E-07	c
95	47.55061737	-122.323359	878.6E-09	7.97E-07	9.96E-06	d
96	47.55015286	-122.322408	48.21E-09	4.82E-08	6.03E-07	d
97	47.54930102	-122.322911	37.32E-09	3.11E-08	3.89E-07	d
98	47.5487143	-122.319556	1.678E-09	8.74E-10	1.09E-08	c
99	47.5525011	-122.32085	-426.5E-09	-3.95E-07	-4.94E-06	d
100	47.55075854	-122.321364	169.1E-09	2.20E-07	2.75E-06	d
101	47.55375709	-122.317191	14.68E-09	3.55E-08	4.44E-07	d
102	47.55190735	-122.316325	-71.34E-09	-6.87E-08	-8.59E-07	d
CH 1	47.61867044	-122.326753	763.4E-09	6.22E-07	7.78E-06	d
2	47.62081865	-122.32636	151.3E-09	1.00E-07	1.25E-06	d
3	47.62137781	-122.326586	-66.48E-09	-5.76E-08	-7.20E-07	d

4	47.62222495	-122.325284	-43.643E-09	-5.09E-08	-6.36E-07	d
5	47.62392431	-122.326606	94.33E-09	1.21E-07	1.51E-06	d
6	47.62581395	-122.326622	270E-09	2.10E-07	2.63E-06	d
7	47.6261373	-122.32652	388.1E-09	3.92E-07	4.90E-06	d
8	47.6268347	-122.325770	334E-09	3.29E-07	4.11E-06	d
9	47.6258609	-122.325423	-55.11E-09	-7.58E-08	-9.48E-07	d
10	47.6258609	-122.325423	-62.74E-09	-3.23E-08	-4.04E-07	d
11	47.6255007	-122.325375	16.91E-09	2.84E-08	3.55E-07	d
12	47.62515873	-122.325366	-66.05E-09	-6.97E-08	-8.71E-07	d
13	47.62457368	-122.325333	34.84E-09	3.36E-08	4.20E-07	c
14	47.62198719	-122.324635	299.3E-09	1.67E-07	2.09E-06	d
15	47.62152465	-122.324015	173.6E-09	2.36E-07	2.95E-06	d
16	47.62090408	-122.324063	146.4E-09	1.63E-07	2.04E-06	d
17	47.62541005	-122.322208	235.3E-09	3.12E-07	3.90E-06	d
18	47.62541005	-122.322208	104.7E-09	1.12E-07	1.40E-06	d
19	47.62667991	-122.322405	44.61E-09	7.11E-08	8.89E-07	d
20	47.62688621	-122.322296	-2.77E-09	-1.99E-09	-2.49E-08	d
21	47.62855386	-122.321289	11.52E-09	1.27E-08	1.59E-07	d
22	47.62692522	-122.321284	7.582E-09	1.60E-08	2.00E-07	d
23	47.62852909	-122.320145	324.7E-09	4.64E-07	5.80E-06	d
24	47.63000493	-122.320179	1.166E-09	1.32E-09	1.65E-08	d
25	47.63128276	-122.320202	7.291E-09	1.80E-08	2.25E-07	c
26	47.63599165	-122.319196	104.8E-09	4.91E-08	6.14E-07	d

27	47.63722551	-122.317875	115.8E-09	1.26E-07	1.58E-06	d
28	47.63722551	-122.317875	-127E-09	-1.59E-07	-1.99E-06	c
29	47.63774282	-122.317110	1.4883E-09	5.45E-10	6.81E-09	d
30	47.63610929	-122.314775	-174.2E-09	-1.10E-07	-1.38E-06	d
31	47.63239528	-122.310617	-85.73E-09	-1.04E-07	-1.30E-06	c
32	47.63393002	-122.309971	28.72E-09	1.13E-08	1.41E-07	d
33	47.63322801	-122.309940	87.9E-09	1.51E-07	1.89E-06	d
34	47.63216187	-122.313708	-71.15E-09	-2.21E-07	-2.76E-06	c
35	47.63194124	-122.314430	-4.957E-09	5.06E-08	6.33E-07	c
36	47.63184681	-122.313686	295.3E-09	1.56E-07	1.95E-06	d
37	47.63182468	-122.312994	-104.7E-09	-1.86E-07	-2.33E-06	c
38	47.63182468	-122.312994	430E-09	1.97E-07	2.46E-06	c
39	47.63151113	-122.313224	-19.97E-09	-1.15E-08	-1.44E-07	d
40	47.63146774	-122.313491	87.48E-09	1.01E-07	1.26E-06	c
41	47.63038012	-122.313678	85E-09	3.41E-08	4.26E-07	c
42	47.62898111	-122.312951	-80.92E-09	-3.22E-08	-4.03E-07	c
43	47.62860697	-122.313582	-230.6E-09	-1.18E-07	-1.48E-06	d
44	47.62860076	-122.31404	-79.9E-09	-1.02E-07	-1.28E-06	d
45	47.62844144	-122.314489	-99.87E-09	-2.17E-07	-2.71E-06	d
46	47.62865116	-122.314952	-102.5E-09	-7.72E-08	-9.65E-07	d
47	47.62869437	-122.316163	68.38E-09	7.07E-08	8.84E-07	d
48	47.62855288	-122.316577	76.11E-09	4.05E-08	5.06E-07	d
49	47.62856372	-122.318401	42.13E-09	5.92E-08	7.40E-07	d
50	47.62882369		30.13E-09	5.48E-08	6.85E-07	d

		-122.318237				
51	47.63004232	-122.317383	-60.8E-09	-0.00000019	-2.38E-06	d
52	47.63119938	-122.316769	-42.28E-09	-1.08E-07	-1.35E-06	c
53	47.63169949	-122.316137	322.9E-09	1.75E-07	2.19E-06	d
54	47.63038458	-122.312919	-268.4E-09	-6.56E-07	-8.20E-06	d
55	47.62810966	-122.31468	-206.5E-09	-3.73E-07	-4.66E-06	d
56	47.6271648	-122.314665	95.2E-09	1.57E-07	1.96E-06	d
57	47.62609996	-122.312643	88.45E-09	1.21E-07	1.51E-06	d
58	47.62577574	-122.312594	111.1E-09	1.70E-07	2.13E-06	d
59	47.62526888	-122.313599	26.46E-09	5.15E-08	6.44E-07	d
60	47.62534603	-122.314463	-62.11E-09	-7.07E-08	-8.84E-07	d
61	47.62489776	-122.314735	64.3E-09	9.46E-08	1.18E-06	d
62	47.62422775	-122.315542	241.3E-09	1.30E-07	1.63E-06	d
63	47.62479528	-122.315655	-5.394E-09	-5.04E-09	-6.30E-08	d
64	47.62533646	-122.315874	23.03E-09	3.44E-08	4.30E-07	d
65	47.62303906	-122.316889	37.47E-09	1.05E-07	1.31E-06	c
66	47.62112151	-122.318231	-34.99E-09	-1.34E-08	-1.68E-07	d
67	47.62199961	-122.319125	-31.35E-09	-1.97E-08	-2.46E-07	d
68	47.6216383	-122.318890	-368.31E-09	-3.13E-07	-3.91E-06	d
69	47.62128749	-122.318908	-51.32E-09	-5.99E-08	-7.49E-07	d
70	47.61926731	-122.319639	92.14E-09	9.24E-08	1.16E-06	d
71	47.61863467	-122.319168	146.1E-09	1.41E-07	1.76E-06	d
72	47.61835141	-122.318440	278.9E-09	2.05E-07	2.56E-06	d
73	47.46803934	-128.902934	-12.83E-09	-9.86E-09	-1.23E-07	d

74	47.46766275	-128.902905	55.84E-09	7.10E-08	8.88E-07	d
75	47.4668002	-128.903047	124.7E-09	1.72E-08	2.15E-07	d
76	47.46681759	-128.90340	519.6E-09	5.23E-07	6.54E-06	c
77	47.6170421	-122.319176	-45.63E-09	-6.33E-08	-7.91E-07	d
78	47.61680067	-122.319432	326.1E-09	6.28E-07	7.85E-06	d
79	47.61652121	-122.319342	131E-09	2.29E-07	2.86E-06	d
81	47.61698645	-122.320414	9.137E-09	1.27E-08	1.59E-07	d
82	47.61851432	-122.320115	76.69E-09	9.83E-08	1.23E-06	d
83	47.61871873	-122.319686	-5.686E-09	-4.04E-09	-5.05E-08	d
84	47.61959988	-122.318065	80.92E-09	1.34E-07	1.68E-06	d
85	47.61931539	-122.315620	134E-09	1.25E-07	1.56E-06	d
86	47.61898305	-122.315717	-26.83E-09	-3.34E-08	-4.18E-07	d
87	47.61890273	-122.314321	196.8E-09	2.00E-07	2.50E-06	d
88	47.61910067	-122.314318	415.7E-09	4.11E-07	5.14E-06	d
89	47.62131619	-122.314662	-91.71E-09	-6.79E-08	-8.49E-07	d
90	47.62156835	-122.314699	-110.8E-09	-6.50E-08	-8.13E-07	d
91	47.62235962	-122.314608	-90.1E-09	-1.16E-07	-1.45E-06	d
92	47.62494251	-122.314694	253.4E-09	2.37E-07	2.96E-06	d
93	47.62532883	-122.314596	135.3E-09	2.13E-07	2.66E-06	d
94	47.62594135	-122.314708	88.94E-09	7.97E-08	9.96E-07	d
95	47.62662458	-122.314606	-56.03E-09	-8.81E-08	-1.10E-06	d
96	47.6265752	-122.315378	156.1E-09	2.96E-07	3.70E-06	d
97	47.62565001	-122.315643	177.3E-09	2.70E-07	3.38E-06	d
98	47.62377799	-122.323148	15.16E-09	1.91E-08	2.39E-07	c

99	47.62129454	-122.323140	1.089E-09	6.43E-10	8.04E-09	d
100	47.62093442	-122.323104	60.07E-09	8.20E-08	1.03E-06	d
101	47.62080213	-122.323559	-154.8E-09	-1.74E-07	-2.18E-06	d
102	47.61946446	-122.324068	-12.69E-09	-8.95E-09	-1.12E-07	
Industrial			411.4E-06	5.8990E-06	7.37E-05	
Diesel			973.7E-09	3.4589E-08	4.32E-07	
Car			6.351E-06	1.9896E-07	2.49E-06	

Appendix III – Cleveland HS Susceptibilities

Leaf Sample	Susceptibility (Bartingtons)
DW1	-206.6
DW100n	-21.2
DW105n	148.7
DW108n	3.8
DW109n	31.1
DW110	-5
DW115	0
DW118	-55.8
DW119	13.7
DW12	22.1
DW121n	-31.1
DW122n	-7.9
DW123n	-0.9
DW129	-33.1
DW132n	22.9
DW133n	-27.4
DW140n	3.5
DW141n	6.7
DW146n	6.5
DW149	-18.7
DW149n	19.8
DW152	-18.1
DW153	-319.7

DW156	-0.3
DW157	6.3
DW159	-9
DW164	19.8
DW168	43.3
DW169	-18
DW17	-10.9
DW175n	17.3
DW178n	-35.2
DW181n	-10.8
DW183n	-14.3
DW189	1.8
DW19	23.1
DW192n	52.5
DW194	-38.7
DW196	8.3
DW197n	6.3
DW199n	50.7
DW200n	83.8
DW202n	-21.3
DW203n	63.1
DW205	0
DW211n	14.6
DW219	-82.7
DW22	-9.3
DW222	-52.4
DW224	-23.4
DW231n	-4.1
DW234n	24
DW236n	10
DW239n	-5.2
DW28	19.4
DW31n	-3.7
DW4	-78.8
DW45n	-73.5
DW46	-3.3
DW47	0
DW48	31.4
DW49	20.6
DW53	14.9

DW54	29.4
DW57	52.3
DW58	-20.2
DW59	8.1
DW60	102
DW63n	37.2
DW64	-10.2
DW65	-35.2
DW68	0
DW7	27.7
DW72	-6.6
DW73	-27.2
DW75	-97.1
DW80	12.3
DW81n	-10.6
DW82n	-0.4
DW83n	7.8
DW84n	2.6
DW85n	0
DW87	-14.9
DW89n	-23.2
DW9	-142.2
DW90n	-6.5
DW91n	-7.8
Dw116	-9.8
Dw213n	5.7

Appendix IV – SIRM Ratios

Sample	Intensity (300 mT)	Intensity (1 T)	Ratio (1 T/300 mT)
1	0.84	0.75	0.892857143
3	0.8	0.81	1.0125
7	2.0049	1.9988	0.996957454
17	1.9873	1.9776	0.995119006
32	1.9985	2.0345	1.01801351
34	1.7902	2.0932	1.169254832
40	2.0187	1.9984	0.989944023
55	1.9802	1.9981	1.009039491
87	1.9927	2.007	1.007176193

90	0.77	0.77	1
91	2.0029	1.8915	0.944380648
92	1.9905	2.0277	1.018688772
94	0.73	0.86	1.178082192
95	0.98	0.79	0.806122449
96	0.78	0.79	1.012820513
97	0.97	0.82	0.845360825
98	0.83	0.84	1.012048193
99	0.82	0.85	1.036585366
100	0.78	0.78	1
101	0.79	0.78	0.987341772
102	0.73	0.86	1.178082192
101c	1.9993	1.9992	0.999949982
26c	2.0051	2.0046	0.999750636
4c	2.0042	2.0038	0.999800419
56c	2.002	2.0096	1.003796204
84c	2.0014	2.004	1.001299091
86c	2.0052	2.0016	0.998204668
99c	1.9591	1.9106	0.975243734
Industrial	0.92	1.21	1.315217391
Diesel	0.117	0.124	1.05982906
Car	0.1246	0.095	0.762439807

Appendix V – Fe amounts per leaf density

Sample DV	Ms (mAm^2/kg)	Mass-normalized Ms	Fe weight %
1	1.218	1.35333E-05	0.0014
2	3.832	4.25778E-05	0.0043
3	0.6753	7.50333E-06	0.0008
4	3.776	4.19556E-05	0.0042
5	2.351	2.61222E-05	0.0026
6	1.266	1.40667E-05	0.0014
7	2.019	2.24333E-05	0.0022
8	4.835	5.37222E-05	0.0054
9	3.865	4.29444E-05	0.0043
10	4.429	4.92111E-05	0.0049
11	1.873	2.08111E-05	0.0021
12	1.032	1.14667E-05	0.0011

13	0.4572	0.00000508	0.0005
14	0.9748	1.08311E-05	0.0011
15	-0.4389	-4.87667E-06	-0.0005
16	0.9745	1.08278E-05	0.0011
17	0.05456	6.06222E-07	0.0001
18	0.2664	0.00000296	0.0003
19	-0.2337	-2.59667E-06	-0.0003
20	-0.2121	-2.35667E-06	-0.0002
21	1.005	1.11667E-05	0.0011
22	1.739	1.93222E-05	0.0019
23	-0.8633	-9.59222E-06	-0.0010
24	-0.09984	-1.10933E-06	-0.0001
25	1.55	1.72222E-05	0.0017
26	2.472	2.74667E-05	0.0027
27	1.398	1.55333E-05	0.0016
28	-1.116	-0.0000124	-0.0012
29	0.282	3.13333E-06	0.0003
30	1.757	1.95222E-05	0.0020
31	1.874	2.08222E-05	0.0021
32	0.7763	8.62556E-06	0.0009
33	0.36	0.000004	0.0004
34	10.66	0.000118444	0.0118
35	5.057	5.61889E-05	0.0056
36	4.657	5.17444E-05	0.0052
37	0.4534	5.03778E-06	0.0005
38	-0.8363	-9.29222E-06	-0.0009
39	0.4453	4.94778E-06	0.0005
40	0.8836	9.81778E-06	0.0010
41	-0.5984	-6.64889E-06	-0.0007
42	-0.04511	-5.01222E-07	-0.0001
43	0.2949	3.27667E-06	0.0003
44	1.696	1.88444E-05	0.0019
45	0.3554	3.94889E-06	0.0004
46	1.457	1.61889E-05	0.0016
47	3.224	3.58222E-05	0.0036
48	0.5306	5.89556E-06	0.0006
49	0.88953	9.88367E-06	0.0010
50	0.8124	9.02667E-06	0.0009
51	1.307	1.45222E-05	0.0015
52	1.532	1.70222E-05	0.0017

53	1.75	1.94444E-05	0.0019
54	1.898	2.10889E-05	0.0021
55	2.85	3.16667E-05	0.0032
56	0.684	0.0000076	0.0008
57	-0.3705	-4.11667E-06	-0.0004
58	1.179	0.0000131	0.0013
59	1.21	1.34444E-05	0.0013
60	-0.7774	-8.63778E-06	-0.0009
61	2.414	2.68222E-05	0.0027
61	1.499	1.66556E-05	0.0017
62	0.6588	0.00000732	0.0007
63	3.583	3.98111E-05	0.0040
64	3.126	3.47333E-05	0.0035
66	0.6567	7.29667E-06	0.0007
67	-0.07737	-8.59667E-07	-0.0001
68	-0.2505	-2.78333E-06	-0.0003
69	0.393	4.36667E-06	0.0004
70	0.7575	8.41667E-06	0.0008
71	0.451	5.01111E-06	0.0005
72	0.288	0.0000032	0.0003
73	0.7416	0.00000824	0.0008
74	-0.121	-1.34444E-06	-0.0001
75	1.254	1.39333E-05	0.0014
76	0.93	1.03333E-05	0.0010
78	-0.76	-8.44444E-06	-0.0008
79	-1.206	-0.0000134	-0.0013
80	0.2392	2.65778E-06	0.0003
82	-0.6246	-0.00000694	-0.0007
83	0.03045	3.38333E-07	0.0000
84	0.5337	0.00000593	0.0006
85	3.296	3.66222E-05	0.0037
86	0.06704	7.44889E-07	0.0001
87	0.3538	3.93111E-06	0.0004
88	1.061	1.17889E-05	0.0012
89	0.3634	4.03778E-06	0.0004
90	1.962	0.0000218	0.0022
91	5.353	5.94778E-05	0.0059
92	3.234	3.59333E-05	0.0036
93	1.577	1.75222E-05	0.0018
94	0.101	1.12222E-06	0.0001

95	5.446	6.05111E-05	0.0061
96	1.092	1.21333E-05	0.0012
97	2.258	2.50889E-05	0.0025
98	10.35	0.000115	0.0115
99	5.595	6.21667E-05	0.0062
100	2.392	2.65778E-05	0.0027
101	3.418	3.79778E-05	0.0038
102	4.335	4.81667E-05	0.0048
CH			
1	4.485	4.98333E-05	0.0050
2	1.978	2.19778E-05	0.0022
3	0.4758	5.28667E-06	0.0005
4	1.14	1.26667E-05	0.0013
5	2.611	2.90111E-05	0.0029
6	2.43	0.000027	0.0027
7	2.174	2.41556E-05	0.0024
8	4.166	4.62889E-05	0.0046
9	0.6565	7.29444E-06	0.0007
10	0.3277	3.64111E-06	0.0004
11	2.876	3.19556E-05	0.0032
12	0.4618	5.13111E-06	0.0005
13	1.601	1.77889E-05	0.0018
14	2.077	2.30778E-05	0.0023
15	2.913	3.23667E-05	0.0032
16	0.954	0.0000106	0.0011
17	1.438	1.59778E-05	0.0016
18	1.435	1.59444E-05	0.0016
19	1.446	1.60667E-05	0.0016
20	1.121	1.24556E-05	0.0012
21	1.502	1.66889E-05	0.0017
22	1.669	1.85444E-05	0.0019
23	2.053	2.28111E-05	0.0023
24	2.245	2.49444E-05	0.0025
25	1.273	1.41444E-05	0.0014
26	1.187	1.31889E-05	0.0013
27	0.509	5.65556E-06	0.0006
28	0.491	5.45556E-06	0.0005
29	4.573	5.08111E-05	0.0051
30	0.1857	2.06333E-06	0.0002
31	1.004	1.11556E-05	0.0011

32	0.6359	7.06556E-06	0.0007
33	0.5589	0.00000621	0.0006
34	0.1804	2.00444E-06	0.0002
35	-0.257	-2.85556E-06	-0.0003
36	1.777	1.97444E-05	0.0020
37	-7.28	-8.08889E-05	-0.0081
38	2.156	2.39556E-05	0.0024
39	0.07148	7.94222E-07	0.0001
40	0.5514	6.12667E-06	0.0006
41	-0.2856	-3.17333E-06	-0.0003
42	-0.3107	-3.45222E-06	-0.0003
43	-0.3401	-3.77889E-06	-0.0004
44	1.107	0.0000123	0.0012
45	0.3425	3.80556E-06	0.0004
46	0.5506	6.11778E-06	0.0006
47	1.32	1.46667E-05	0.0015
48	0.653	7.25556E-06	0.0007
49	1.494	0.0000166	0.0017
50	1.014	1.12667E-05	0.0011
51	2.567	2.85222E-05	0.0029
52	0.4413	4.90333E-06	0.0005
53	1.805	2.00556E-05	0.0020
54	1.211	1.34556E-05	0.0013
55	1.369	1.52111E-05	0.0015
56	2.767	3.07444E-05	0.0031
57	2.681	2.97889E-05	0.0030
58	2.106	0.0000234	0.0023
59	1.279	1.42111E-05	0.0014
60	0.8047	8.94111E-06	0.0009
61	-0.00508	-5.64444E-08	0.0000
62	0.9885	1.09833E-05	0.0011
63	0.889	9.87778E-06	0.0010
64	1.505	1.67222E-05	0.0017
65	1.327	1.47444E-05	0.0015
66	0.4647	5.16333E-06	0.0005
67	1.145	1.27222E-05	0.0013
68	0.7492	8.32444E-06	0.0008
69	1.088	1.20889E-05	0.0012
70	0.7646	8.49556E-06	0.0008
71	2.134	2.37111E-05	0.0024

72	2.362	2.62444E-05	0.0026
73	0.5102	5.66889E-06	0.0006
74	2.285	2.53889E-05	0.0025
75	2.159	2.39889E-05	0.0024
76d	7.24	8.04444E-05	0.0080
77	1.216	1.35111E-05	0.0014
78	8.517	9.46333E-05	0.0095
79	2.906	3.22889E-05	0.0032
81	1.662	1.84667E-05	0.0018
82	1.247	1.38556E-05	0.0014
84	3.74	4.15556E-05	0.0042
85	1.294	1.43778E-05	0.0014
86	0.5723	6.35889E-06	0.0006
87	2.566	2.85111E-05	0.0029
88	3.658	4.06444E-05	0.0041
89	0.5818	6.46444E-06	0.0006
90	0.2604	2.89333E-06	0.0003
91	0.6377	7.08556E-06	0.0007
92	1.069	1.18778E-05	0.0012
93	2.962	3.29111E-05	0.0033
94	0.6646	7.38444E-06	0.0007
95	0.7741	8.60111E-06	0.0009
96	4.117	4.57444E-05	0.0046
97	0.02546	2.82889E-07	0.0000
98	2.609	2.89889E-05	0.0029
99	5.875	6.52778E-05	0.0065
100	0.9764	1.08489E-05	0.0011
101	0.5902	6.55778E-06	0.0007
102	0.6354	0.00000706	0.0007
Industrial	576.6	0.006406667	0.6407
Diesel	1.468	1.63111E-05	0.0016
Car	16.13	0.000179222	0.0179

Appendix VI – Background Figures

Air Quality Index (AQI) Values	Levels of Health Concern	Colors
0 to 50	Good	Green
51 to 100	Moderate	Yellow
101 to 150	Unhealthy for Sensitive Groups	Orange
151 to 200	Unhealthy	Red
201 to 300	Very Unhealthy	Purple
301 to 500	Hazardous	Maroon

Figure VI.1: Air Quality Index levels of health concern according to the EPA.

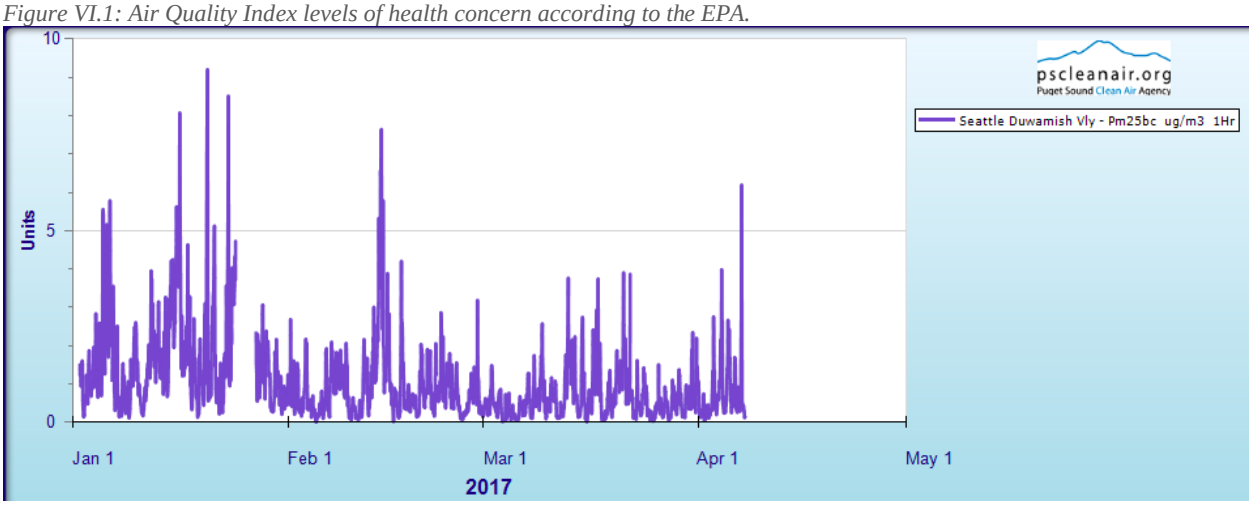

Figure VI.2: Puget Sound Clean Air Agency chart of $PM_{2.5}$ concentrations from January to April of 2017.

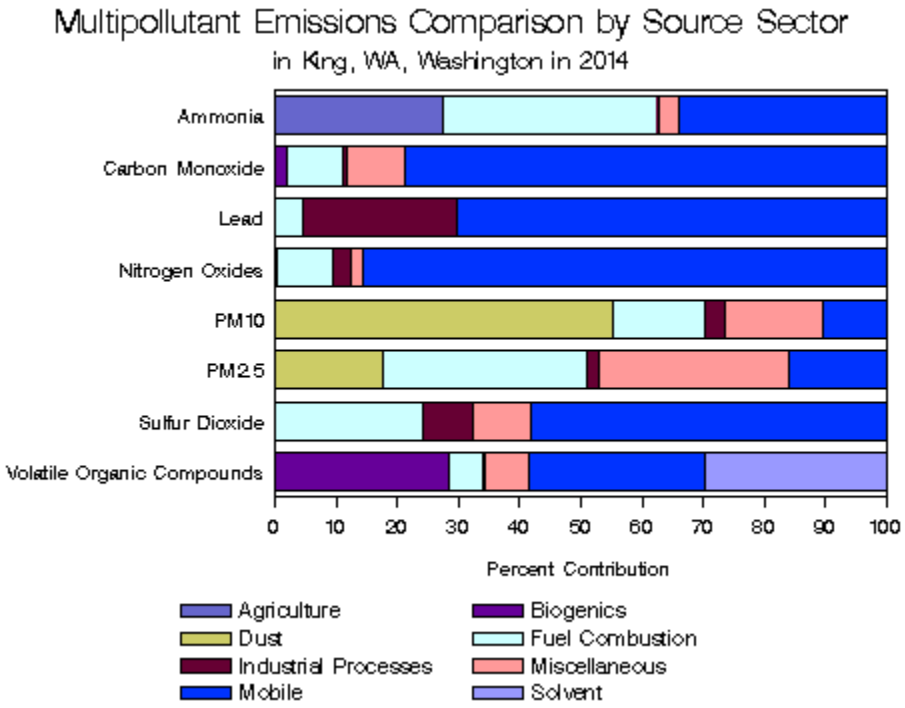

Figure VI.3: Emissions sources of pollutants in King County, WA 2014.

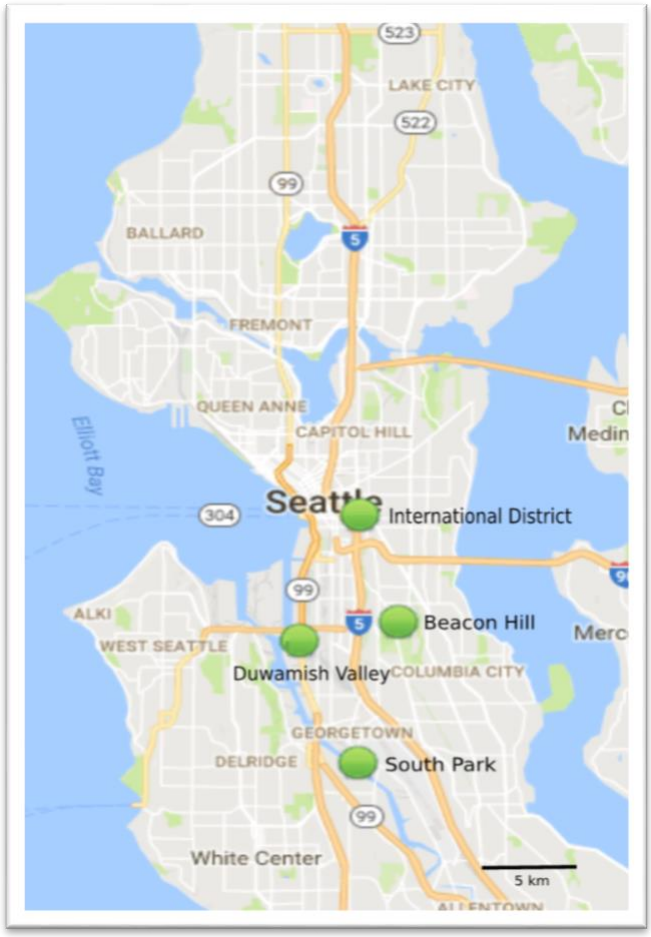

Figure VI.4: Map of the Puget Sound Clean Air Agency's air monitor station location.

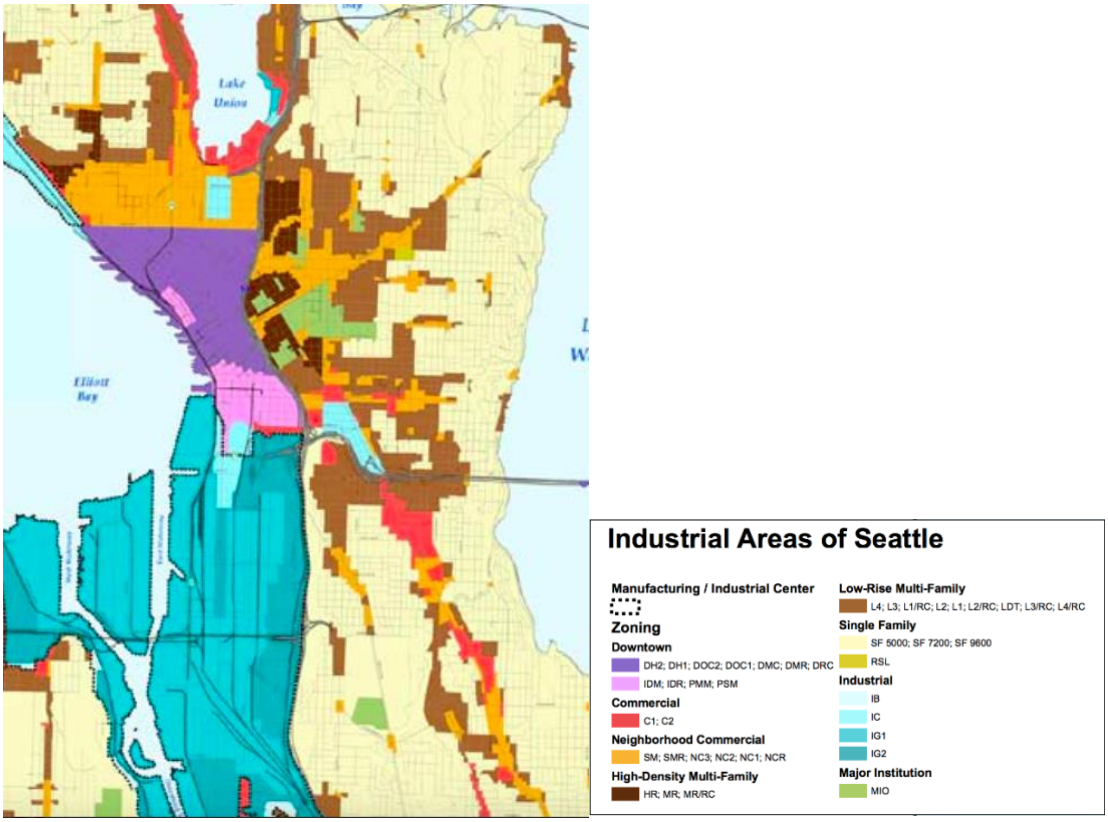

Figure VI.5: Map of land use of Seattle (Seattle Planning Commission Report 2007), with industrial mostly in the southwest.

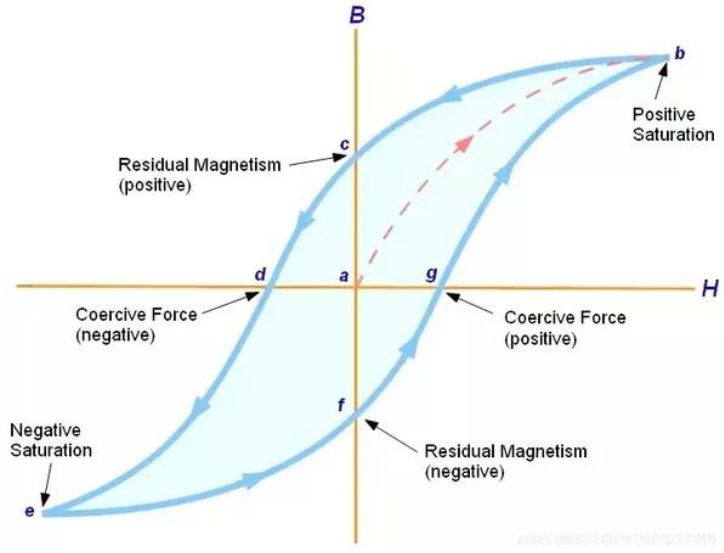

Figure VI.6: Graphic of a typical magnetic hysteresis loop. Ms at points b and e, Mr at points c and f, and Hc at points d and g.

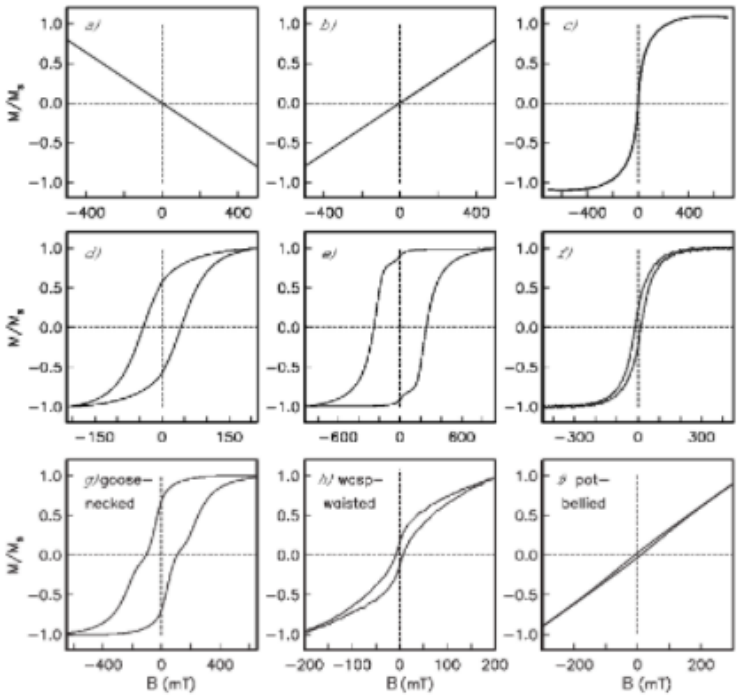

Figure VI.7: Patterns of hysteresis loops. a) diamagnetic, b) paramagnetic, c) superparamagnetic, d) uniaxial, single domain, e) magnetocrystalline, single domain, f) pseudo-single domain, g) magnetite and hematite, h) SD/SP magnetite, i) SD/SP magnetite, finer grains (Figure from Tauxe et al 1996)

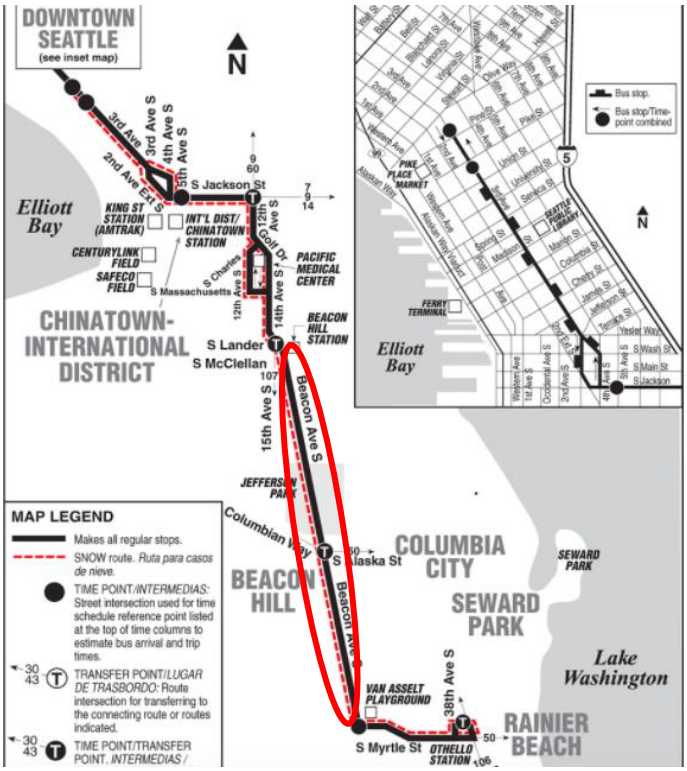

Figure VI.8: Bus route 36 goes through Beacon Avenue in South Seattle.

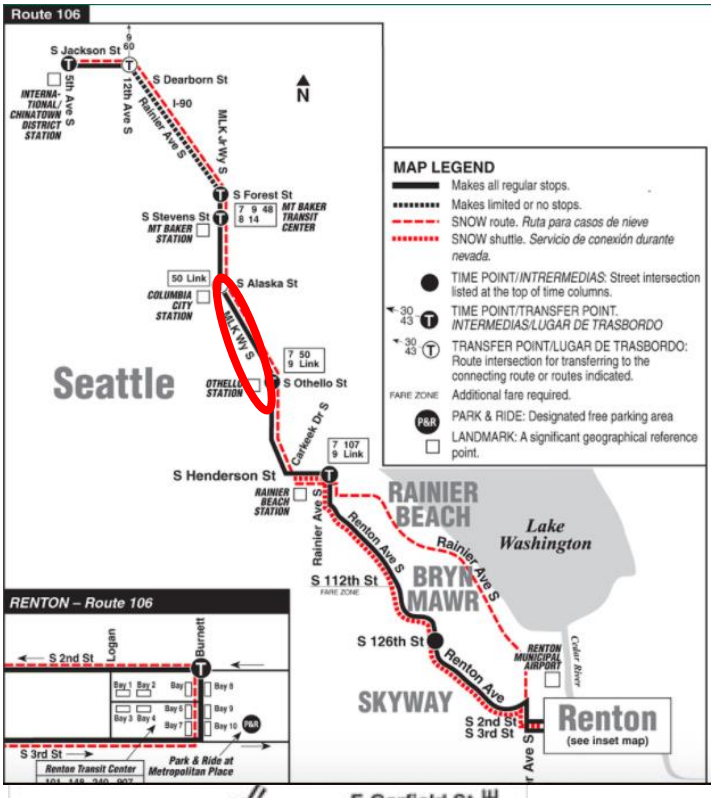

Figure VI.9: Bus route 106 goes through Martin Luther King Avenue in south Seattle.

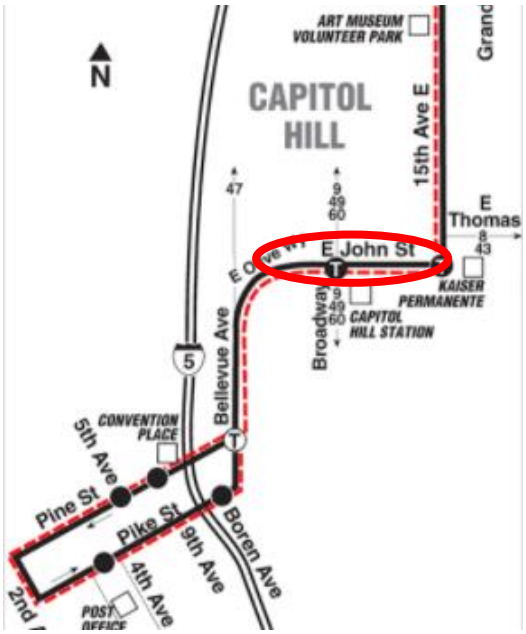

Figure VI.10: Bus route 10 goes through E John Street in